AD-A228 718

DTIC FILE COPY

(2)

OFFICE OF NAVAL RESEARCH

PUBLICATIONS / PATENTS / PRESENTATIONS / HONORS REPORT

DTIC
ELECTE
NOV 05 1990
S D
D S

for

1 October 1989 through 30 September 1990

for

Contract N00014-90-J-1553

R&T No. 414-Q-013---02

A Theoretical Search for Supervelocity Semiconductors

M. A. Littlejohn and K. W. Kim, Co-Principal Investigators
Department of Electrical and Computer Engineering
North Carolina State University
Raleigh, North Carolina 27695-7911

Reproduction in whole, or in part, is permitted for any purpose of the United States Government.

*This document has been approved for public release and sale; its distribution is unlimited.

90 10 25 079

a. Papers submitted to refereed journals (and not yet published).

K.W. Kim, M.A. Stroscio, and J.C. Hall, "Frequencies of Confined Longitudinal-Optical Phonon Modes in Short-Period Strained Semiconductor Superlattices," accepted for publication in the Proceedings of the SPIE International Symposium on Optical & Optoelectronic Applied Science and Engineering, July, 1990.

M.A. Littlejohn, J.L. Pelouard, W.C. Koscielniak, and D.L. Woolard, "Device Simulation Augmented by the Monte Carlo Method," accepted for publication in the Proceedings of the Workshop on Computational Electronics, May 21-25, 1990, Univ. of Illinois, Urbana, IL.

K.W. Kim, H. Tian, and M.A. Littlejohn, "Analysis of Delta-Doped and Uniformly-Doped HEMTs by Ensemble Monte Carlo Simulation," submitted to IEEE Electron Device Letters.

L.F. Register, M.A. Littlejohn, and M.A. Stroscio, "Comments on Evaluation of Feynman Path Integrals by Analytic Continuation," submitted to Physical Review B.

L.F. Register, M.A. Stroscio, and M.A. Littlejohn, "Path Integral Monte Carlo Calculation of Carrier Self-Energies," submitted to Physical Review B.

J.L. Pelouard and M.A. Littlejohn, "The Role of Nearly-Ballistic Transport in the Emitter-Base Junction of HBTs," submitted to IEEE Transactions on Electron Devices.

J.L. Pelouard and M.A. Littlejohn, "Transport in the Collector-Base Junction of HBTs," submitted to the IEEE Transactions on Electron Devices.

D.L. Woolard, M.A. Littlejohn, R.J. Trew, and C.T. Kelly, "Hydrodynamic Transport Model with Non-Parabolic Energy Bands," submitted to Physical Review B.

D.L. Woolard, H.L. Grubin, M.A. Littlejohn, M.A. Stroscio, and C.T. Kelly, "A Comparison of the Wigner Distribution Function Transport Model with the Quantum-Corrected Hydrodynamic Transport Model," submitted to Superlattices and Microstructures.

H. Tian, K.W. Kim, and M.A. Littlejohn, "Influence of DX Centers and Surface on Delta-Doped HEMT Performance," submitted to J. Appl. Phys.

DTIC COPY INSPECTED 6

Accession For
NTIS GRA&I
DTIC TAB
Unannounced
Justification
By
Distribution
Availability Codes
Dist | Avail and/or Special
A-1

b. Papers published in refereed journals

W.C. Koscielniak, J.L. Pelouard and M.A. Littlejohn, "Dynamic Behavior of Photocurrent in a GaAs Metal-Semiconductor-Metal Photodetector with Sub-Half-Micron Electrode Pattern," Appl. Phys. Lett. 54, 567 (1989).

W.C. Koscielniak, M.A. Littlejohn and J.L. Pelouard, "Analysis of a GaAs Metal-Semiconductor-Metal (MSM) Photodetector with 0.1 μm Finger Spacing," IEEE Electron Dev. Lett. 10, 209 (1989).

L.F. Register, M.A. Stroscio and M.A. Littlejohn, "Efficient Path-Integral Monte Carlo Technique for Ultrasmall Device Applications," Superlattices and Microstructures 6, 233 (1989).

J.L. Pelouard and M.A. Littlejohn, "Indium-Phosphide-Based Heterojunction Bipolar Transistors," Proceedings of the First International Conference on Indium Phosphide and Related Materials for Advanced Electronics and Optical Devices, Proceedings of SPIE-The International Society for Optical Engineering, vol. 1144, p. 582 (1989).

J.L. Pelouard, M.A. Littlejohn and H.P. Belgal, "Monte Carlo Study of Ballistic and Quasi-Ballistic Electron Transport in Semiconductors," Proceedings of the Sixth International Conference on the Numerical Analysis of Semiconductor Devices and Integrated Circuits, edited by J.J. Miller, Boole Press, Ltd., p. 255, Dublin, Ireland (1989).

L.F. Register, M.A. Littlejohn and M.A. Stroscio, "Path Integral Monte Carlo Methods for Ultra-Small Device Applications," Proceedings of the Sixth International Conference on the Numerical Analysis of Semiconductor Devices and Integrated Circuits, edited by J.J. Miller, Boole Press, Ltd., p. 266, Dublin, Ireland (1989).

D.L. Woolard, J.L. Pelouard, R.J. Trew, M.A. Littlejohn and C.T. Kelly, "Hydrodynamic Hot-Electron Transport Simulations Based on the Monte Carlo Method," Solid State Electronics 32, 1347 (1989).

L.F. Register, M.A. Littlejohn and M.A. Stroscio, "Polar Optical Phonon Scattering of Charge Carriers in Alloy Semiconductors: Effects of Phonon Localization," Solid State Electronics 32, 1387 (1989).

W.C. Koscielniak, J.L. Pelouard and M.A. Littlejohn, "Intrinsic and Extrinsic Response of GaAs Metal-Semiconductor-Metal Photodetectors," IEEE Photonics Technol. Lett. 2 125 (1990).

K.W. Kim, M.A. Stroscio, and J.C. Hall, "Frequencies of Confined Longitudinal-Optical Phonon Modes in GaAs/GaP Short-Period Strained-Layer Superlattices," J. Appl. Phys. 67, 6179 (1990).

W.C. Koscielniak, J.L. Pelouard, and M.A. Littlejohn, "Dark-Current Characteristics of GaAs Metal-Semiconductor-Metal (MSM) Photodetectors," IEEE Trans. Electron Devices ED-37, 1623 (1990).

M.A. Stroscio, K.W. Kim, and J.C. Hall, "Variation in Frequencies of Confined Longitudinal-Optical Phonon Modes due to Changes in the Effective Force Constants Near Heterojunction Interfaces," Superlattices and Microstructures 7, 115 (1990).

c. Books (and sections thereof) submitted for publications.

none

d. Books (and sections thereof) published.

none

e. Patents filed.

none

f. Patents granted.

none

g. Invited presentations at topical or scientific/technical society conferences.

J.L. Pelouard, M.A. Littlejohn and H.P. Belgal, "Monte Carlo Study of Ballistic and Quasi-Ballistic Electron Transport in Semiconductors," presented at the Sixth International Conference on the Numerical Analysis of Semiconductor Devices and Integrated Circuits, July 11-14, 1989, Dublin, Ireland.

L.F. Register, M.A. Littlejohn and M.A. Stroscio, "Path-Integral Monte Carlo Methods for Ultra-Small Device Applications," presented at the Sixth International Conference on the Numerical Analysis of Semiconductor Devices and Integrated Circuits, July 11-14, 1989, Dublin, Ireland.

M.A. Littlejohn, J.L. Pelouard, W.C. Koscielniak, and D.L. Woolard, "Device Simulation Augmented by the Monte Carlo Method," presented at the Workshop on Computational Electronics, May 21-25, 1990, Univ. of Illinois, Urbana, IL.

h. Contributed presentations at topical or scientific/technical society conference.

D.L. Woolard, J.L. Pelouard, R.J. Trew, M.A. Littlejohn and C.T. Kelly, "Hydrodynamic Hot-Electron Transport Simulations Based on The Monte Carlo Method," presented at the Sixth International Conference on Hot Carriers in Semiconductors, July 23-28, 1989, Scottsdale, AZ.

L.F. Register, M.A. Littlejohn and M.A. Stroscio, "Polar Optical Phonon Scattering of Charge Carriers in Alloy Semiconductors: Effects of Phonon Localization," presented at the Sixth International Conference on Hot Carriers in Semiconductors, July 23-28, 1989, Scottsdale, AZ.

D.L. Woolard, M.A. Stroscio, M.A. Littlejohn, R.J. Trew, and H.L. Grubin, "A New Non-parabolic Hydrodynamic Transport Model with Quantum Corrections," presented at the Workshop on Computational Electronics, May 21-25, 1990, Univ. of Illinois, Urbana, IL.

K.W. Kim, M.A. Stroscio, and J.C. Hall, "Frequencies of Confined Longitudinal-Optical Phonon Modes in Short-Period Strained Semiconductor Superlattices," presented at the SPIE International Symposium on Optical & Optoelectronic Applied Science and Engineering, July 8-13, 1990, San Diego, CA.

i. Honors/awards/prizes.

Mr. L.F. Register - Awarded Semiconductor Research Corporation (SRC) Fellowship for 1989 academic year, one of the 20 fellowships awarded nationally.

Dr. M.A. Littlejohn - Received the Certificate of Appreciation for Patriotic Civilian Service from the Secretary of the Army. This is the second highest commendation given to civilians by the Department of Defense.

j. Graduate students and postdoctorals supported under the CRP for the year ending 1 October 1990.

Mr. L.F. Register - Ph.D. student (degree awarded in December 1989).

Mr. D.L. Woolard - Ph.D. student

Mr. W.C. Koscielniak - Ph.D. student

ANNUAL REPORT

TO

THE OFFICE OF NAVAL RESEARCH
ARLINGTON, VA 22217

FOR

A THEORETICAL SEARCH FOR SUPERVELOCITY SEMICONDUCTORS

ONR Contract No. N00014-90-J-1553
R&T No. 414-Q-013---02
NCSU FAS No. 5-30451

Submitted By

North Carolina State University
The Department of Electrical and Computer Engineering
Raleigh, North Carolina 27695-7911

For the Period July 1, 1989 - June 30, 1990

Dr. M. A. Littlejohn
Principal Investigator
Soc. Sec. No. 242-60-6419
(919) 737-5247

Dr. K. W. Kim
Principal Investigator
Soc. Sec. No. 211-62-7519
(919) 737-5229

90 10 25 079

EXECUTIVE SUMMARY

This document presents a final report to the Office of Naval Research for the research program entitled "A Theoretical Search For Supervelocity Semiconductors". This program has been funded by ONR since 1974 in the Department of Electrical and Computer Engineering at N.C. State University. The research has resulted in more than 65 refereed publications and numerous conference presentations from its inception. Major contributions to the field of hot electron transport and semiconductor device modeling have been achieved, new computational methods have been developed (e.g. path integral Monte Carlo techniques), and the work has helped stimulate commercial ventures in the applications of quaternary semiconductor materials to electronic and optical devices. In addition, there have been twenty-four Ph.D. and M.S. students who have received degrees at N.C. State University with research support from this contract. Three visiting faculty members from Japan came to the University to work with the faculty investigators supported under this ONR contract during the 1979-1983 time period. A visiting professor from the French CNRS Microstructures and Microelectronics Laboratory in Bagneux (near Paris) spent a sabbatical year at N.C. State during 1988-89, and he devoted full-time working on this program at no cost to ONR. During the current funding period, a visiting scholar from China is a member of our research group working on projects which directly impact this ONR program.

This initial phases of this work centered around the development of Monte Carlo simulation techniques which allow the study of detailed physics of hot electron transport in a variety of compound semiconductor materials. The original emphases were concerned with electronic materials phenomena. Later work considered the utilization of these materials in realistic device structures where physical boundary conditions must be imposed on the carrier transport. More recently, the work has focused on the domain of ultra-small materials and device phenomena where microscopic non-local transient effects such as velocity overshoot, ballistic and nearly-ballistic transport, and quantum transport become important or dominant. During the past four years we have begun new research into the applications of the Feynman "integral over paths" approach to quantum transport as well as the study of hot electron effects in new

device structures, such as the hot electron spectrometer, heterojunction bipolar transistor, small dimension metal-semiconductor-metal photodetectors, and delta-doped high electron mobility transistors. Also, we have been exploring some new approaches to device modeling which combine the Monte Carlo method with the method of moments of the Boltzmann transport equation (hydrodynamic transport model) for studying specific device structures, such as small-dimension n^+-n-n^+ majority carrier devices and the high electron mobility transistor. During the past year we have incorporated quantum correction terms into the hydrodynamic model and applied this model to resonant tunneling structures. Quite recently, we have applied a new ansatz distribution function as a constitutive relation to close the moment equations in the hydrodynamic transport model. Initial results of this approach have been physically satisfying and computationally promising. New work on the theory of optical phonon modes in heterostructures has demonstrated the importance of the effects of reduced dimensionality on transport dominated by the LO phonon interaction near heterointerfaces. As a result of this work, a new concept for velocity enhancement in pseudomorphic device structures has been presented to ONR.

→ Recent efforts

During the last report period, we focused our efforts on new research in four areas along with the continuation of our basic research directions encompassing the study of hot electron transport in materials and devices. These four areas included 1) the study of quantum transport in resonant tunneling and related ultra-small heterobarrier device structures using the Feynman path integral and the transmission matrix method, 2) the study of the physics of hot electron and heterojunction device structures, 3) some new approaches to the merging of Monte Carlo methods with moment equation methods with resulting improvements to the hydrodynamic transport model, and 4) new Monte Carlo simulation in order to study pseudomorphic devices, delta-doped structures, and submicron MOSFETs. (RH) ←

TABLE OF CONTENTS

1.0 INTRODUCTION 1

2.0 RESEARCH RESULTS 2

2.1 Background 2

2.2 Summary of Research Results 6

2.3 Publications and Presentations 43

3.0 LIST OF REFERENCES 46

4.0 PERSONNEL 50

Appendix A: List of Refereed Publications on This Program Since 1975.

Appendix B: Papers Published During Contact Period.

Appendix C: Resumes of Principal Investigators.

1.0 INTRODUCTION

In October, 1974, the Office of Naval Research initiated sponsorship of a basic research program in the Department of Electrical and Computer Engineering at North Carolina State University. The general goal of this research program has been and continues to be the investigation of high-speed carrier transport in III-V compound semiconductors, III-V alloy materials, other advanced electronic and optical materials, and novel device structures which utilize these materials. Four faculty members at N. C. State have been primarily involved and supported by this project. They are M. A. Littlejohn, J. R. Hauser and T. H. Glisson, presently Professors in the ECE Department, and Dr. K. W. Kim who joined the ECE faculty in August, 1988 and who has served as a PI on the effort since January, 1989. This research program has made significant contributions to the understanding and knowledge base of hot electron transport in materials and devices. It has provided scientific guidance to the U. S. Navy in the formulation of a part of its basic and applied research program. Numerical concepts developed under this project have been transferred to other Universities, including the University of Illinois, and we continue these inter-institutional collaborations. During the past year, two faculty members and two graduate students from NCSU spent extended time with Prof. K. Hess, Director of the National Center for Computational Electronics at the University of Illinois. Also, during the last year, collaborations with Dr. H. L. Grubin of Scientific Research Associates, Inc. and Dr. G. J. Iafrate of the U. S. Army Research Office in the area of quantum transport in semiconductor devices have been initiated. Also, our research results have helped stimulate commercial ventures, particularly in the development of GaInAsP-based materials and devices. To-date, this program has resulted in 57 referred publications in the literature, 3 additional manuscripts are currently in press, and 8 manuscripts have been submitted or are in preparation for submission to the technical literature. A listing of these publications is given in Appendix A. In addition, numerous invited talks and presentations have been given at conferences and workshops throughout the United States and in other countries. The program has contributed significantly to the educational program at N. C. State University with more than twenty-five Ph.D., M.S. and undergraduate students having received support

under this ONR contract. Currently, four Ph.D. students are working toward their degrees on this project. Two of these Ph.D. students are U.S. Citizens. A visiting scholar from China is also working on research related to this program.

This ONR program has been efficient and productive. The high quality of this research will continue to be maintained in the future. This report will summarize the progress and accomplishments made during the past twelve-month ONR reporting period.

2.0 RESEARCH RESULTS

2.1 Background

Since its inception, semiconductor technology has been stimulated by requirements for electronic systems with ever-increasing capabilities to process information faster, more functionally and more efficiently. These requirements have motivated the scaling down of integrated circuit (IC) device dimensions into the submicron (less than ten thousand angstroms) and ultrasubmicron (less than one thousand angstroms) regions. Today, we have entered an era where nanostructure physics and fabrication motivate our research efforts in semiconductor electronics [1]. As fabrication technology has allowed such devices to be realized, many new and fundamental questions have emerged concerning the underlying physics of small (atomic level) dimensions in semiconductor devices. Important issues now under consideration for ultrasubmicron devices include nonequilibrium transport dealing with such topics as quasi-ballistic transport, overshoot phenomena and quantum transport. A great deal of progress has been achieved in our understanding of these important device effects, although major work remains to be done as our ability to fabricate very small electronic device structures continues to expand and mature [2,3].

The ability to fabricate small devices has been continually refined over the last ten years through impressive improvements in materials growth technologies. Molecular beam epitaxy (MBE), metalorganic chemical vapor deposition (OMCVD), and atomic layer epitaxy (ALE) have provided the capability

to fabricate a wide variety of materials and heterostructure combinations with near perfect interfaces, doping control and compositional uniformity with atomic level dimensions. The development of ALE may very well prove to be the ultimate growth technology since it allows the deposition of one monolayer of device quality materials through a controllable, self-limiting mechanism, and is especially useful for the deposition of heterojunctions [4]. The ability to grow layers with dimensions of a few angstroms opens the domain of quantum transport to experimental study and verification. Thus, topics resulting from size quantization in condensed matter must be investigated from theoretical viewpoints with tools which are either partially developed or through the development of new tools which are not now available. Quantization effects arising from geometrical size constraints, proximity effects resulting from closely packed arrays of devices, and general solid-state considerations not heretofore considered questionable (effective mass approximation, the role of contacts and the like) must be addressed from a fundamental point of view. Moreover, from a device physics point-of-view, it is desirable to have a microscopic description of the physics of small dimensions which is amenable to phenomenological treatment, so that its properties can be meaningfully incorporated into futuristic device concepts and simulations.

Theoretical methods to address carrier transport have also progressed rapidly over the last ten-fifteen years, in a manner similar to research in semiconductor thin film epitaxial growth technology. In fact, this is a natural progression in many ways and is to be expected. The progress achieved in materials growth of structures with quantum dimensions dictates that new approaches be developed and refined to study quantum transport phenomena. However, a significant change in direction is now warranted. Past transport theory and device modeling approaches have relied on particle or quasi-particle approaches where the electrons are treated as rigid mobile entities which undergo interactions with the transport medium. The treatment of the interaction often involves wave concepts. However, the model is basically a particle model. In the current regime of quantum transport, we may no longer be able to consider the carriers as particles. It is quite likely that their physical behavior will be governed either partially or completely by wave phenomena.

The quasi-particle methods attempt to retain as much of the classical formalism as possible in order to be able to express results in terms of parameters which are of the greatest experimental interest, such as carrier velocity and diffusion constant. This is a flexible approach. However, much care is required to ensure that all important effects are properly included because of the approximations involved in the formulations. On the other hand, more fundamental quantum approaches, such as operator-eigenfunction methods, adhere closely to the actual quantum states present in the device structure when scattering is not included. Scattering processes (dissipation) can be added using perturbation theory from quantum mechanics. These techniques can obtain the greatest sensitivity to the resulting carrier confinement and the lattice potentials. However, they are relatively inflexible in studying non-linear dynamical properties in the presence of strong dissipation, such as is present in the electron-phonon interaction at high electric fields.

Another approach to quantum transport relies on the "integral over paths" method, originally proposed by Dirac and formulated by Feynman [5]. Path integral methods rely on an influence functional technique in which the source of the dissipation has been integrated over all phonon modes. This results in a model influence functional where the phonon-scattering dissipation can be represented as an interaction with a collection of harmonic oscillator modes in which the translational invariance of the carriers is preserved. The resulting model includes constant or oscillatory electric and magnetic fields, carrier screening, scattering and dissipation, carrier confinement, background temperature and initial conditions can be dealt with as readily as for a free particle [6].

The work at N. C. State University supported by the ONR has progressed over the past fifteen years from the realm of particle models to quasi-particle models to quantum transport models. We have relied primarily on the Monte Carlo method to study and solve transport problems in III-V compound semiconductors. Our techniques for modeling materials physics and device phenomena extend to device dimensions around one thousand angstroms [7-8], and we are confident in these models for predicting steady state and transient device effects down to these dimensions. However, in order to remain in the forefront of transport physics and device research, we must continue and increase our progress into the realm of

dimensions where physical effects can be studied in device regions with dimensions less than one thousand angstroms.

As one new direction for our research, we have chosen to pursue the path integral method. This is in contrast to other methods now being studied and supported by ONR, such as the application of the density matrix formalism and Wigner distribution function approaches including the use of moment equations [9]. We have made substantial progress in the path integral approach during the past four years and we believe that path integral methods will play an increasingly more significant role in developing an understanding of quantum transport in devices. Currently, we are aware of only one other U.S. university program directed toward applying the path integral method to semiconductor devices. This is the program at the University of Illinois under the direction of Prof. Karl Hess. Our program is very complimentary to the one at Illinois, and we are in fact collaborating with those personnel through the use of the NSF Supercomputing Center and the National Center for Computational Electronics there. One of our former students who recently finished his Ph.D. degree joined Prof Hess' group in January, 1990 and thus we expect this interaction to increase. We propose to spend a major effort collaborating with Prof. Hess' group in applying the path integral to specific device structures such as mesoscopic devices [10] during the next year, thereby further establishing its utility as a method for modeling quantum transport in devices. In addition, we will continue to explore the Monte Carlo transport method for study of novel device structures where theoretical underpinning is required. One particular class of devices which we will continue to study is based on hot electron injection across potential barriers (e.g. heterojunctions and planar-doped barriers) where the transport mechanisms which determine device behavior are poorly or incompletely understood. Of great importance here is the fact that these devices offer the potential to compare experiment and theory. Also, these devices can be used to aid in our understanding of quasi-ballistic transport [3]. For example, we have explored the concept that ballistic-like behavior can be predicted even when scattering effects are significant [11]. The type of scattering and the range of carrier energies are critical in this regime. Another novel class of structures which will also be studied in detail by the Monte Carlo method is based on the rapidly-emerging pseudomorphic or strained-layer devices. These

structures permit extended compositional ranges and, thus, have a number of potential advantages such as higher transconductance and channel carrier density. Recent studies on strain-induced piezoelectric fields have opened yet another possibility in realizing ultra-fast switching devices, resulting in an increased importance on the study of carrier transport in these devices. Other novel devices which are currently being analyzed include delta-doped field-effect transistors and quantum well structures, based on studies which have begun during the past year. Finally, we have initiated research which incorporates Monte Carlo methods into the quasi-particle approach based on moments of the Boltzmann transport equation with quantum mechanical corrections. Preliminary results show the utility of this approach for modeling microwave and millimeter wave devices which are important to the DoD's MMIC program.

We want to re-iterate the important interactions which have developed between our research group and other researchers during the last year. These interactions increase the impact of this program on the field of semiconductor device physics and allow our research efforts to be far more productive through increased intellectual efforts and enhanced facilities and resources. During the 1990 funding period, we have intensified our research collaborations with Prof. K. Hess at the University of Illinois, Dr. H. Grubin of Scientific Research Associates, and Drs. M. Stroscio and G. Iafrate of the U. S. Army Research Office. These research collaborations have resulted in several joint publications based on mutual research interests, expertise and capabilities. There have been several visits between these laboratories and the logistics for increased collaborations are excellent.

2.2 Summary of Research Results

2.2.1 Quantum Transport

This section will be divided into two parts. The first section will provide a summary of the current status of our work on the development of Path-Integral Monte Carlo (PIMC) methods for the study of the electronic properties of ultrasmall devices. The application of PIMC is based on the Feynman path-integral (FPI) formalism of quantum mechanics. The second section will provide a demonstration of PIMC methods in the calculation of carrier-phonon coupling effects. In particular, carrier self-energies

are calculated by PIMC techniques for a single-crystal semiconductor (GaAs) and for GaAs quantum wires as a function of wire size.

A. Summary of Path-Integral Monte Carlo (PIMC) Research For Ultra-Small Device Applications

A.1. Introduction

Proper treatment of scattering processes such as charge-carrier-phonon coupling is crucial for accurate modeling of the electronic properties of semiconductor devices. A powerful and conceptually appealing treatment of carrier-phonon coupling is provided by the Feynman Path-Integral (FPI) formalism of quantum mechanics [5,12]. The power of the FPI formalism in treating coupling processes was demonstrated first in quantum electrodynamics (QED) [13], but soon its advantages in the formally similar treatment of carrier-phonon coupling in bulk semiconductors also was realized [14]. Further, the reduction in device sizes to dimensions on the order of the thermal de Broglie wavelength of charge carriers offers few conceptual difficulties for the full quantum mechanical FPI formalism, while greatly reducing the value of the semiclassical treatment of carrier-phonon scattering as spatially localized, instantaneous events. However, the reduction of device dimensions does pose great practical problems to application of the FPI formalism. For analytical evaluation, both the device potentials and the net effects of coupling potentials must be modeled as either linear or quadratic in the carrier coordinates to make the calculations tractable. Thus, while a variational technique introduced by Feynman [14] has been used with great success to model carrier-phonon coupling in bulk semiconductors [15-20], extension of the FPI formalism, analytically, to the study of ultrasmall structures has been slowed, though not halted [21-23], by approximations required to model built-in device potentials.

The alternative to analytical evaluation of FPIs is, of course, numerical evaluation. In this section, the feasibility of numerical evaluation of FPIs in ultra-small device applications is considered. In Section A.2 the FPI formalism is reviewed briefly. In Section A.3 a practical path-integral Monte Carlo (PIMC) method for equilibrium calculations is described. In Section A.4, various basic nonequilibrium PIMC methods and their limitations are presented. Because, to the best of our knowledge, no nonequilibrium

PIMC method has proven widely applicable to ultrasmall device modeling, the goal in this latter section is to exhibit the fundamental problems yet to be overcome.

A.2. FPI Formalism

In quantum mechanics, the time evolution of a particle's wave function $\Psi(x,t)$ can be obtained from $\Psi(x_b, t_b) = \int_{-\infty}^{+\infty} K(x_b,t_b;x_a,t_a)\Psi(x_a,t_a)dx_a$ where $K(x_b,t_b;x_a,t_a)$ is the quantum mechanical propagator or Green's function. In the FPI formalism $K(x_b,t_b;x_a,t_a)$ is given by

$$K(x_b,t_b;x_a,t_a) = \int_{x_a}^{x_b} \exp\left\{ \frac{i}{\hbar} \int_{t_a}^{t_b} \left(\frac{1}{2}m\dot{x}^2(t) - V[x(t)]\right) dt \right\} Dx(t) \qquad (1)$$

where $\frac{1}{2}m\dot{x}^2(t)$ is the kinetic energy, $V[x(t)]$ is the potential energy and the "$\int_{x_a}^{x_b} \cdots Dx(t)$" is a notational convenience signifying an integral over all conceivable paths $x(t)$ from point x_a to point x_b [5,12]. To evaluate Eq. (1), the integral over paths, the "path-integral", must be subdivided; i.e., the paths must be broken down into, for example, straight line segments or Fourier components [5]. Also, by considering imaginary-time arguments in the propagator, it can be shown that the equilibrium density matrix subject to a Maxwell-Boltzmann distribution in energy at temperature T is given by

$$\rho(x_b,x_a;T) = \int_{x_a}^{x_b} \exp\left\{ -\frac{1}{\hbar} \int_{0}^{\hbar/k_BT} \left(\frac{1}{2}m\dot{x}^2 + V[x(t)]\right) dt \right\} Dx(t) \qquad (2)$$

where k_B is Boltzmann's constant [5]. For both equilibrium and nonequilibrium calculations, the net effects of coupling charge carriers to harmonic systems, e.g. phonons, can be incorporated exactly into path-dependent influence functionals inside the path-integrals [5]. Though this property is largely the motivating force for developing numerical FPI techniques for ultrasmall device applications, inclusion of influence functionals is not a primary obstacle to the development of these techniques and their consideration here would complicate the discussion needlessly.

A.3. Equilibrium (Imaginary-Time) PIMC

For numerical evaluation of FPIs, to achieve a reasonable degree of resolution in the path configurations, the number of path segments or Fourier components used to describe the paths, though finite, must be large. The resulting high dimensional (path) integral inherently is no amenable to evaluation by uniform sampling techniques and, thus, path-integral Monte Carlo (PIMC) methods must be used. Though there are a variety of methods for numerically evaluating imaginary-time FPIs [24], the method most amenable to ultrasmall device applications appears to be direct sampling [25,26]. Paths $x_n(t)$ are selected stochastically with a probability

$$p[x_n(t)] \propto \exp\left\{-\frac{1}{\hbar}\int_0^{\hbar/k_BT}\frac{1}{2}m\dot{x}_n^2(t)dt\right\}. \tag{3}$$

The equilibrium density matrix then is obtained from

$$\rho(x_b,x_a;T) = \rho_f(x_b,x_a;T)\frac{1}{N}\sum_{n=1}^{N}\exp\left\{-\frac{1}{\hbar}\int_0^{\hbar/k_BT} V[x_n(t)]\,dt\right\} \tag{4}$$

where $\rho_f(x_b,x_a;T)$ is the free-space density matrix and N is the total number of sample paths. Despite - or, more accurately, because of - the simplicity of this method, it has several properties that allow its practical application to modeling equilibrium charge carrier behavior in ultrasmall devices: (1) Either in terms of Fourier coefficients of using a sequential bisection technique [27], paths can be selected from Gaussian probability distributions with no unwanted correlation between successively-generated paths. (2) Paths can be stored and reused to model various potential structures and can be normalized readily with respect to temperature, and, thus, the generation of paths is in effect a start-up cost. (3) By reusing paths, small changes in the density matrix between similar potential structures can be evaluated accurately, including changes much smaller than the statistical fluctuations obtained in evaluation of each structure independently. (4) Energy values can be obtained directly from the probability density normalization constants. (5) Because it is a Monte Carlo technique, little additional cost is incurred in treating potentials that vary

in multiple dimensions, e.g. the charge-carrier-phonon coupling potential. With this equilibrium PIMC method, for example, energy level splittings in coupled quantum well systems of a few percentage points of the nominal value can be accurately resolved in about an hour on a VAXstation 3200 [26]. Though such calculations can be performed more readily using other, non-PIMC techniques, these latter techniques are not as amenable to physically accurate treatment of charge-carrier-phonon coupling processes in ultrasmall devices. With PIMC, however, it should be a straightforward procedure to introduce these coupling processes into future calculations.

A.4. Nonequilibrium (Real-Time) PIMC

Though nonequilibrium and equilibrium FPI calculations pose similar analytical computational problems, nonequilibrium PIMC calculations pose far more severe numerical problems than do equilibrium PIMC calculations. For nonequilibrium calculations, because the argument of the exponential in Eq. (1) is purely imaginary, these is no inherent normalizable probability distribution from which paths can be chosen stochastically. A variety of methods have been tried to overcome this fundamental problem. The most direct is to impose a decaying probability distribution for selecting paths away from classical paths, and then increase the spread in the distribution function until the solution converges [28]. Another functionally related method is suggested by rewriting Eq. (1) in the equivalent form,

$$K(x_b,t_b;x_a,t_a) = \int_{x_a}^{x_b}\int_{x_a}^{x_b} w[x'(t)-x(t)]\exp\left\{\frac{i}{\hbar}\int_{t_a}^{t_b}\left(\frac{1}{2}mx'^2(t)-V[x'(t)]\right)dt\right\}D_x'(t)Dx(t), \qquad (5)$$

where $w[x'(t)-x(t)]$ is a normalized window in $x'(t)$ about $x(t)$ [29,30]. The window is taken small enough that the potential function may be approximated either linearly or quadratically within the window. Therefore, the path-integral over $x'(t)$ can be performed analytically. The result of the first integral is a function of $x(t)$ that, not coincidentally, decays away from classical paths providing a normalizable probability distribution for selecting paths. Therefore, the second integral can be performed using PIMC techniques. With both of these methods the absolute value of the contribution for each sample path, an

exponential in a purely imaginary argument, is independent of the resolution in the path configurations, i.e. of the number of path segments or Fourier terms per path. However, also with both methods, the average value of these contributions decreases geometrically with linear increases in the resolution in the path configurations. Consequently, the required number of Monte Carlo samples increases geometrically with linear increases in path resolution, limiting these methods to short time transient applications. A fundamentally different approach is provided by viewing real-time FPIs as the analytic continuation of, for example but not restricted to, imaginary-time FPIs. For one such method [31,32], first, values of a FPI along the negative imaginary-time axis, where the FPI takes the form of Eq. (2) but with $\hbar/k_BT$ replaced by the magnitude of the imaginary-time period, are found using equilibrium PIMC methods. Next, some type of curve fit to the imaginary-time solutions is performed. Last, an analytic continuation back to the real-time axis is made for the curve fit. However, this approach has been limited by instabilities that arize during the analytic continuation of the curve fit, though not necessarily from the curve fit as evidenced by the next method. The next and final nonequilibrium PIMC method presented, another analytic continuation method but one that requires no curve fit, is analogous to and can be derived from the direct sampling equilibrium PIMC method described in Section A.3. Path variations $x'_n(t)$ from the constant velocity path $x_o(t)$ from x_a to x_b are chosen with a probability

$$p[x'_n(t)] \propto \exp\left\{-\frac{1}{\hbar}\int_{t_a}^{t_b}\frac{1}{2}m\dot{x}'^2_n(t)dt\right\}. \tag{6}$$

The real-time FPI then is obtained from

$$K(x_b,t_b;x_a,t_a) = K_f(x_b,t_b;x_a,t_a)\frac{1}{N}\sum_{n=1}^{N}\exp\left\{-\frac{1}{\hbar}\int_{t_a}^{t_b}V[x_o(t)+x'_n(t)e^{i\pi/2}]dt\right\} \tag{7}$$

where $K_f(x_b,t_b;x_a,t_a)$ is the free-space propagator [33,34]. Here, analytic continuations are performed for each sample before summation. Beyond returning the time argument to the real-time axis, the effect of the analytic continuations is to displace the previously selected path variations into complex position

space where, presumably, the analytic continuation of V(x) is known. The value of the real-time FPI, in theory, then can be found by summing the results of the individual analytic continuations. Unfortunately, for potential functions that are analytic everywhere in the complex plane, as the size of the path variations $x'_n(t)$ increases, the magnitudes of $\exp\left\{-\frac{1}{\hbar}\int_0^{\hbar/k_BT} V[x_o(t)+x'_n(t)e^{i\pi/2}]dt\right\}$ tend to increase much faster than the probabilities for selecting the path variations decrease. Therefore, excluding linear and some quadratic potentials - for which analytic solutions exist already - and near diagonal elements of the propagator for certain barrier potentials for short time periods, the summation of Eq. (7) does not converge absolutely - and possibly not at all. Thus, again the numerical solutions are unstable. An interesting alternative would be to use potentials functions that are analytic and bounded everywhere in the complex plane except at isolated poles; however, it is not clear what theoretical and practical effects the resulting introduction of essential singularities into the calculations would have.

A.5. Conclusion

With existing methods, PIMC offers a practical approach to modeling the equilibrium electronic properties of ultrasmall devices, an approach that should provide physically accurate treatments of carrier-phonon coupling processes in the future. In contrast fundamental computational problems so far limit existing nonequilibrium PIMC methods to short-period transient-time applications. While future increases in computer power should allow transient-time applications of somewhat longer time periods with existing methods, it appears that new PIMC methods must be found to fully overcome these problems and allow modeling of long-period transient-time and steady-state nonequilibrium behavior. However, the great advantages that would be offered by a practical, widely applicable nonequilibrium PIMC method, for modeling charge-carrier transport in ultrasmall devices as well as in other areas of research, motivate a continued search.

B. Self-Energy Calculations: An Example of the Application of PIMC Methods

As a demonstration of the use of the PIMC method to calculate carrier-phonon coupling effects, in this section carrier self-energies are calculated for free-space (single crystal) as a function of temperature, and for "quantum wires" as a function of wire size at 77.3K and 300K. After Degani and Hipolito [34], the self energy Σ at finite temperatures is defined by

$$\Sigma = \langle E \rangle - \langle E_o \rangle \tag{8}$$

where $\langle E \rangle$ and $\langle E_o \rangle$ are the polaron and uncoupled carrier expected energies as defined by

$$\langle E \rangle = \frac{d}{d(\frac{1}{k_B T})} (\frac{F}{k_B T}) \tag{9}$$

where F is the free energy of the system [5], k_B is Boltzmann's constant, and T is the absolute temperature. The values of $\langle E \rangle$ and $\langle E_o \rangle$ are calculated from Eq. (9) using Metropolis importance sampling and a finite difference approximation [26].

Figure 1 shows the PIMC calculated free-space self-energies of electrons in GaAs as a function of temperature from 10K to 1000K. The solid curve is for only one path set, but the error bars at 77.3 and 300K show the small (0.12% and 0.24% respectively) RMS deviation based on 10 path sets at these points. Because there was no varying potential energy function to consider, the cpu time required for each such calculation beyond that required to calculate the influence functionals was negligible. The dashed curve at low temperatures $k_B T \ll \hbar\omega$, shows results based on the variational method calculations of finite temperature free-energies of Saitoh [36]. The calculations appear to converge at very low temperature, but the PIMC results demonstrate a somewhat more rapid falloff in self-energy with increasing temperature that the variational results, though in either case the falloff is extremely slow. The qualitative structure of this self-energy vs. temperature curve has been exhibited previously by Degani and Hipolito [35] using a variational FPI method; however, quantitative comparison is not possible because their results were given for quantum wire structures, to be considered below.

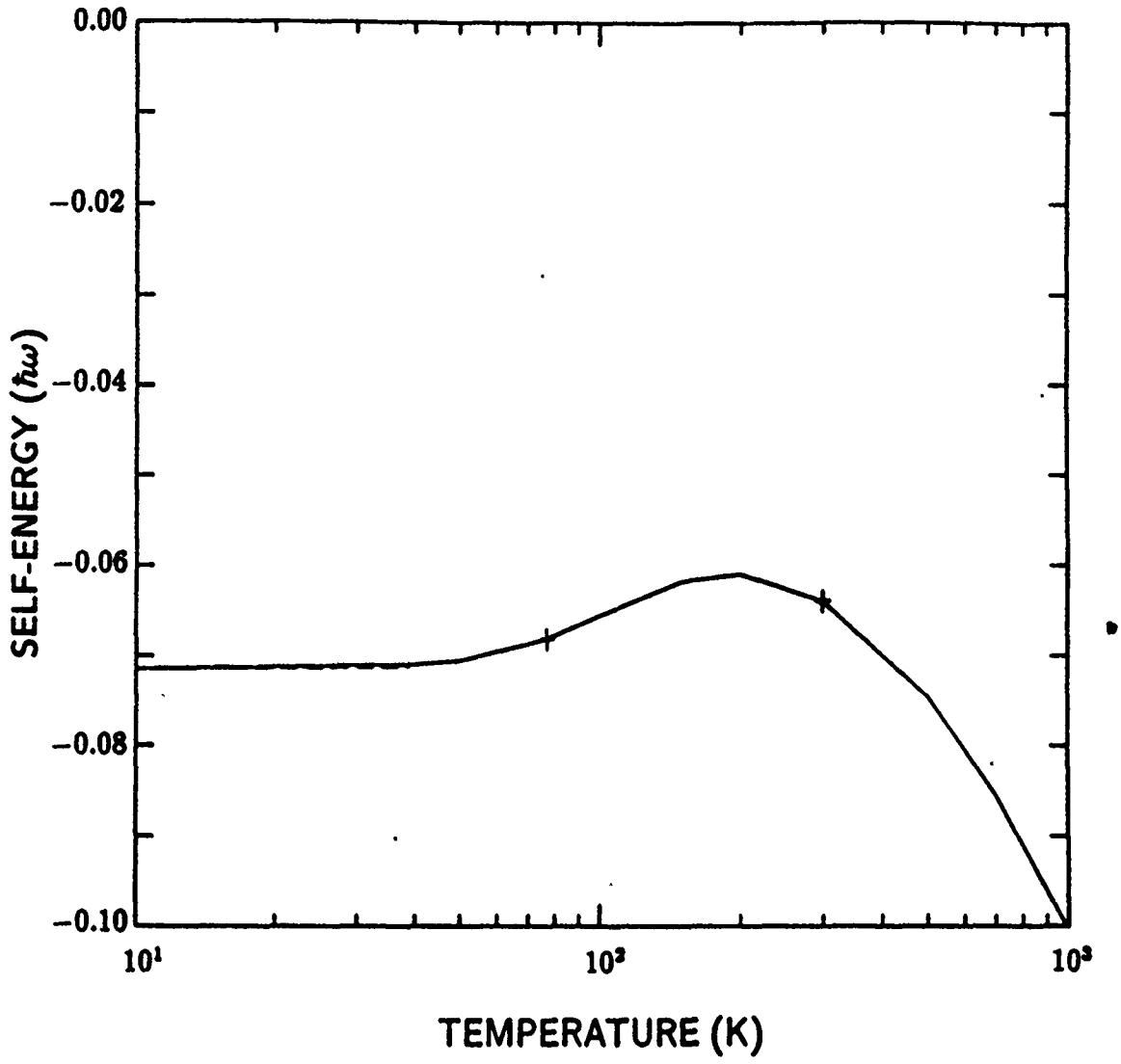

Figure 1. Electron free-space self energies as a function of temperature. The solid line represents PIMC results for a set of 1000 paths. The dashed line represents results based on the variational calculations of low-temperature free-energy by Saitoh [36].

Figure 2a and 2b display the means and RMS deviations in PIMC calculated self-energies of square quantum wire structures (carrier confinement in two dimensions) of widths varying from 0Å and 200Å. The quantum well depth was taken to be 0.2158eV. Each such calculation, a combination of two separate free-energy calculations, required approximately two hours of cpu time on the VAXstation 3200 at 77.3K and one-half hour at 300K. For reference, the isolated closed circles in Figs. 5.2a and 5.2b are OK, infinite well depth results obtained analytically by Degani and Hipolito [37] using a variational non-FPI method. The large RMS deviations in the PIMC results at 77.3 for the midrange of well widths is the result a large majority contribution to the probability density from a small minority of the stochastically sampled paths. However, again, the RMS deviations shown here are for sets of only 1,000 paths each and can be reduced readily by increasing the number of paths used; the root of the expected mean-square deviation of the man found here for all ten path sets from the true mean is one-third that shown. At first for both temperatures, judged by the means, the PIMC obtained self-energies increase as the well width decreases and the electrons become more localized. However, as the well narrows further, the self-energies begin to decrease again, the result of reduced electron confinement as the electron energy levels are forced up and out of the well. The 0Å limit is just the free-space condition again as the quantum well vanishes. This ultimate decrease in self-energy with well width, of course, is not obtained under an infinite well depth approximation for which carrier confinement to the well is complete regardless of the wire dimensions [35,37]. As can be seen, judged by the means and allowing for the 0.0034 $\hbar\omega$ and 0.0075 $\hbar\omega$ free-space energy shifts from 0K to 77.3K and 300K, respectively, exhibited in Fig. 1, the isolated 0K non-FPI-method results of Degani and Hipolito agree well with the PIMC results obtained here. However, the agreement of their variational FPI-method results mentioned above to both the PIMC results and their own non-FPI results is poor. In particular, inexplicably, at a width of 100Å their FPI-method results at both 0K and 77.3K exhibited no significant confinement effects on the electron self-energies, in marked contrast to both the PIMC results and their own non-FPI-method results. This lack of agreement, perhaps, can be considered a testament to the difficulties involved in applying the FPI formalism analytically in ultrasmall devices structures.

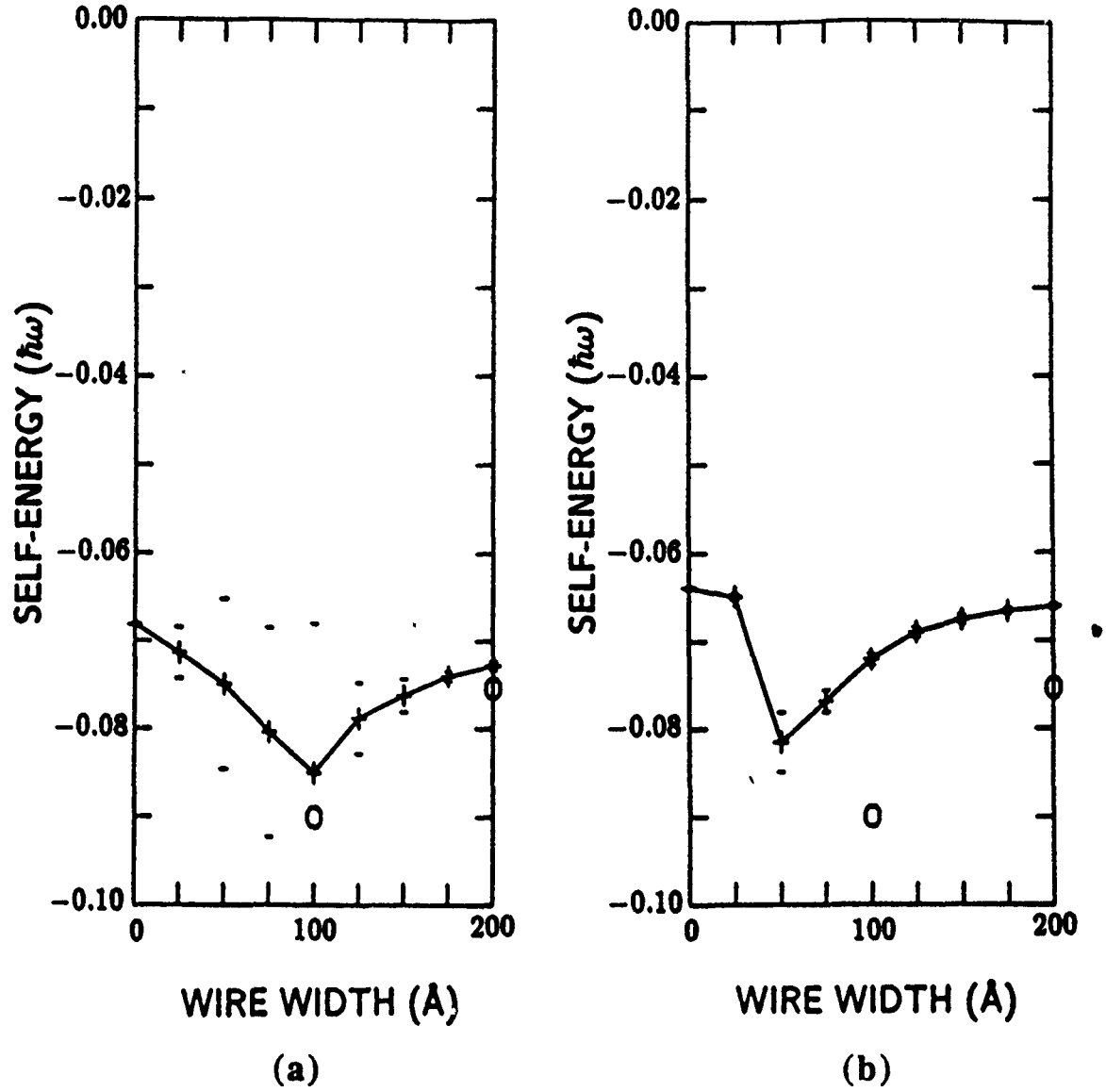

Figure 2. Mean and RMS deviations of PIMC calculated self-energies in square quantum wires as a function of width at (a) 77K and (b) 300K, with isolated analytically-obtained results at 0K (open circles) after Degani and Hipolito [35].

2.2.2 Monte Carlo Study of Ballistic and Quasi-Ballistic Transport in Semiconductors

This section summarizes our research which deals with electron transport across potential barriers. We have studied two particular types of barriers, which are the planar-doped barrier and the abrupt heterojunction barrier. While much of the following discussion focuses on the planar-doped barrier, the results are more generic and seem to apply to potential barriers in general, at least where the potential changes (variations) occur over distances smaller than the electron mean free path at the total barrier energy. The general nature and applicability of the physical effects and resultant physical models merit further investigation.

The distribution function experiences fundamental changes when an ensemble of carriers passes through an abrupt potential barrier. By imposing continuity of total particle energy and the parallel component of wave vector, there are two important consequences on the velocity distribution function. First, the normal component of the velocity vector is shifted to high positive values by an amount equal to the ballistic velocity; that is, the velocity gained by a particle accelerated without collisions through a potential energy equal to the barrier height. Secondly, the width of the distribution is reduced by the nonparabolicity of the energy bands and by the reduction of the effective mass in crossing the barrier (provided this is the case). This effect is substantial, producing an extreme non-equilibrium distribution function with excess energy (for barrier heights well above the thermal energy) and a large forward component of momentum. This situation is much the same for realistic barriers. For abrupt heterojunctions with interfacial space charge layers, the injected velocity distribution function is essentially indistinguishable from an ideal abrupt barrier. For planar-doped barriers, where carrier injection occurs over a finite high field region a few hundred angstroms thick, the velocity distribution function differs only slightly from an ideal abrupt barrier. In this case, there is a "tail" in the velocity distribution which decreases toward zero from the ballistic velocity. Thus, the planar-doped (or delta-doped) barrier is not quite as effective in transferring the barrier energy to the ensemble due to scattering events in the high field region. However, the basic nature of the velocity distribution function remains phenomenologically similar to that for an ideal abrupt barrier.

The particle motion away from these barriers is not controlled by normal diffusive processes with diffusion velocities of around 5 x 10^6 cm/sec. The extreme non-equilibrium transport allows for more than an order of magnitude increase in the ensemble average velocity (~10^8 cm/sec) over short distances while the non-equilibrium populations are reduced to related (or thermal) distributions through isotropic scattering events which tend to randomize the distribution of particle velocities. The transport of the ensemble during this transition period is very important to high-speed device behavior. However, it is very difficult phenomena to incorporate in device simulation and models.

In 1985, two groups reported experimental evidence for hot electron transport in barrier injection devices [38,39]. These and later results established the existence of a peak in the electron energy distribution function at the barrier injection energy [40,41]. This peak, observable a significant distance from the barrier, was attributed to ballistic transport in both homojunction planar-doped barriers and heterojunction barriers.

Recently, Hess and Iafrate explored these results in an effort to elucidate further the processes of ballistic transport and velocity overshoot [42]. They developed definitions for these terms, classified the basic experimental results, and concluded that, while the basic physics of ballistic transport is well understood qualitatively, much quantitative work remains to be done, especially with respect to device applications.

The purpose of this study is to investigate transport in the base region of GaAs planar-doped barriers used as ballistic launchers. Our results expand the definitions of Hess and Iafrate and further classify electronics in the velocity distribution function as to their role in ballistic and quasi-ballistic transport in semiconductors.

The basic structure of a planar-doped barrier has been discussed at length in the literature [38-43]. Ideally, the device has a triangular potential barrier represented by two regions of constant electric field strength. A plan-doped barrier transistor (PDBT) is formed by constructing two such barriers separated by a base region with zero electric field strength. From Monte Carlo simulations, the electron velocity

distribution function at the top of the barrier has been found to be a Maxwellian distribution with essentially no negative velocity electrons [43]. This distribution is also that found in the abrupt emitter of heterojunction bipolar transistors (HBTs) [44]. this is an ensemble effect in both devices since, once an electron is transported over the barrier, the probability for back-scattering is very small [42-44]. These conditions correspond to those originally described by Bethe for thermionic current in Schottky diodes [8], and have been verified carefully for HBTs using Monte Carlo simulations [44]. Thus we concluded that the emitter current of a PDBT, as well as an HBT, is primarily a thermionic current.

The velocity distribution function at the edge of the base region consists of two components. First, there is a very narrow peak centered at a high velocity. This velocity equals the theoretical free-flight velocity calculated for an electron accelerated in a non-parabolic band gaining kinetic energy equal to the barrier height (field time distance). Also, there is a small tail in the distribution function extending from zero velocity, increasing with velocity and merging with the narrow peak. This is very similar to the case for an HBT [44], although the presence of the tail shows that the planar-doped barrier is not as effective s the abrupt emitter barrier of an HBT in orienting the electron velocity in the transport direction.

As the electrons are transported from the emitter into the base, there is a change in the velocity distribution function. This effect is shown in Figure 3 where two dominant features can be seen. The first is the peak discussed above centered at the free-flight velocity. This narrow peak remains for a substantial distance into the base beyond the mean free path length. However, the emergence of a very broad peak centered at a low velocity can be seen also. Thus, there is a redistribution of the electrons from the narrow peak to the broad peak, suggesting that some electrons have been transported far into the base with either no interactions or else interactions with small deviation angle and energy loss. Other electrons have experienced isotropic, velocity-randomizing interactions leading to a velocity-relaxed population that contributes to a highly diffusive current (Maxwellian distribution). Again, the same phenomena occurs in an HBT [44]. Thus, it appears that electrons in the base of a PDBT (and an HBT) can be divided into three generic populations, ballistic, quasi-ballistic and velocity-relaxed. This classification is consistent with the definition for nearly-ballistic transport given by Hess and Iafrate [42].

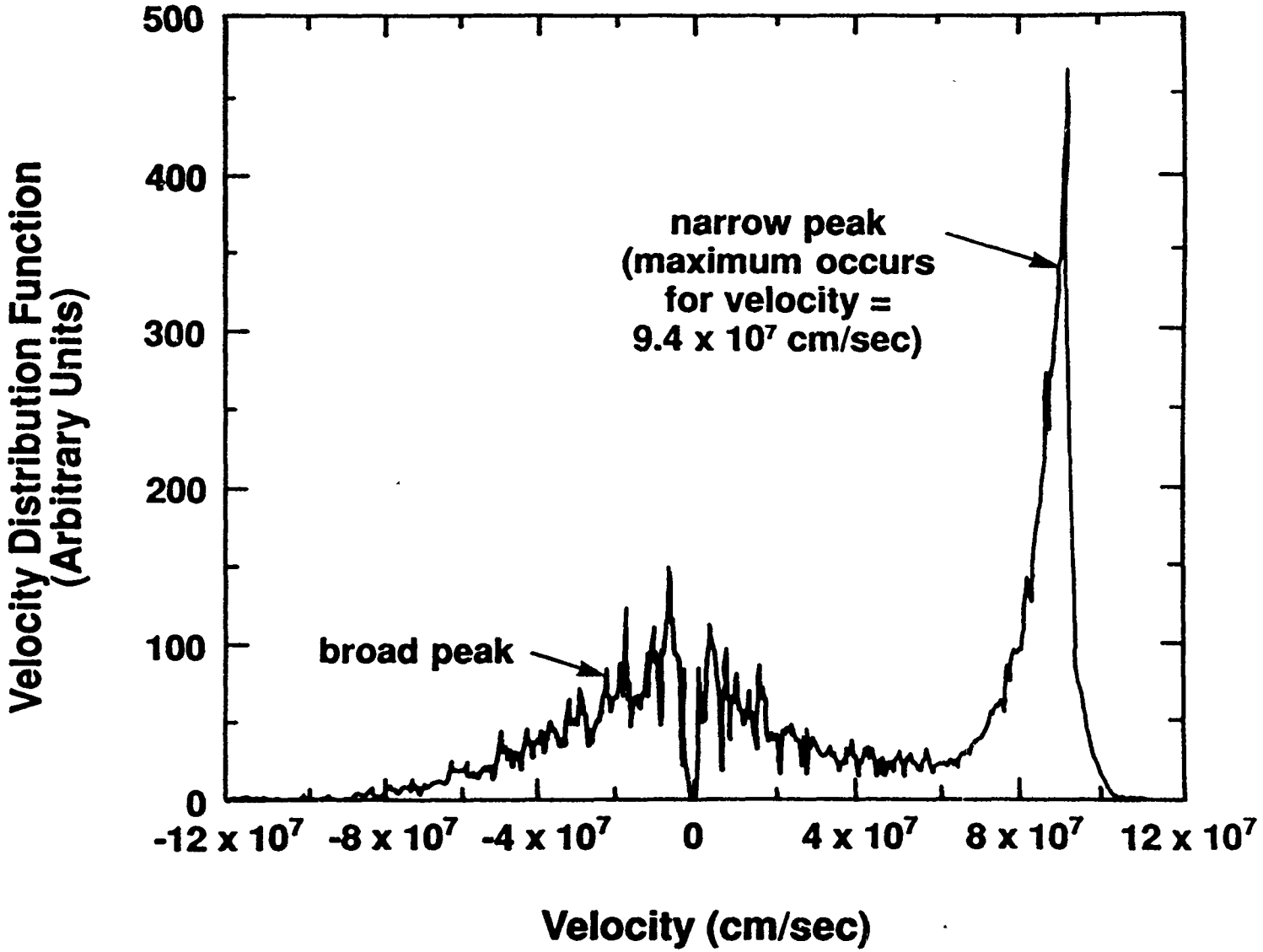

Figure 3. Velocity distribution function in the base of a PDBT at a distance of 50 nm from a 0.225 eV barrier. The narrow peak centered at the free flight velocity was the singular velocity distribution at the edge of the barrier; the broad peak was not present.

In order to investigate the proposition that the total electron distribution can be divided into three populations, we have performed Monte Carlo simulations using the following three definitions.

i) An electron is in the ballistic population until it experiences one interactions.

ii) An electron is in the quasi-ballistic population if it experiences very few ($\leq$N) anisotropic interactions. As anisotropic interaction is defined as an interaction in which the angle between the initial and final electron velocity following an interaction is less than a threshold angle, Θ_a. Here, Θ_a and N will be determined empirically from the Monte Carlo simulations.

iii) An electron is in the velocity-relaxed population if it experiences one or more isotropic interactions $\Theta > \Theta_a$, or more than N anisotropic interactions.

Monte Carlo simulations with several values of Θ_a and N were performed and the velocity distribution functions of the ballistic (f_o), quasi-ballistic (f_1 to f_N) and velocity-relaxed populations (f_T) were computed 50nm into the base region from a 0.225eV barrier. The purpose of the simulations was to identify Θ_a and N such that the narrow peak in the total velocity distribution mainly is due to the ballistic and quasi-ballistic populations, and the broad peak is due to the velocity-relaxed population. Figure 4 shows the results of these simulations. In this figure, we plot the area under the function $[f_t - (f_o + \ldots + f_N)]$ versus N for different values of Θ_a, where f_t is the total distribution. Also shown is the area under a Gaussian function fitted to the broad peak in the total velocity distribution. From these curves, and from many other simulations, we conclude that reasonable empirical values are N = 3 and $\Theta_a = 70°$. The results of these simulations support the concept that it is possible to deconvolve the two peaks of the velocity distribution function using the simple criteria described above, and that the narrow peak is indeed due to ballistic and quasi-ballistic electrons while the broad Gaussian peak is due to velocity-relaxed electrons. It is interesting to note that similar simulations of HBTs have shown that the contributions to the base current from the ballistic and quasi-ballistic populations are negligible for i > 3 [44]. This lends further support to the generic definitions for the ballistic and quasi-ballistic populations in ballistic launcher structures,

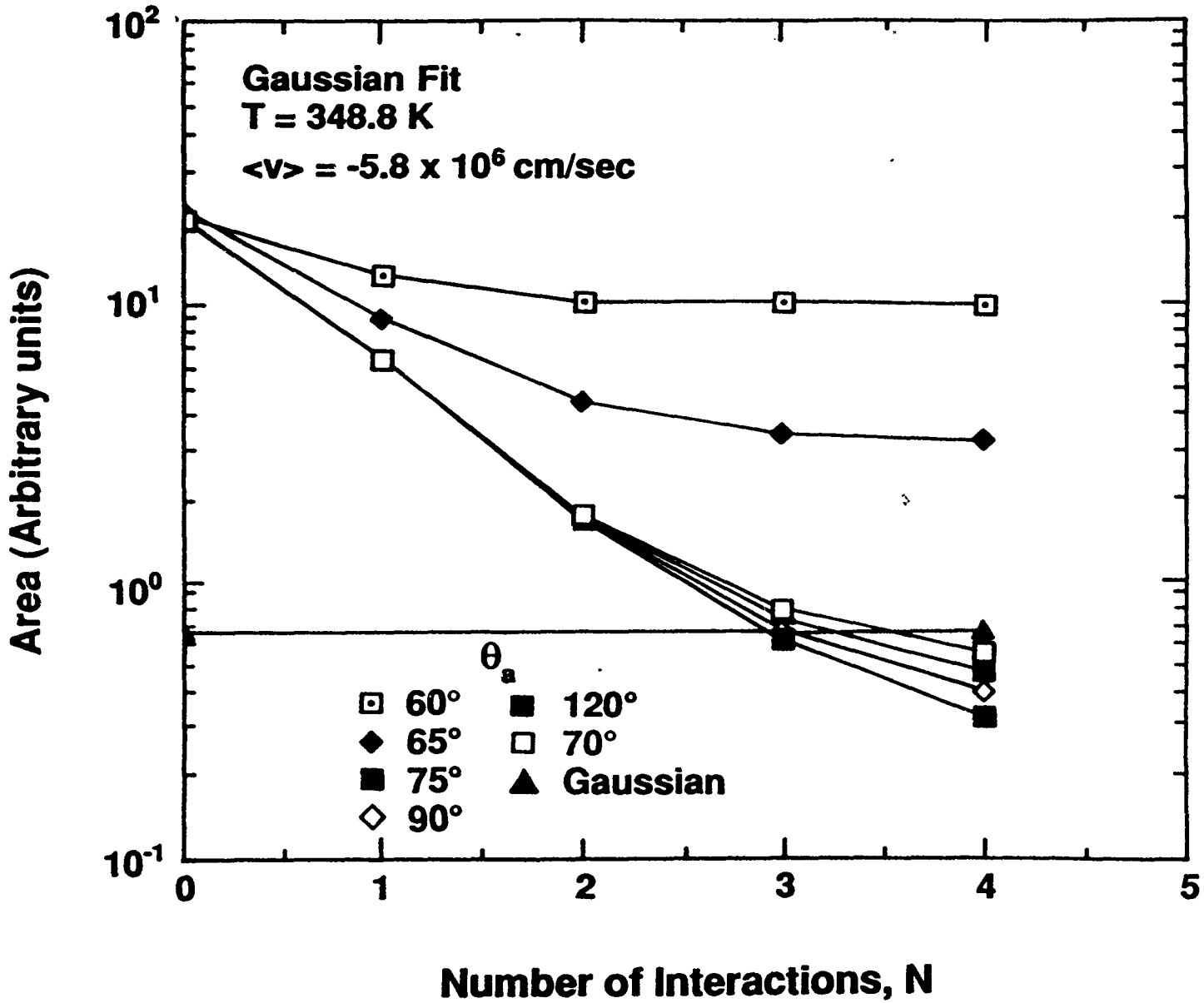

Figure 4. Area under the velocity distribution function $[f_t - (f_0+f_1+...+f_N)]$ as a function of N with Θ_a as a parameter. Here, f_t is the total distribution function and f_i, i=0,...,N are the ballistic and quasi-ballistic distribution functions.

and extends the definitions of Hess and Iafrate [42].

An analytical model, based on the definitions for ballistic, quasi-ballistic and velocity-relaxed populations, has been developed in order to obtain quantitatively the spatial variation of the various physical variables. The model is based on the decay of the electron flux, $\Phi_i(x)$, of the ith ballistic or quasi-ballistic population due to interactions in the base region. By developing a difference equation of Φ_i, we can describe the exchange of flux within the ballistic and quasi-ballistic populations for each differential region of the velocity distribution. The resulting recursive differential equation is

$$\frac{d\Phi_i(z,v_i)}{dz} = -\frac{\lambda_t}{v_i}\Phi_i(z,v_i) + \frac{\lambda_{an}}{v_{i-1}}\Phi_{i-1}(z,v_{i-1}) \tag{10}$$

where λ_t is the total scattering rate λ_{an} is the anisotropic scattering rate and v_i is the electron velocity of the ith population. The equation for each value of i can be solved analytically if λ_t and λ_{an} are assumed to be constant. This assumption is valid for the energy range considered here. Thus, if we know the value fo the flux of ballistic electrons z = 0, Φ_o $(0,v_o)$, we can solve for $\Phi_i(z,v_i)$ for i = 1 to 3. We obtain $\Phi_o(0,v_o)$ from the expression for the velocity distribution function at the edge of the base [9]. Thus, we can construct the velocity distribution functions, $f_i(z)$, of the i = 0 to 3 populations for all values of z in the base. The electron density, $n_i(z)$, average velocity, $v_i(z)$, and current density, $J_i(z)$, of the i = 0 to 3 populations are calculated from the velocity distribution functions. The total ballistic and quasi-ballistic current density, $J_{qb}(z)$, is then given by

$$J_{qb}(z) = \sum_{i=0}^{\infty} J_i(z) = \sum_{i=0}^{3} J_i(z) \tag{11}$$

Since the velocity distribution function of the velocity-relaxed electrons is Gaussian, the drift-diffusion formalism can be used to calculate the population density, $n_r(z)$, of these electrons. This analysis results in the following equations:

$$J_r(z) = qD_n \frac{dn_r(z)}{dz} + q\mu_n E n_r(z). \tag{12}$$

Monte Carlo simulations were carried out to validate this model. Electrons were injected from the top of the emitter barrier with initial momenta selected from a semi-Gaussian function (only positive z-directed momenta). An ideal collecting plane was assumed at the end of the base region. Figure 5 shows the close agreement obtained between the model and Monte Carlo simulations for $n_i(z)$,$J_i(z)$ and $n_r(z)$. The values of the total scattering rate, λ_t, and the anisotropic scattering rate, λ_{an}, obtained from these curve fits were .138 x 10^{13}/sec and 1.2 x 10^{13}/sec, respectively. A comparison of these values with the total scattering rate (~ 1.2 x 10^{13}/sec) used in the Monte Carlo simulations show that polar optical scattering is indeed the primary anisotropic scattering process in the range of energies considered here (less than ~ 0.3 eV), and that the model can be used for any material once the total and anisotropic scattering rates are identified for the particular study. Figure 6 demonstrates the results of applying such a model to a GaAs planar doped barrier with a 0.225 eV barrier height. This figure shows that the current flow is dominated by the quasi-ballistic transport for distances much greater than the electron mean free path before the traditional drift-diffusion current begins to dominant. This same effect is observed from Monte Carlo simulations of heterojunctions bipolar transistors [44]. In general, there is excellent agreement between the model and Monte Carlo simulations.

In summary, we have classified electron transport in the base of a planar-doped barrier transistor in terms of ballistic, quasi-ballistic and velocity-relaxed populations. Simle criteria have been developed to define these populations in terms of the degree of anisotropy of the scattering and the number of anisotropic interactions that an electron experiences during transport. Empirically, an interaction is classified as anisotropic if the electron velocity deviates less than 70° due to the interaction. Also, the maximum number of anisotropic interactions which an electron can experience and remain in the quasi-ballistic population is empirically determined to be equal to three. These definitions allow the construction of a simple analytical model which describes the spatial variation of the ballistic and quasi-ballistic current in the base region. This model agrees well with Monte Carlo simulations. Despite its simplicity, the success of this model in describing the decay of ballistic and quasi-ballistic populations makes it useful in device modeling that does not require intensive computer resources. At this stage, the model does not

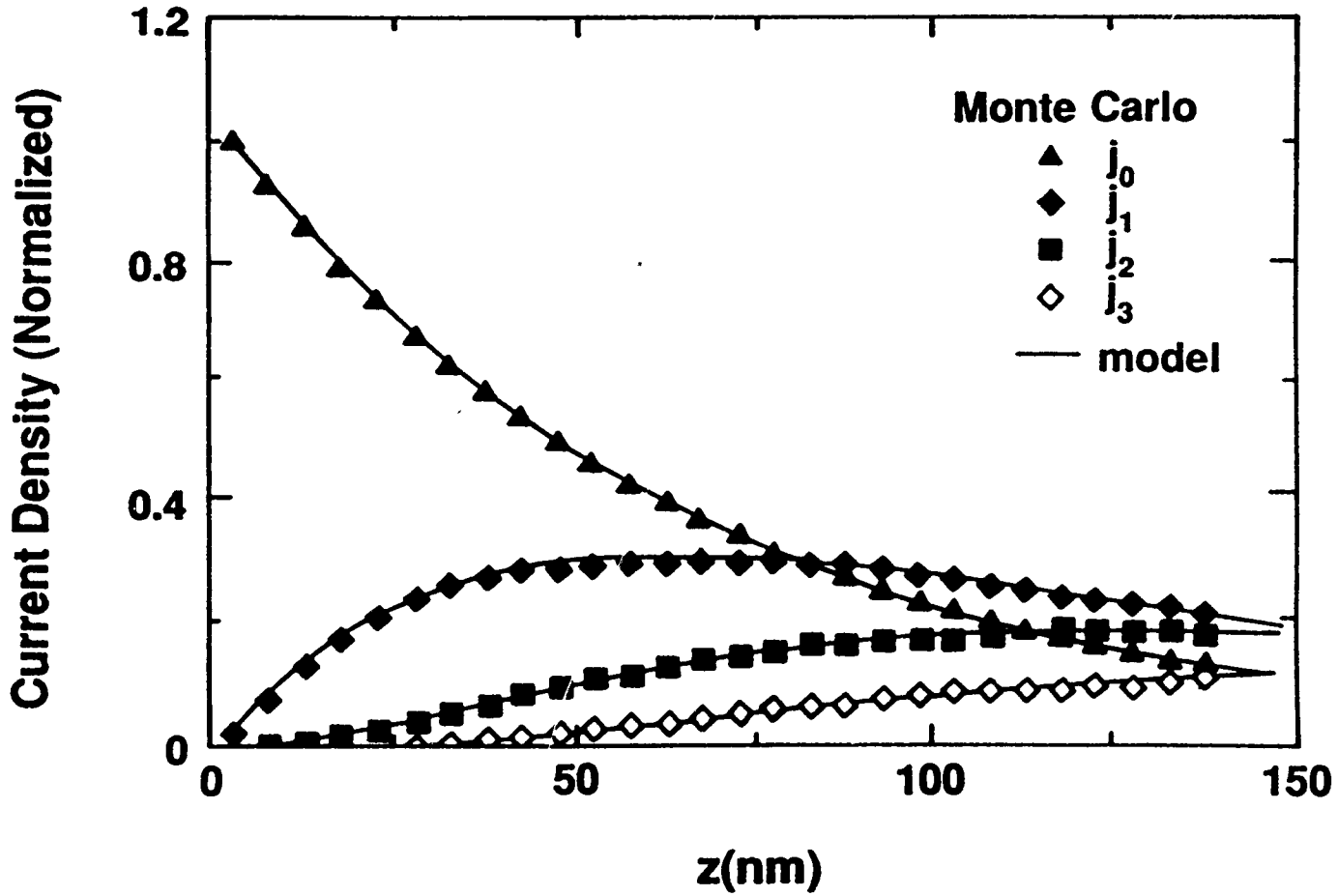

Figure 5a. Comparison of analytical model with Monte Carlo simulations of ballistic (j_0) and quasi-ballistic current densities versus distance into the base of a PDBT.

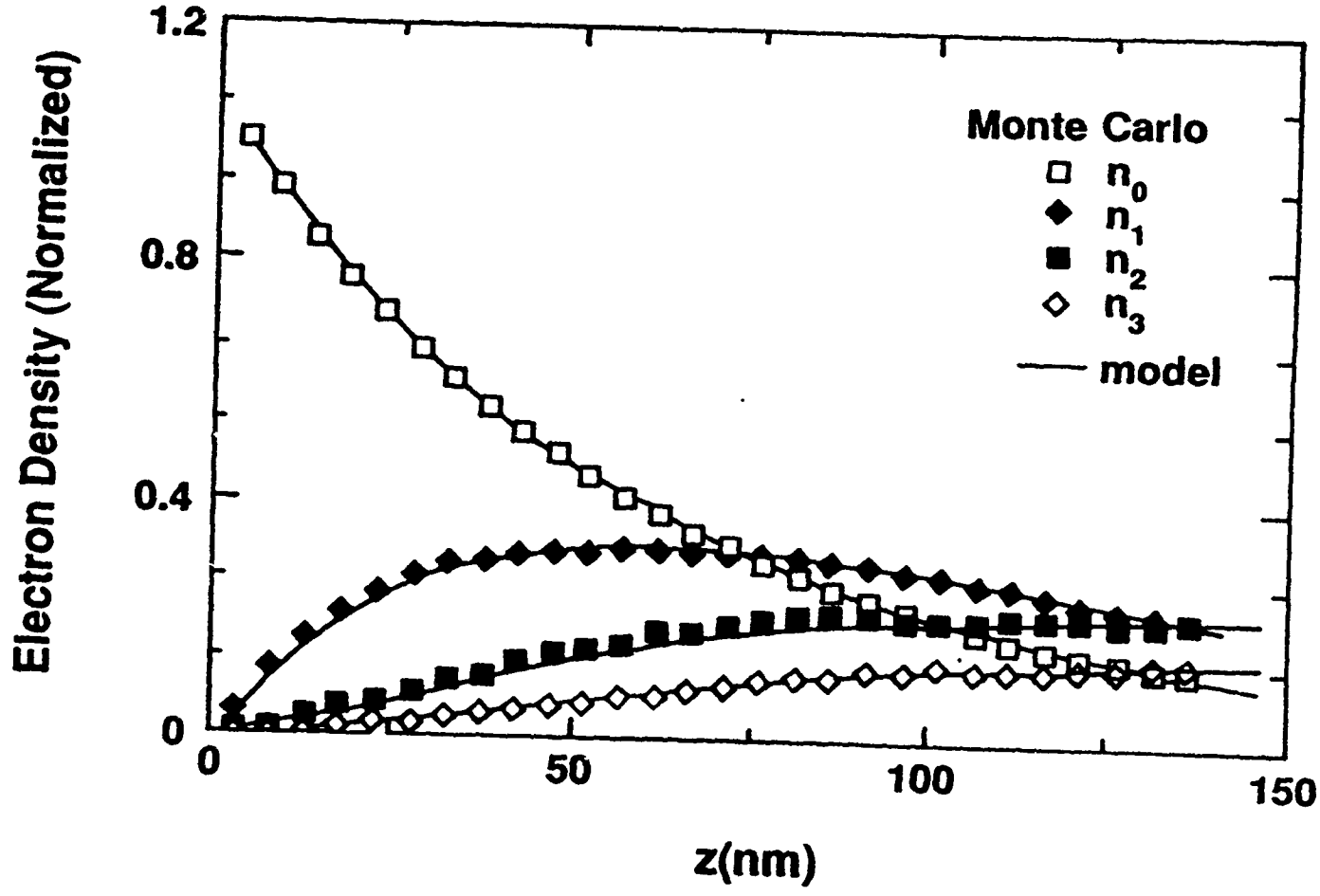

Figure 5b. Comparison of analytical model with Monte Carlo simulations of the ballistic (n_0) and quasi-ballistic electron densities versus distance into the base of a PDBT.

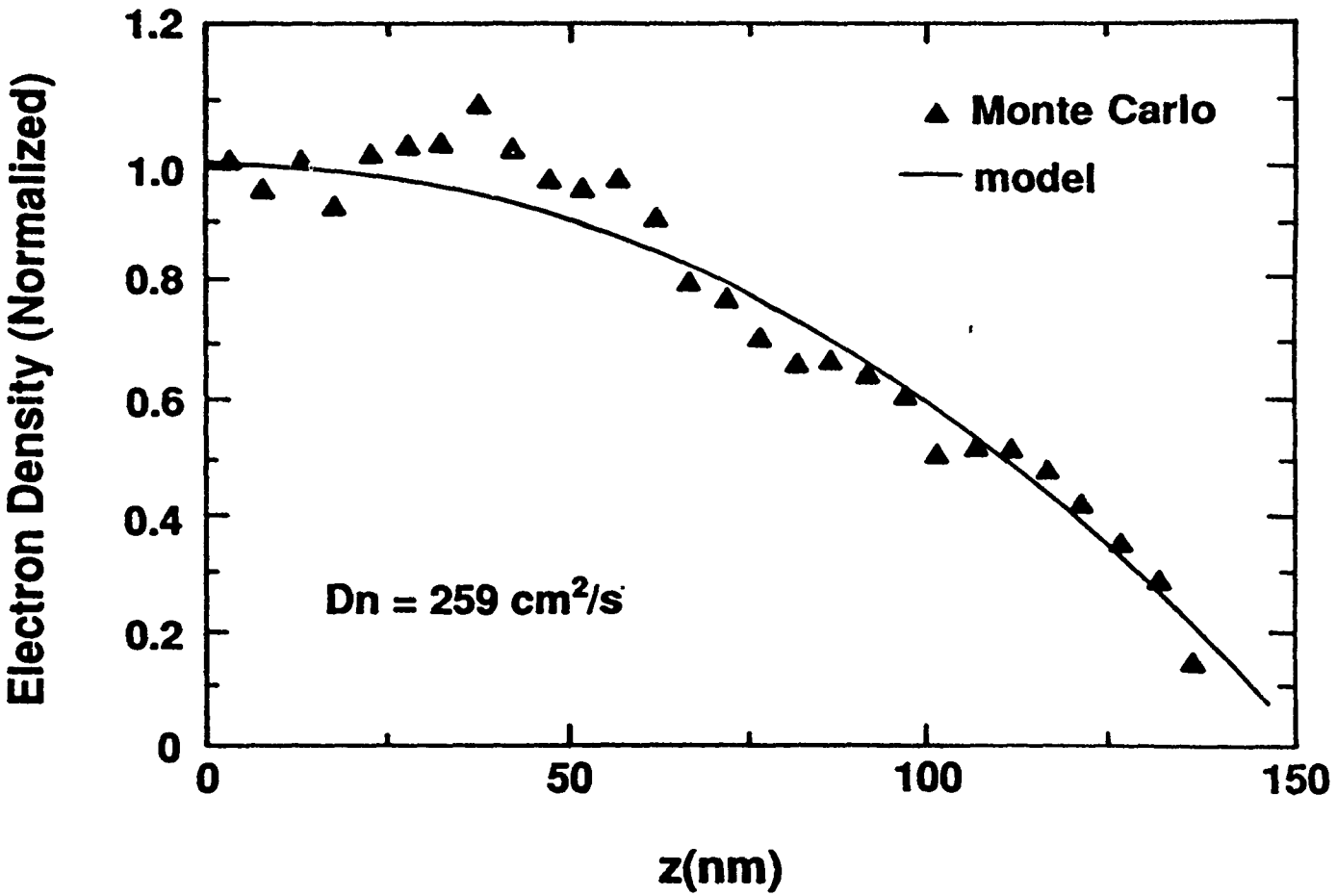

Figure 5c. Comparison of analytical model with Monte Carlo simulations of velocity-relaxed electron density versus distance into the base of a PDBT. The fitted value of D_n results in an electron mobility in the base of 8600 cm^2/vsec.

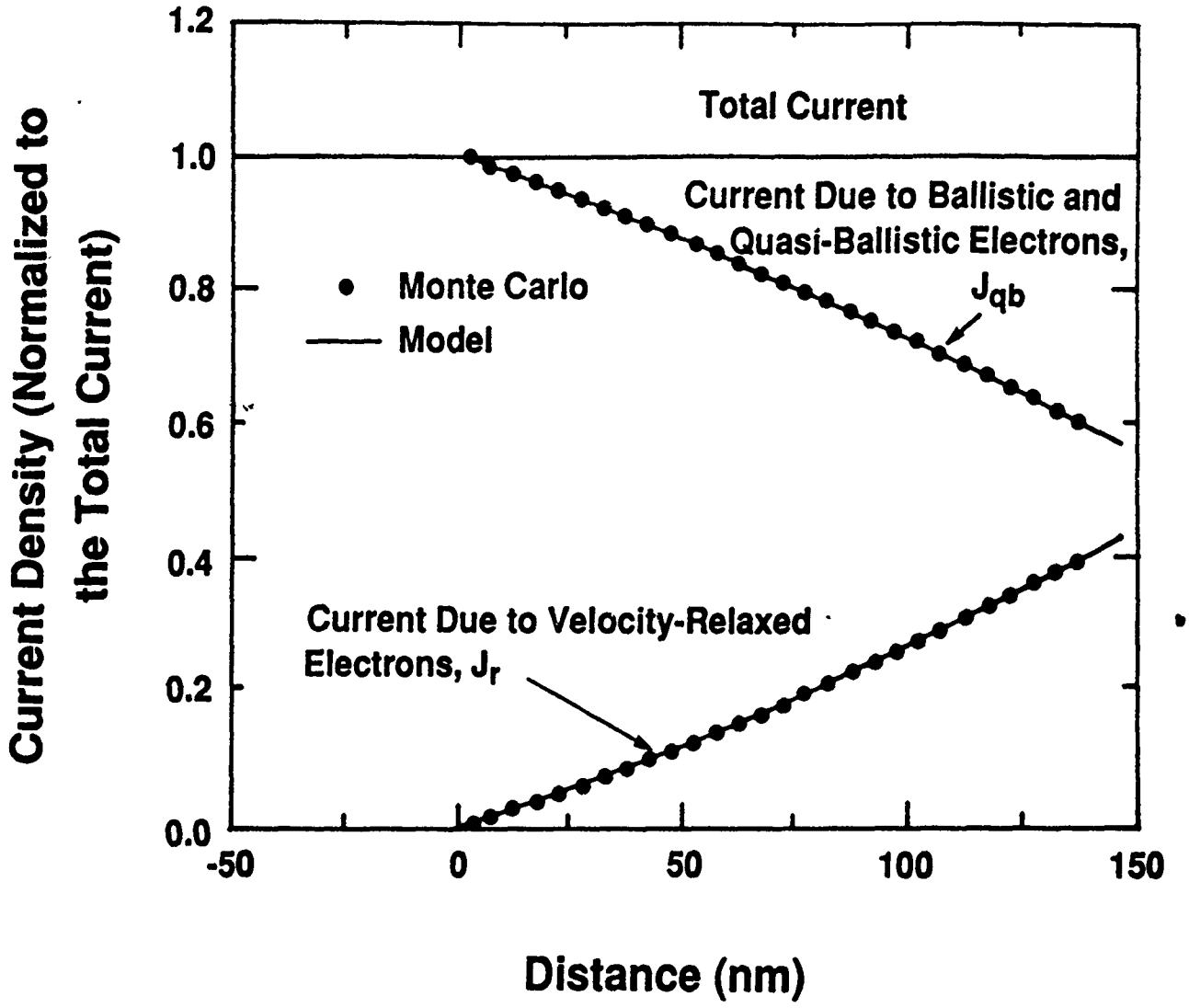

Figure 6. Current versus distance in a GaAs planar-doped barrier with a barrier height of 0.225 eV. The data points are from Monte Carlo simulations. The solid curves are calculated from the analytical model described in the text.

take into account the transfer of electrons to the lateral or satellite valleys, Thus, it is valid only for the range of energies where intervalley transfer is negligible. However, the ideas presented here can be extended to include the effects of intervalley scattering.

2.2.3 A Hydrodynamic Hot-Electron Transport Model

We have explored a new approach for modeling hot electron transport in submicron III-V compound semiconductor devices during the past three years which we believe can have a significant impact on the development of device models for microwave and millimeter wave circuit simulators. Currently, this area is critical for the DoD's MMIC program, and there is an urgent need for computer-aided design approaches in the development of high frequency electronic systems. Often the design of such circuits is done empirically and by trial and error. We would like to contribute to the development of an approach to millimeter wave circuit design which is analogous to approaches now used in the design of silicon integrated circuits. There are at least two needs for the implementation of such an approach. First, models are required for the description of high frequency circuit effects brought about by the interactive nature of circuits elements which are normally considered discrete and isolated at low frequencies. Thus, at very high frequencies, these elements cannot be considered as independent circuit elements interconnected by lossless wires, but their mutual interactions must be considered as well as the nature and physical layout of their interconnections. Secondly, specific device models must be developed which take into consideration the nonequilibrium effects which occur and can dominate the performance of submicron compound semiconductor devices. Examples are quasi-ballistic transport and velocity overshoot, which are becoming practical limitations of current device structures rather than the esoteric topics they were once considered.

We are addressing the need for increased physical understanding in device models through advanced modeling concepts, such as the Feynman path integral and, on a more practical level, through the use of hydrodynamic approaches to device modeling. This (hydrodynamic) approach allows nonequilibrium effects to be included in a rigorous way within device models which are more readily accepted

by circuit and device engineers. These device models can be applied for dimensions which well exceed the current technological limits of device fabrication.

The basic transport model used in this research is based upon the semiclassical hydrodynamic conservation equations for the average electron density, average electron momentum and average electron energy. The general model includes particle relaxation times, momentum relaxation times and energy relaxation times as a function of average carrier energy for the Γ, L and X conduction band valleys of GaAs. The model also contains electron temperature tensors and heat flow vectors which also have average energy dependence. The relaxation times in the model result from intravalley and intervalley particle scattering and represent rates of exchange of particles between valleys and rates of loss of average momentum and average energy between and within the individual valleys. The electron temperature tensor and heat flow vector depend upon the electron velocity distribution about the average electron velocity and ultimately affect transport when spatial variations in average velocity and average energy exist.

In the initial stages of the project [47], the extreme heuristic assumption was made that the temperature tensor, heat flow vector and relaxation times were all simple functions of average energy. These general transport parameters were then calculated using the Monte Carlo method in conjunction with the ergodic principle applied directly to the integral definition for the parameters. This approach was taken to approximately include the effects of nonparabolicity in the conduction bands and to make as few assumptions as possible about the form of the electron distribution in momentum space. A direct or indirect assumption traditionally made is to assume that the distribution has a displaced Maxwellian form which leads to incorrect results even for the stationary transport case. The above heuristic approach offered a slight improvement in accuracy and, if developed, offers a future hydrodynamic/Monte Carlo model which could quickly and accurately describe many electronic structures.

The initial investigations of the hydrodynamic model have been based on single conduction band valley cases to simplify the difficulties associated with determining solutions. Solutions were obtained for the model by combining a very efficient local Newton-based solver with a perturbation-in-doping based

continuation method. The first simulation results [48] of the hydrodynamic model indicated a general improvement over the more conventional drift-diffusion model with results closer to those of a Monte Carlo transport model. The results also showed an extreme dependency on the functional form of the heat flow vector. The heat flow vector was shown to have a large impact on the resultant cooling in average energy observed at the source end of an N^+–N–N^+ structure. The complete results from this study are shown in Figs. 7-12 with Fig. 12 indicating an excessive cooling at the source which did not agree with the Monte Carlo results. Another important result discovered in these initial investigations was an inability, due to neglecting any form of velocity or kinetic energy dependency in the temperature tensors, to find high bias solutions for the model.

Since simulation results indicated it was important to include additional accuracy into the model through more physically correct effective temperature dependencies, a new derivation was performed. As in the previous work the new hydrodynamic model was based on a unique set of moments. The usual approach is to take moments of the electron momentum which yield a set of conservation equations for density, momentum and energy. Then addition assumptions are used to mathematically close the moment process at the conservation of energy equation. The traditional assumption is to either directly or indirectly assume a displaced Maxwellian distribution. Under this assumption one can express the moment equations in terms of the variables density n, average velocity v, average energy w, and thermal temperature T. The displaced Maxwellian approximation also yields the constitutive relation $w = \frac{3}{2}k_BT + \frac{1}{2}mv^2$, resulting in a value of the heat flow vector of $\mathbf{q} = 0$ for parabolic bands. Also, a heat flow vector, with higher order differential dependence on energy, is usually included using thermodynamics arguments (phenomenological Wiedemann-Franz law).

The moments used in the new model can be described as moments of the nonparabolic electron velocity. Specifically, the current hydrodynamic model was developed using the moment operators $\Psi_0 = 1$, $\Psi_1 = \mathbf{u}(\mathbf{k})$ and $\Psi_2 = \frac{1}{2}m(\mathbf{k})\mathbf{u}(\mathbf{k})\mathbf{u}(\mathbf{k}) \approx E_c(\mathbf{k})$. Here, the Kane dispersion relation, $\hbar^2k^2/2m^* = E_c(1 + \alpha E_c)$ is used to define the single electron velocity $\mathbf{u}(\mathbf{k})$ and the effective mass

Figure 7. Current density versus applied potential.

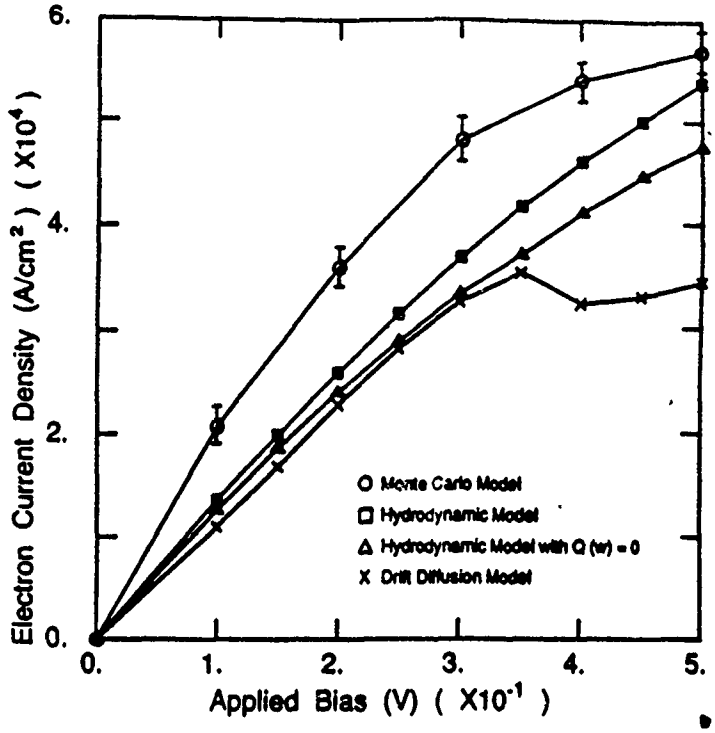

Figure 8. Carrier concentration profile for an applied potential of 0.4 volts.

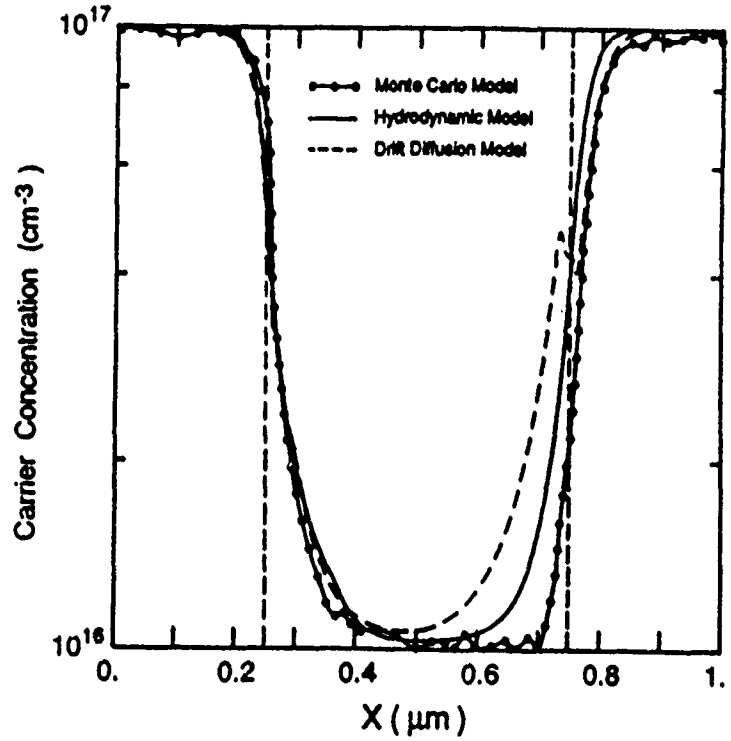

Figure 9. Potential energy profile for an applied potential of 0.4 volts.

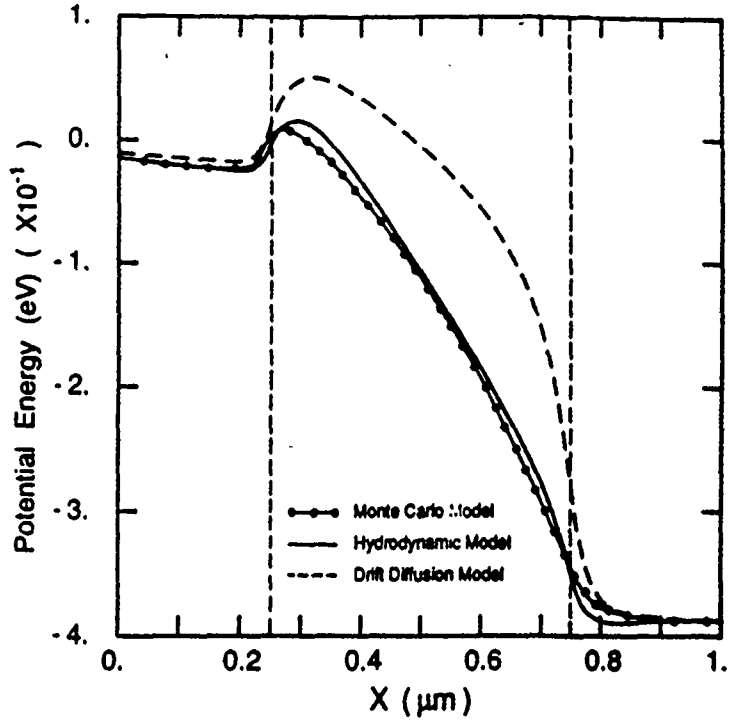

Figure 10. Electric field intensity profile for an applied potential of 0.4 volts.

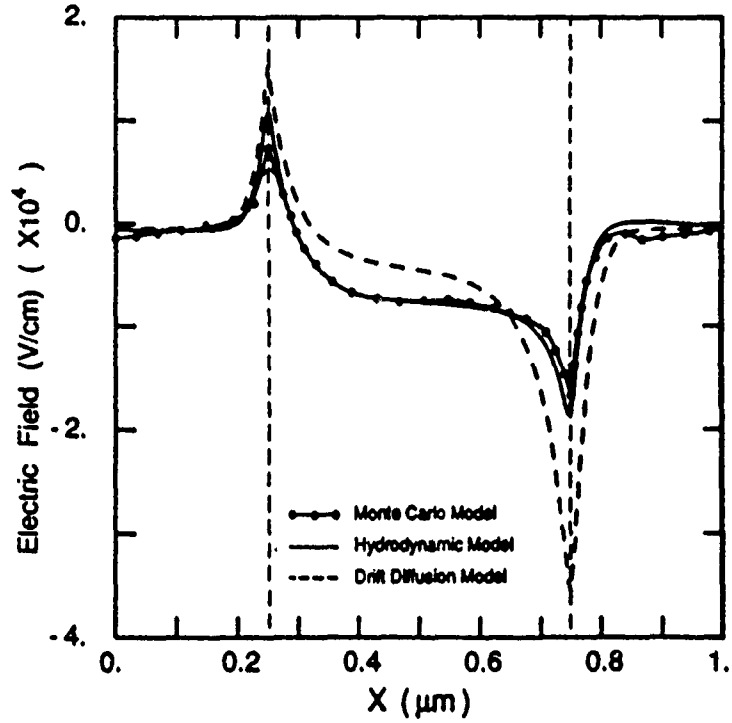

Figure 11. Drift velocity profile for an applied potential of 0.4 volts.

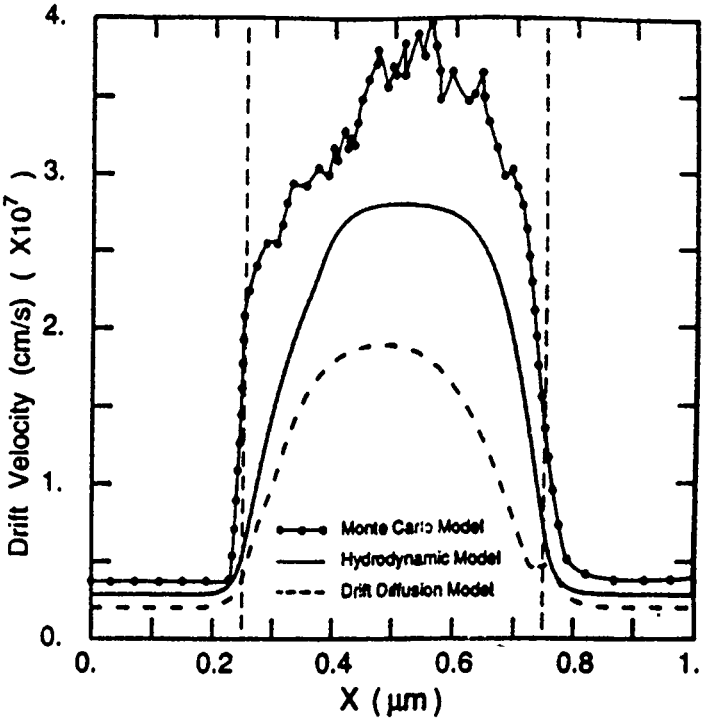

Figure 12. Average energy profile for an applied potential of 0.4 volts.

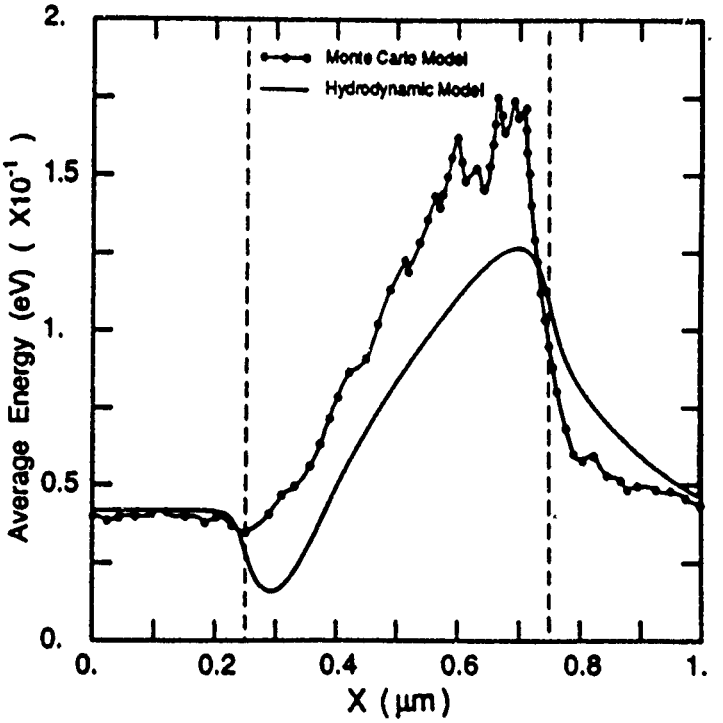

$m(\mathbf{k}) = m^*(1 + 2\alpha\hbar^2k^2/m^*)^{1/2}$. These moment operators were chosen because they lead to a form which can be manipulated more easily, one in which simplifying assumptions can be seen more clearly. Performing the moment process and simplying to first order yields immediately the results:

$$\frac{\partial n}{\partial t} = -\nabla_r\cdot(nv) \tag{13}$$

$$\frac{\partial v}{\partial t} = -v\cdot\nabla_r v + \frac{F}{m^{**}} - \frac{1}{nm^*}\nabla_r\cdot[P_v] \tag{14}$$

$$\frac{\partial w}{\partial t} = -v\cdot\nabla_r w\cdot[P_w] + q) \tag{15}$$

where m^{**}, $[P_v]$, $[P_w]$ and q have integral definitions which depend on f. Here, unlike the parabolic band case, there is a dilemma of two distinctly different effective pressure tensors $\mathbf{P_v}$ and $\mathbf{P_w}$, (for parabolic bands and displaced Maxwellian, $[P_v]$ = To resolve this, stationary Monte Carlo calculations and physical intuition are used to suggest the following ansatz distribution function

$$f = n\left[\frac{m_w(T_w)}{2\pi k_B T_w}\right]^{3/2} \exp\left[\frac{-m_w(T_w)\,|u - v|^2}{2k_B T_w}\right] \tag{16}$$

as a constitutive relation to close the moment equations. Here T_w has been chosen to replace T because $\frac{3}{2}k_B T_w$ accurately approximates the effective thermal energy for the stationary transport case, and $m_w(T_w)$ has been introduced because we expect a non-constant effective mass strongly dependent on T_w. Equation (16) is now used in the definitions for the transport parameters, and the analysis is limited to first and second orders in T_w, to arrive at the the supplemental relations;

$$w = \frac{3}{2}k_B T_w + \frac{m^{**}(T_w)}{2} v\cdot v \tag{17}$$

$$m^{**}(T_w) = m^*(1 + 3\alpha k_B T_w) \tag{18}$$

$$[P_v] = \frac{m^*}{m^{**}} nk_B T_w[I] \tag{19}$$

$$[P_w] = nk_B T_w [I] \tag{20}$$

$$q_i = 5\alpha \left[\frac{m^*}{m^{**}} \right]^2 (k_B T_w)^2 n u_i \tag{21}$$

These relations supply all the necessary equations to express the hydrodynamic transport model for non-parabolic conduction bands in terms of the quantities; electron concentration n, average electron velocity v, average electron energy w and the space-times variable (r,t). Applying these relations reveal the new collisionless nonparabolic hydrodynamic transport model equations to be :

$$\frac{\partial n}{\partial t} = -\nabla_r \cdot (nv) \tag{22}$$

$$\frac{\partial v}{\partial t} = -v \cdot \nabla_r v + \frac{F}{m^* \mu} - \frac{2}{3nm^*} \nabla_r [nv(w - \frac{m^*}{2} v \cdot v)] \tag{23}$$

$$\frac{\partial w}{\partial t} = -v \cdot \nabla_r w + F \cdot v - \frac{2}{3n} \nabla_r \cdot [nv(\omega + \phi)(w - \frac{m^*}{2} v \cdot v)] \tag{24}$$

with nonparabolic correction terms

$$\mu(v,w) = 1 + 2\alpha\omega(v,w)(w - \frac{m^*}{2} v \cdot v) \tag{25}$$

$$\nu(v,w) = \frac{\omega(v,w)}{\mu(v,w)} \tag{26}$$

$$\omega(v,w) = \frac{1}{1 + \alpha m^* v \cdot v} \tag{27}$$

$$\phi(v,w) = \frac{10\alpha}{3} \left[\frac{\omega(v,w)}{\mu(v,w)} \right]^2 (w - \frac{m^*}{2} v \cdot v) \tag{28}$$

The nonparabolic model equations above have been written in a form so that for the parabolic case, α=0, it is easy to observe that μ=ν=ω=1 and ϕ=0. Then, the nonparabolic model conveniently reduces to the more familiar classical hydrodynamic equations in Lagrangian form.

Since we are also interested in models which can be used to study ultrasmall electronic devices investigations into adding quantum corrections to the hydrodynamic equations were performed. To achieve this goal, the previous work of Grubin and Kveskovsky [49] was followed to develop a set of quantum balance equations consistent with the nonparabolic model above. For the initial investigation a slightly restricted version of their quantum hydrodynamic equations were used. Specifically, spatial and nonparabolic effects on the effective mass were neglected and any deficiencies of the general quantum distribution function to agree with Fermi statistics (low temperature effects) were ignored. Development of the quantum correction terms began with the general moment equations of Stroscio [50]. The collisionless one-dimensional forms of the first three moments are:

$$\frac{\partial n}{\partial t} = -\frac{1}{m^*}\frac{\partial}{\partial x}(np_d) \tag{29}$$

$$\frac{\partial p_d}{\partial t} = -\frac{\partial}{\partial x}\left(\frac{p_d^2}{2m^*} + U_{eff}\right)p_d\rangle\rangle \tag{30}$$

$$\frac{\partial}{\partial t}\langle(p-p_d)^2\rangle - \frac{1}{nm^*}\frac{\partial}{\partial x}(n\langle(p-p_d)^3\rangle) - \frac{p_d}{nm^*}\frac{\partial}{\partial x}(n\langle(p-p_d)^2\rangle)$$

$$-\frac{2}{m^*}\frac{\partial}{\partial x}(n\langle(p-p)^2\rangle)\frac{\partial p_d}{\partial x} + \frac{p_d\langle(p-p_d)^2\rangle}{nm^*}\frac{\partial n}{\partial x} \tag{31}$$

where n is the electron density, p is the single electron momentum, p_d is the classical average momentum and U_{eff} is the total effective electric potential. Here Ref. 49 was followed and

$$f_W = \frac{n}{N}\exp\left[\frac{-\beta(p-p_d)^2}{2m^*}\right]\left[1 + \frac{\gamma}{3}\left(1 - \frac{\beta}{m^*}(p-p_d)^2x\right)\frac{\partial}{\partial x}\left(\frac{1}{n}\frac{\partial n}{\partial x}\right)\right], \tag{32}$$

which is the momentum displaced nonequilibrium Wigner distribution function of Ancona and Iafrate [51], was used to obtain $n\langle(p-p_d)^2\rangle = \frac{m^*}{\beta}\left(1 - \frac{2\alpha}{3\beta}\frac{\partial}{\partial x}\left(\frac{1}{n}\frac{\partial n}{\partial x}\right)\right.$ and $n\langle(p-p_d)^3\rangle = 0$ where $\alpha = \hbar^2\beta^2/8m^*$, $\beta = 1/k_BT$ and $\gamma = \alpha/\beta$. These results can be used with Eqs. (29)-(31) to yield the collisionless quantum hydrodynamic equations:

$$\frac{\partial n}{\partial t} = -\frac{\partial (nv)}{\partial x} \tag{33}$$

$$\frac{\partial v}{\partial t} = -v\frac{\partial v}{\partial x} - \frac{1}{m^*}\frac{\partial}{\partial x}(U_{eff} + \frac{Q}{3}) - \frac{1}{nm^*}\frac{\partial (nk_BT)}{\partial x} \tag{34}$$

$$\frac{\partial w}{\partial t} = -v\frac{\partial w}{\partial x} - v\frac{\partial}{\partial x}(U_{eff} + \frac{Q}{3}) - \frac{1}{n}\frac{\partial (nvk_BT)}{\partial x} + \frac{\hbar^2}{12m^*}\frac{\partial}{\partial x}(\frac{1}{n}\frac{\partial n}{\partial x})\frac{\partial v}{\partial x} \tag{35}$$

where $w = \frac{3}{2}k_BT + \frac{1}{2}m^*v^2 - \frac{\hbar^2}{24m^*}\frac{\partial}{\partial x}(\frac{1}{n}\frac{\partial n}{\partial x})$ and $Q = -\frac{\hbar^2}{2m^*}\frac{1}{\sqrt{n}}\frac{\partial^2\sqrt{n}}{\partial^2 x}$. Comparing the above quantum equations to the semiclassical nonparabolic hydrodynamic Eqs. (22)-(24), approximating T_w by T and using the supplemental relations (25)-(28) one can arrive at the quantum corrected collisionless nonparabolic hydrodynamic transport model in one dimension,

$$\frac{\partial n}{\partial t} = -\frac{\partial (nv)}{\partial x} \tag{36}$$

$$\frac{\partial v}{\partial t} = -v\frac{\partial v}{\partial x} - \frac{1}{m^*\mu}\frac{\partial}{\partial x}(U_{eff} + \frac{Q}{3}) - \frac{2}{3nm^*}\frac{\partial}{\partial x}[nv(w - w_q - \frac{m^*}{2}v^2)] \tag{37}$$

$$\frac{\partial w}{\partial t} = -v\frac{\partial w}{\partial x} - v\frac{\partial}{\partial x}(U_{eff} + \frac{Q}{3}) - \frac{2}{3n}\frac{\partial}{\partial x}[nv(\omega + \phi)(w - w_q - \frac{m^*}{2}v^2)] - 2w_q\frac{\partial v}{\partial x} \tag{38}$$

with nonparabolic correction terms $\mu(n,v,w) = 1 + 2\alpha\,\omega(v,w)\,(w - w_q - \frac{m^*v^2}{2})$, $v(n,v,w) = \frac{\omega(v,w)}{\mu(v,w)}$, $\omega(v,w) = (1 + \alpha m^*v^2)^{-1}$, $\phi(n,v,w) = \frac{10\alpha}{3}[\frac{\omega(v,w)}{\mu(n,v,w)}]^2(w - w_q - \frac{m^*v^2}{2})$ and quantum corrections $w_q = -\frac{\hbar^2}{24m^*}\frac{\partial}{\partial x}(\frac{1}{n}\frac{\partial n}{\partial x})$ and $Q = -\frac{\hbar^2}{2m^*}\frac{1}{\sqrt{n}}\frac{\partial^2\sqrt{n}}{\partial^2 x}$.

An initial study has been performed with this quantum hydrodynamic model. The quantum hydrodynamic model was used to analyze a double-barrier heterostructure, $Al_{x_c}Ga_{1-x_c}As$ barriers with x_c=0.3, doped to $10^{14}cm^{-3}$ with source and drain regions of length 200Å and doped to $10^{16}cm^{-3}$. This structure, which has barrier widths of 5Å and a spacing of 50Å, is shown in Fig. 14 with the source and drain regions excluded. In the self-consistent simulations, the heterostructure was treated using the Anderson

treated in a classical manner and we assumed $T_{lattice}$ = 300 K. Simulation results were generated for a number of biases in the range 5 mV to 50 mV which yielded an approximately linear J–$\Psi_{applied}$ characteristic of slope 0.36 kA/cm^2–mV. The profile result of w, and w_q, parameters intrinsic to the energy balance equation, are displayed in Fig. 13 for $\Psi_{applied}$=8mV. Figure 14 shows the corresponding profile for Q along with the conduction band E_c (E_c=U_{eff}).

This study was the first to use the *three* quantum hydrodynamic (QHD) equations to study transport in heterostructure devices. The key additional feature of the QHD equations is the incorporation of the effects of density gradients through the quantum potential. Insofar as a classical solution does not exist in the presence of barriers, Q must at least cancel the effects of the barriers and permit carrier transport. Indeed Q/3 does approximately balance the barrier potential a result consistent with Ref. 49. Also, since this result is near equilibrium, the density should vary everywhere as $N^+exp[-(U_{eff} + Q/3)/k_BT]$ and this is found to be the case.

2.2.4 Transport in Photoexcited Semiconductors

During the past three years, we have begun an effort to study the transport of photoexcited carriers in semiconductors. We have decided to explore the use of Monte Carlo simulation as well as quantum mechanical wave approaches. The specific device which we have chosen to first explore is the GaAs metal-semiconductor-metal (MSM) photodetector with planar (low interelectrode capacitance) structure which is of interest for discrete applications and optoelectronic integrated circuits (OEIC's). The fastest reported MSM detector has an intrinsic bandwidth of 105 GHz, which compares well with bandwidths of other Schottky photodiodes. These low noise, high quantum efficiency detectors are fully MESFET compatible. The most complex high performance OEIC uses a refractory-gate, ion-implanted process with over 2000 devices. There is, however, little simulation work done for devices with submicron distance between fingers. Recently, we have analyzed detectors with dimensions possible to obtain with well refined lithography techniques [52-54]. Some of the preliminary results on temporal response and dark current were reported last year. In this section, we present a more detailed time analysis of photodetec-

rule; $U_{eff} = q\Psi_{eff} - \chi(x)$, where $\chi(x)$ ($\Delta E_c = 0.697 x_c$) is a position dependent electron affinity and the applied potential Ψ_{eff} was determined from solving Poisson's equation. The dissipation mechanisms were treated in a classical manner and we assumed $T_{lattice}$ = 300 K. Simulation results were generated for a number of biases in the range 5 mV to 50 mV which yielded an approximately linear $J-\Psi_{applied}$ characteristic of slope 0.36 kA/cm^2–mV. The profile result of w, and w_q, parameters intrinsic to the energy balance equation, are displayed in Fig. 13 for $\Psi_{applied}$=8mV. Figure 14 shows the corresponding profile for Q along with the conduction band E_c (E_c=U_{eff}).

This study was the first to use the *three* quantum hydrodynamic (QHD) equations to study transport in heterostructure devices. The key additional feature of the QHD equations is the incorporation of the effects of density gradients through the quantum potential. Insofar as a classical solution does not exist in the presence of barriers, Q must at least cancel the effects of the barriers and permit carrier transport. Indeed Q/3 does approximately balance the barrier potential a result consistent with Ref. 49. Also, since this result is near equilibrium, the density should vary everywhere as $N^+\exp[-(U_{eff} + Q/3)/k_BT]$ and this is found to be the case.

2.2.4 Transport in Photoexcited Semiconductors

During the past three years, we have begun an effort to study the transport of photoexcited carriers in semiconductors. We have decided to explore the use of Monte Carlo simulation as well as quantum mechanical wave approaches. The specific device which we have chosen to first explore is the GaAs metal-semiconductor-metal (MSM) photodetector with planar (low interelectrode capacitance) structure which is of interest for discrete applications and optoelectronic integrated circuits (OEIC's). The fastest reported MSM detector has an intrinsic bandwidth of 105 GHz, which compares well with bandwidths of other Schottky photodiodes. These low noise, high quantum efficiency detectors are fully MESFET compatible. The most complex high performance OEIC uses a refractory-gate, ion-implanted process with over 2000 devices. There is, however, little simulation work done for devices with submicron distance between fingers. Recently, we have analyzed detectors with dimensions possible to obtain with well

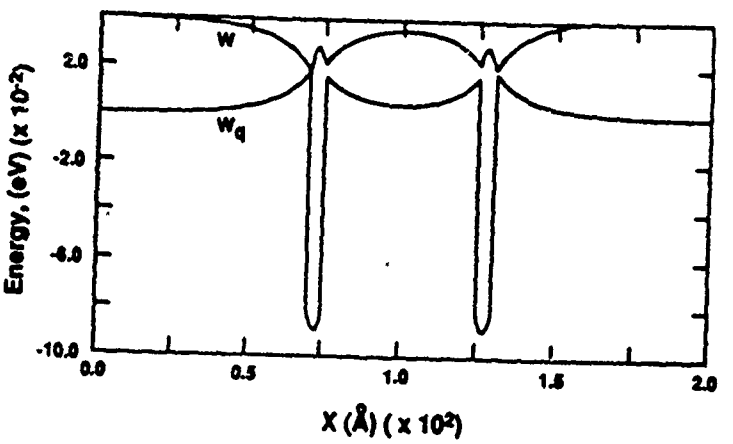

Figure 13. Average energy (w) and quantum correction (w_q) for an applied potential of 8 mV.

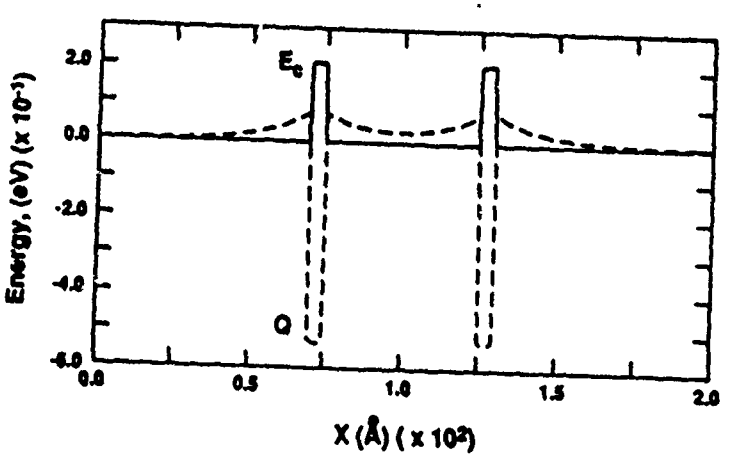

Figure 14. Conduction band edge (E_C) and quantum potential (Q) for an applied potential of 8 mV.

refined lithography techniques [52-54]. Some of the preliminary results on temporal response and dark current were reported last year. In this section, we present a more detailed time analysis of photodetectors with 0.1-1 μm distance between fingers. This range has been considered because it spans devices of current importance as well as those of possible future interest. We have used a self-consistent Monte Carlo (MC) model to simulate intrinsic transport and a lumped-constant circuit model for parasitics. The MC results are used as an input for simulation of the circuit model. This approach is relatively easy to implement. However, the interpretation of the results depends critically on the parasitic lumped-constant circuit parameters.

The GaAs MSM photodetector structure has been illustrated in Ref. 53. We consider two different versions of this detector: discrete and monolithically-integrated. In the discrete version, the bond pads are 50 x 50 μm^2 and the device must be wire bonded to the load. The inclusion of the series wiring inductance affects detector pulse responses. In the monolithic version, one bond pad is replaced with a microstrip transmission line (10 x 50 μm^2), thus reducing the series inductance. All dimensions are chosen to closely model realistic devices. A low bias is essential if the photodetector is to operate in a highly-integrated optoelectronic circuit. It is fortunate that the MSM photodetector offers high performance at relatively low bias voltages. Due to the very low doping concentration of the epitaxial layer, the regions between and below fingers are completely depleted of free carriers [53].

Photodetectors with separations between fingers of 0.1-1 μm were simulated and results are shown in Fig. 15. A self-consistent ensemble Monte Carlo simulation was used to separately determine electron and hole currents for a large number (15000-25000) of photoexcited carriers. The very sharp electron peak for the device with a 0.5 μm distance between fingers is due to a higher electric field than in other devices. Although the intrinsic responses were calculated for the detectors with a lightly doped epitaxial layer, one can expect that very similar results would be obtained if the devices were processed directly on a semi-insulating substrate. We observe that extremely short current pulses are possible. However, other factors have a strong influence on output signal of the device.

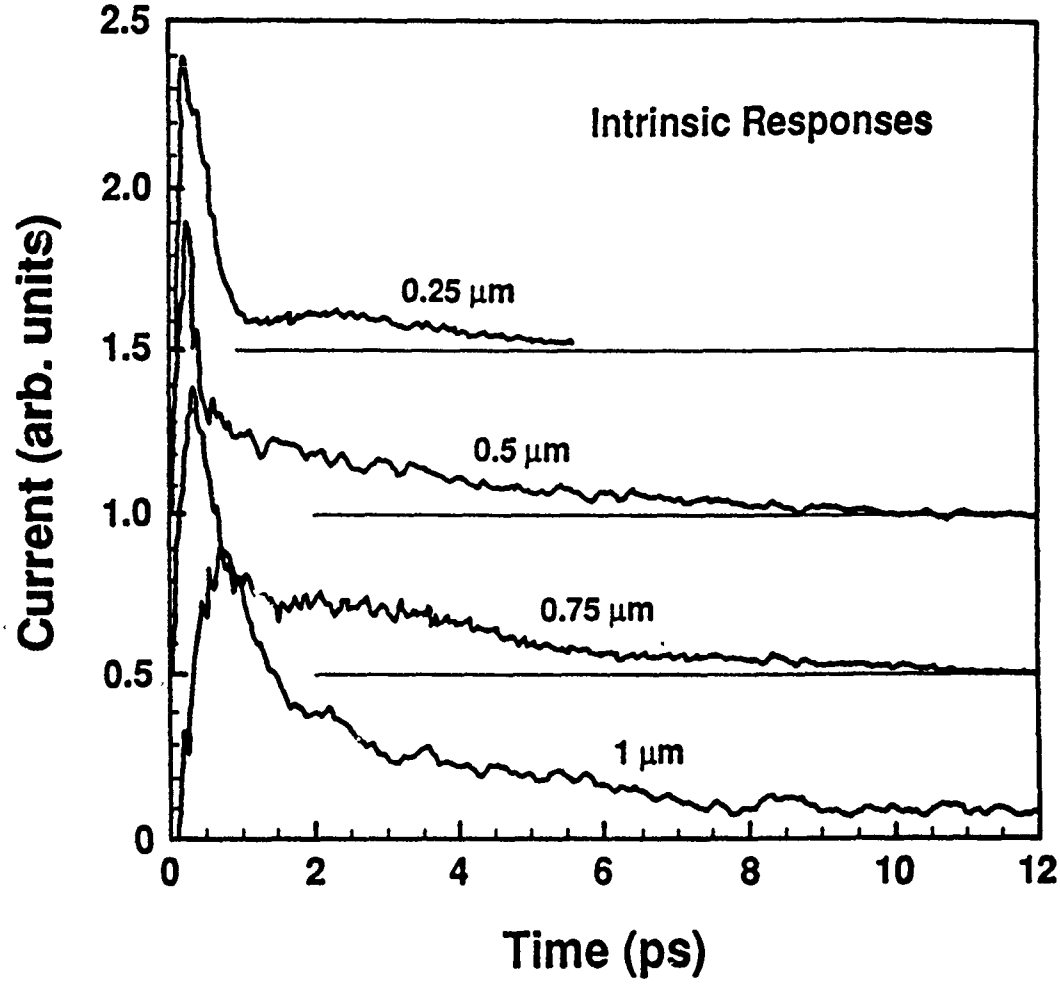

Figure 15. Comparison of intrinsic responses (no parasitics) for photodetectors with submicron electrode pattern (≤1 μm). As interfinger spacing increases from 0.5 μm to 1 μm, the longer hole tail decays become more evident.

The parasitic circuit of a photodetector (Fig. 16) can have a very detrimental effect on time response. Briefly, parasitic elements are estimated in the following way. Here, CPD is modeled as a capacitance between parallel microstriplines. Also, RF and LF are the resistive and inductive parts of the finger impedance (skin depth at 100 GHz has been included). In the discrete version, CPP is the capacitance between bond pads, CPG is the capacitance between the bond pad and ground, and LL is the wire bond inductance (0.06 nH). In the monolithic version LL1, LL2, CLG, CLL represent the microstripline. Other parasitics (RD, CFG) are less important, but were included. The calculated intrinsic responses can now be used to determine the responses of photodetectors with parasitics. In Fig. 17 we present the normalized output voltages vs time for the discrete detectors. The FWHM is 3.77 ps, 3.5 ps, 3.28 ps, 3.08 ps, 2.86 ps for the discrete devices with spacings between fingers of 0.1 μm, 0.25 μm, 0.5 μm, 0.75 μm, and 1 μm, respectively. Due to the long hole tails and oscillations present in some devices (monolithic), the FWHM can not be used unambiguously to estimate the bandwidth. Therefore, we define the maximum repetition frequency as follows. If t_{min} is the time for the pulse to reach 3% of maximum (or -3% if pulse becomes negative), and t_{max} is the time to reach the same value before the pulse settles to zero, then the maximum repetition frequency is simply $1/(t_{max} - t_{min})$. Based on this definition, the maximum repetition frequency is calculated and results are shown in Fig. 18 for the intrinsic, monolithic and discrete detectors.

The experimental results related to the MSM photodetectors are somewhat limited. Although there are detectors fabricated with a submicron electrode pattern, there is little experimental data which could be used for the purpose of comparison with simulated results. An exception to this situation is the detector fabricated and tested at IBM [55]. In Fig. 19 we present the experimental data and the simulated results using the approach described above. In general, there is good agreement between these two results. However, the relatively slow leading edge of the experimental pulse is difficult to explain. This could be a circuit effect.

Thus, in this phase, we have investigated the transit behavior of the GaAs MSM photodetectors. The intrinsic responses have been simulated using Monte Carlo method and used in a detailed analysis of

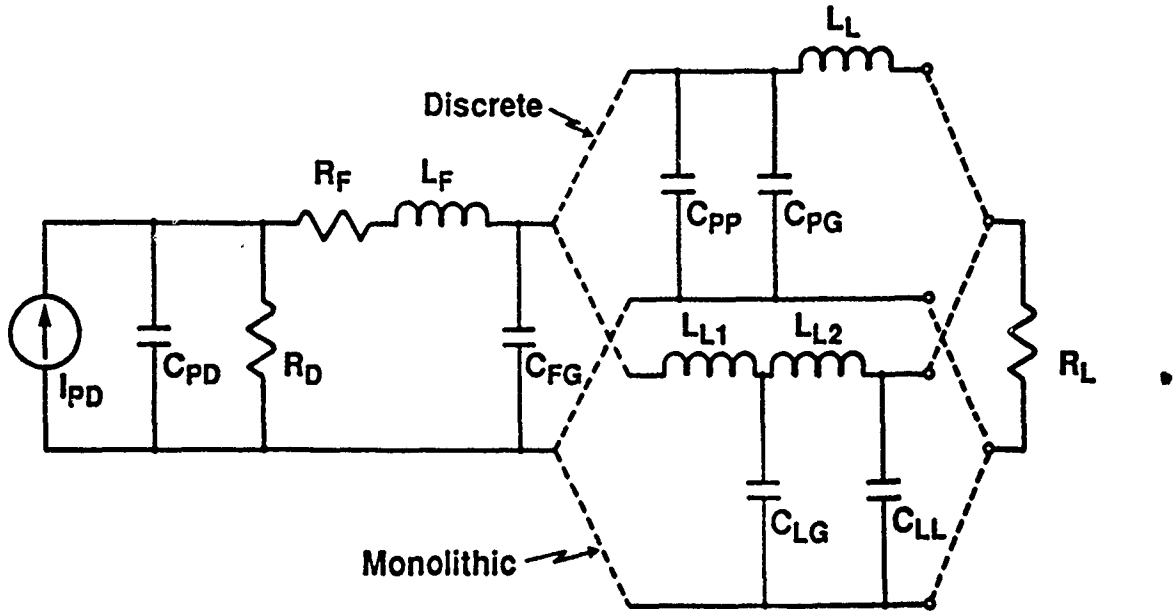

Figure 16. Equivalent circuit of a MSM photodetector. The intrinsic current, I_{PD}, obtained from Monte Carlo simulation of the intrinsic device, is used to excite the parasitic circuit. The parasitic elements depend on whether the discrete or monolithic version of the photodetector is considered.

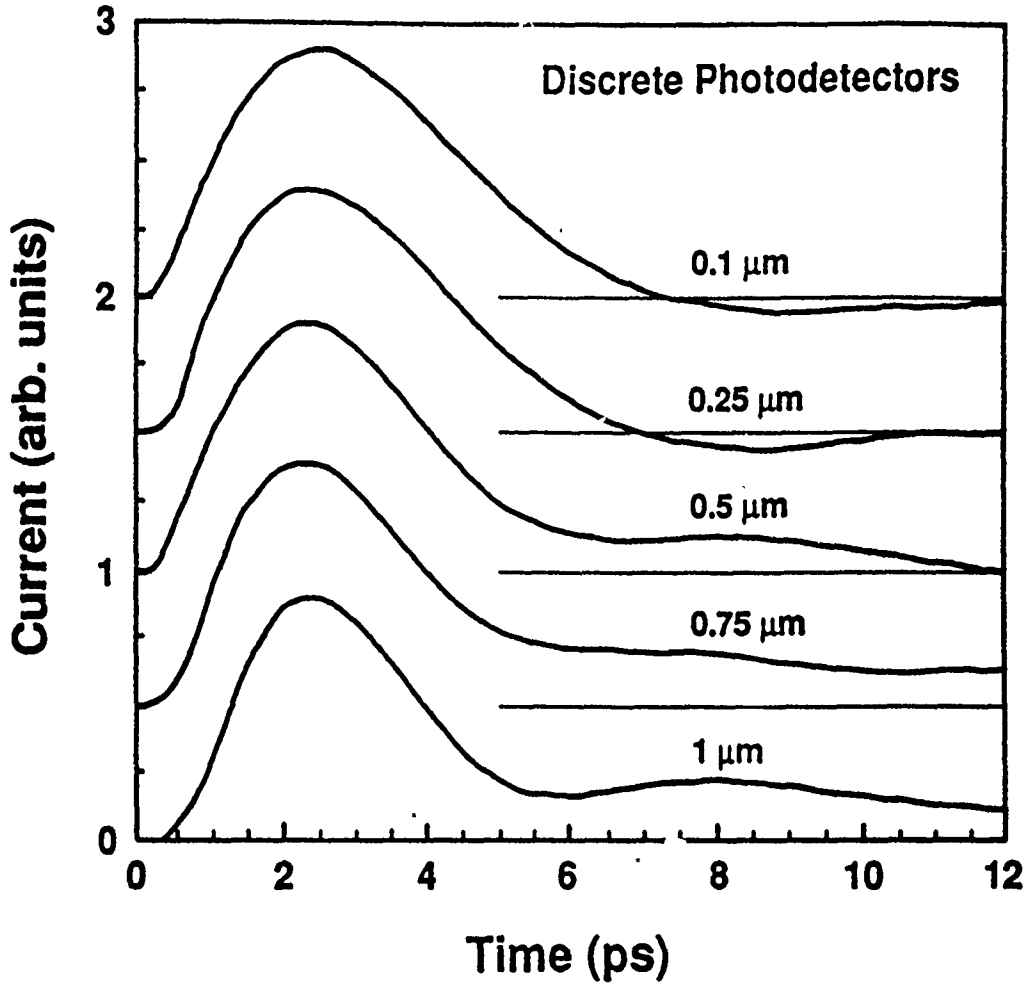

Figure 17. Time responses of discrete photodetectors with parasitics. The full-width-half-maximum (FWHM) decreases as interfinger spacing increases. The maximum repetition frequency, however, is determined by the slow hole decay tail rather than by the FWHM.

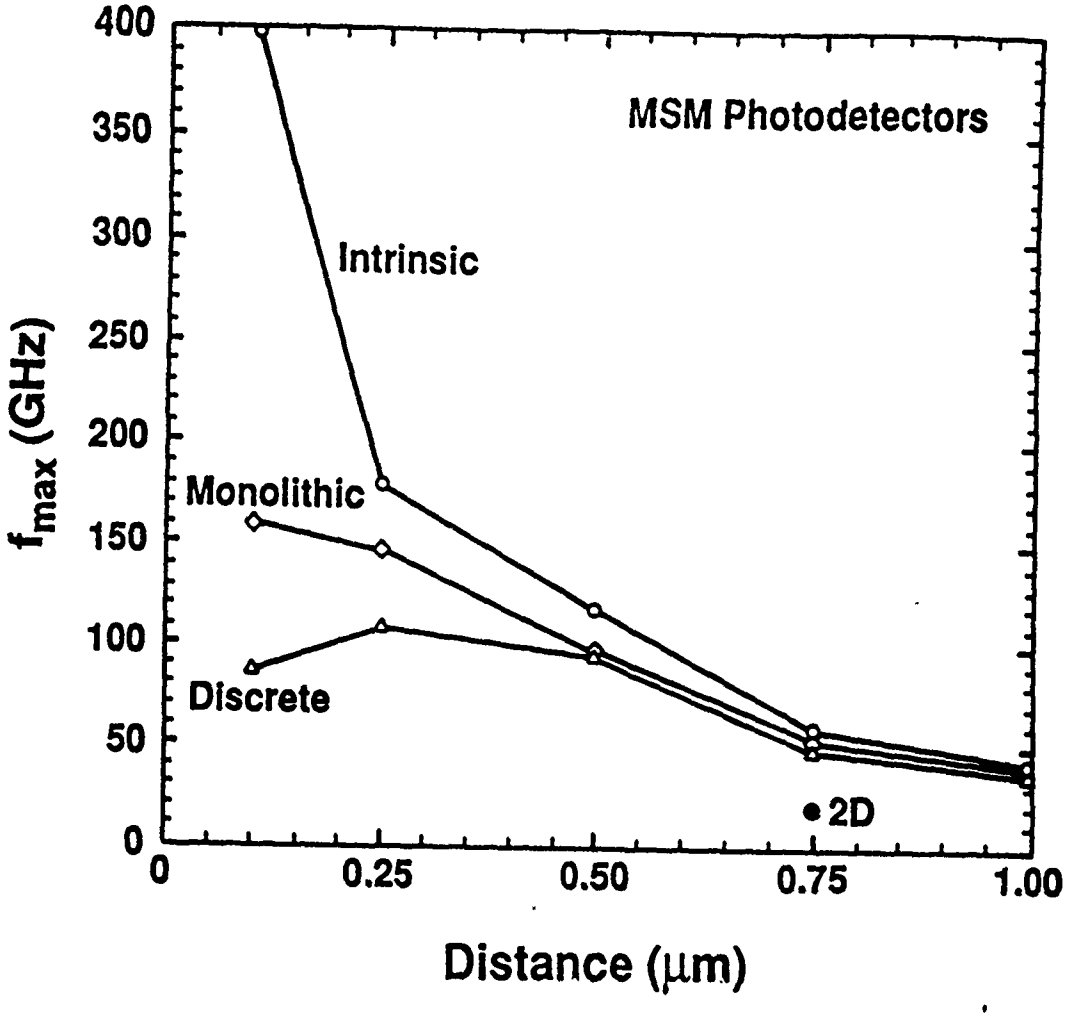

Figure 18. Maximum repetition frequency versus interfinger spacing for all devices simulated. The intrinsic detector is especially fast for small interfinger spacing. The parasitic circuit, however, strongly affects the maximum repetition frequency.

the discrete and monolithic versions of the detectors. Instead of relying on the FWHM to determine the bandwidth, we defined the maximum repetition frequency since this is a better estimate of the device speed. Conducted studies reveal that the GaAs MSM photodetectors are indeed suitable for very fast detection of optical signals in both discrete and monolithic versions. These studies also reveal the utility of the Monte Carlo method to augment other device and circuit simulation techniques.

2.2.5 Theory of Optical-Phonon Modes in Heterostructures

During the past year, we have initiated a research project on the theory of optical-phonon modes in heterostructures. It has been experimentally verified that the phonon modes as well as carrier wave functions are significantly affected by the presence of heterointerfaces. Thus, the characteristics of optical-phonon modes in the layered structures are distinctively different from their bulk counterparts. Questions arise as to the validity of the conventional three dimensional (bulk) treatments of optical-phonon modes in heterostructure devices, especially when interactions by the longitudinal-optical (LO) phonon modes become a dominant energy loss mechanism. Our main objective is to study the effects of reduced dimensionality on optical-phonon modes from various aspects.

In spite of the short period of time during which this research has been performed, we have made substantial progress. Three papers have been already published or accepted by major journals. Two additional papers have been submitted for publication and two more are currently in preparation. As a result of the progress, this research project will be supported by separate grants from ONR and ARO which have been recently awarded to us.

For brevity, this section will focus on the study of confined LO-phonon frequencies in short-period strained-layer superlattices. The main emphasis will be on the development of a simple model which can calculate the frequencies of confined LO phonons in strained-layer III-V superlattices grown in the <001> direction. A discrete (rather than continuum) approach based on a linear-chain model is applied. The frequency shift arising simultaneously from both confinement and strain is accounted for by properly modifying the force constants to incorporate the strain effects into the linear-chain model. For a specific

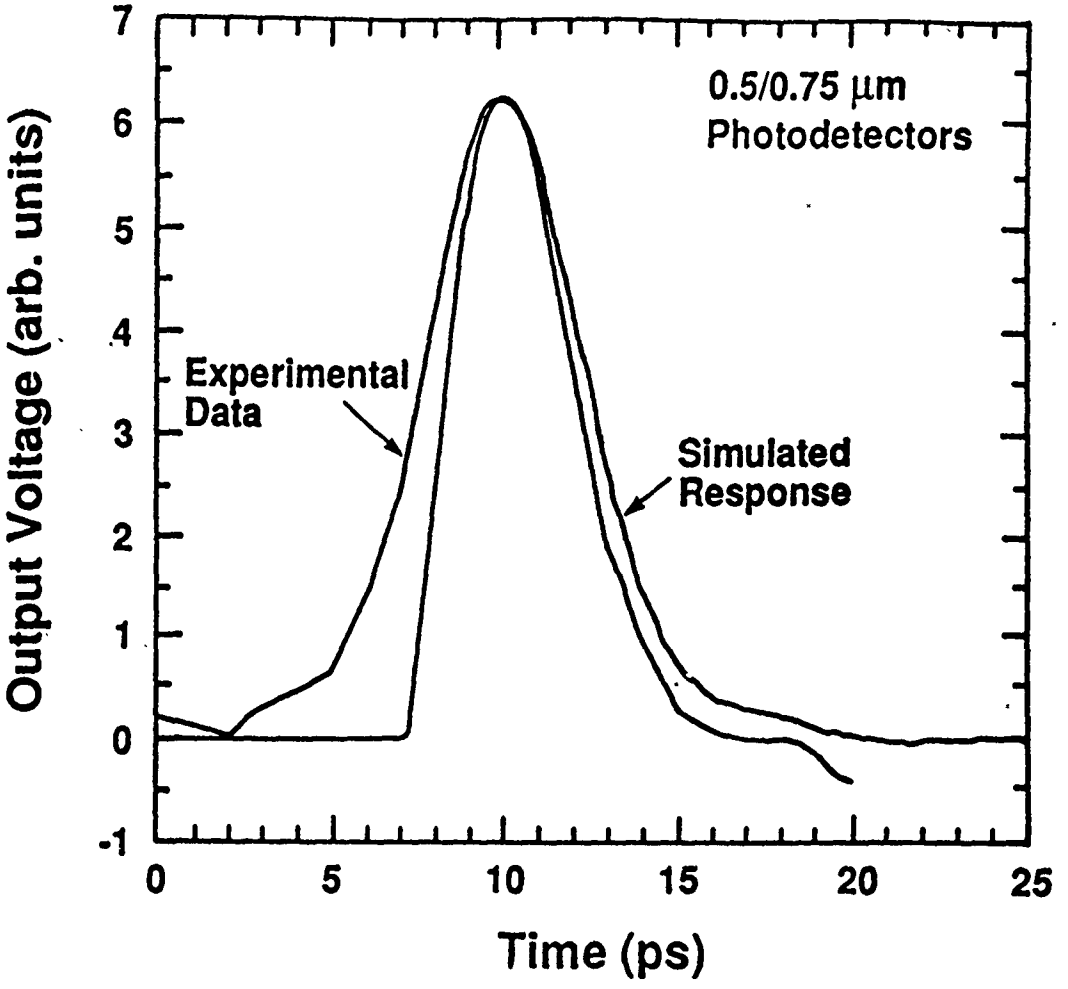

Figure 19. Comparison of experimental response of a GaAs MSM photodetector to its simulated response. The finger width is 0.75 μm and the interfinger spacing is 0.5 μm.

example, the frequency shifts are calculated for GaAs/GaP short-period superlattices, and compared with the existing Raman data of Armelles et al. [56] for the lowest order confined LO modes.

Figure 20 shows a typical schematic drawing for the linear-chain model in a superlattice. As can be seen in the figure, the z axis is chosen as the growth direction of the lattice in this study. Hence, for the longitudinal modes of our interest, the atomic displacement is in the z direction. In the absence of strain, the force constant in each layer is estimated based on the frequencies of corresponding bulk LO modes at the zone center. Thus, the force constant in one layer is modeled independent of the rest of the structure, and is the same as the bulk value of the material. The resulting characteristic equations can predict the frequency shifts due to confinement in LO modes with accuracy.

When a strain is applied, the characteristic equation of motion needs modification to implement the effects of strain. From the analyses of Ganesan et al. [57] and Cerdeira et al. [58], the dynamical equation for the LO modes with $\vec{k}\approx 0$ can be approximated as, to the first order in strain,

$$\bar{m}\ddot{u}_i = -\sum_k K_{ik}u_k = -\left[K_{ii}^{(0)}u_i + \sum_{klm}\frac{\partial K_{ik}}{\partial \varepsilon_{lm}}\varepsilon_{lm}u_k\right] \tag{39}$$

in bulk diamond- and zinc-blende-type semiconductors. Here, u_i is the ith component of the relative displacement of the two atoms in a unit cell; $\bar{m}$ is the reduced mass of the two atoms; $K_{ii}^{(0)} = \bar{m}\omega_o^2$ is the effective bulk force constant for LO modes (ω_o) in the absence of strain; and $\frac{\partial K_{ik}}{\partial \varepsilon_{lm}} = K_{iklm}^{(1)}$ is the change in effective force constant due to an applied strain ε_{lm}. The indices i, k, l, and m represent x, y, or z. In Eq. (39), the effect of mismatched lattice constants is included through ε_{lm} which depends explicitly on the lattice constants. From the symmetry considerations in elasticity theory, it can be shown that in cubic crystals the tensor $K^{(1)}$ has only three independent components [58];

$$K_{xxxx}^{(1)} = K_{yyyy}^{(1)} = K_{zzzz}^{(1)} = \bar{m}p,$$

$$K_{xxyy}^{(1)} = K_{yyzz}^{(1)} = K_{zzxx}^{(1)} = \bar{m}q,$$

$$K_{xyxy}^{(1)} = K_{yzyz}^{(1)} = K_{zxzx}^{(1)} = \bar{m}r.$$

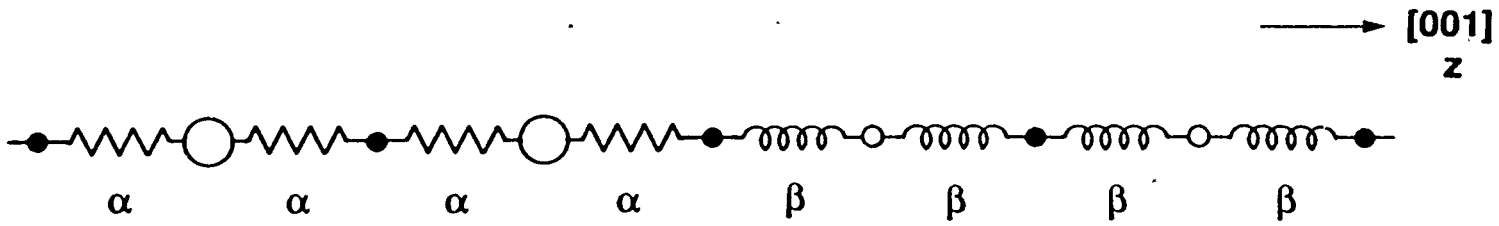

Figure 20. Schematic drawing for the linear-chain model of a superlattice. The z axis is chosen as the growth direction of the lattice, and α and β represent the force constants in each layer.

All other components in which x, y, or z appears an odd number of times become zero. Thus, for the LO modes in the z direction, Eq. (39) can be simplified as

$$\bar{m}\ddot{u}_z = -K_{zz}^{(0)}u_z - \bar{m}\{\, p\varepsilon_{zz} + q(\varepsilon_{xx}+\varepsilon_{yy})\,\}u_z - 2\bar{m}r\varepsilon_{xz}u_x - 2\bar{m}r\varepsilon_{yz}u_y. \tag{40}$$

When the strain is applied along the major crystal axes (i.e., x, y, and z), which is the case for strained-layer structures grown in the <001> direction, the ε_{xz} and ε_{yz} terms vanish and the dynamical equation becomes

$$\bar{m}\ddot{u}_z = -\left[\, K_{zz}^{(0)} + \bar{m}\{\, p\varepsilon_{zz} + q(\varepsilon_{xx}+\varepsilon_{yy})\,\}\right] u_z. \tag{41}$$

As a result, the effect of strain on the effective force constant for LO modes can be obtained as

$$\frac{\Delta K}{K_{zz}^{(0)}} = \frac{\bar{m}}{K_{zz}^{(0)}}\{\, p\varepsilon_{zz} + q(\varepsilon_{xx}+\varepsilon_{yy})\,\} = \frac{1}{\omega_o^2}\{\, p\varepsilon_{zz} + q(\varepsilon_{xx}+\varepsilon_{yy})\,\}. \tag{42}$$

Therefore, within the nearest neighbor approximation, the effects of strain can be included in the linear-chain model for strained-layer structures by modifying the force constants in each layer based on the ratio given in Eq. (42).

It is well established that the strain in individual layers of a strained-layer pseudomorphic superlattice can be calculated by matching up lattice constants in the plane parallel to the heterointerfaces. The resulting biaxial stress subjects each layer under biaxial compressive or tensile strain in the parallel direction, and uniaxial tensile or compressive strain in the perpendicular direction (i.e., along the crystal growth direction). When isolated from the substrate, the lattice constant parallel to the interface $a_{\parallel}$ can be theoretically obtained by minimizing the the elastic energy of each period (i.e., two alternating layers) under the assumption that the lattice mismatch is accommodated by uniform deformation, and is given as follows [59]:

$$a_{\parallel} = a_1\left[\, 1 + \frac{fG_2d_2}{G_1d_1 + G_2d_2}\right] = a_2\left[\, 1 - \frac{fG_1d_1}{G_1d_1 + G_2d_2}\right] \tag{43}$$

where the index 1 (2) represents the layer with smaller (larger) bulk lattice constant a_1 (a_2) respectively, d

is the layer thickness, and f is the mismatch between the two layers. The bulk shear modulus G can be written in terms of elastic constants c_{11}, c_{12} of each material as [59]:

$$G_i = 2\left[c^i_{11} + c^i_{12} - \frac{2(c^i_{12})^2}{c^i_{11}} \right], \quad i = 1,2 . \tag{44}$$

Then, the nonzero components of the strain tensor in each layer are

$$\varepsilon^i_{xx} = \varepsilon^i_{yy} = \frac{a_{\|} - a_i}{a_i}, \quad \varepsilon^i_{zz} = -\left[\frac{2c^i_{12}}{c^i_{11}} \right] \varepsilon^i_{xx}, \quad i = 1,2 . \tag{45}$$

For the strained-layer quantum wells and superlattices coupled to the substrate, the strain is accommodated by only one type of layer. In this case, the thickness of the other layer can be considered very large in Eq. (43). For comparison with other calculations, direct application of Eqs. (42) and (45) to the linear-chain model also results in the frequency shift due to strain in the absence of confinement effects as

$$\Delta\omega^i_\varepsilon = \left[\frac{q_i}{\omega^i_o} + \frac{p_i}{\omega^i_o}\left(\frac{s^i_{12}}{s^i_{11} + s^i_{12}}\right) \right] \varepsilon^i_{xx}, \quad i = 1,2 , \tag{46}$$

which is correct to the first order in strain, where s_{11} and s_{12} are elastic compliances.

The frequencies of LO-phonon modes have been calculated in the GaAs/GaP short-period strained-layer superlattices using the linear-chain model described above. The material parameters for GaAs and GaP used in the calculation can be found in Ref. 60 except the p and q values for GaAs which are from Ref. 61. Two different cases have been considered for the distribution of strain: Table I shows the results when the superlattices are isolated from the substrates and, thus, the strain is accommodated by both GaAs and GaP layers based on their thicknesses (i.e., Eq. (43)); and Table II shows the results when the strain is applied only to the GaP layers (i.e., lattice-matched to the GaAs substrate). In both cases, superlattices with two monolayers of GaP and two, four, and six monolayers of GaAs (i.e., $(GaAs)_2/(GaP)_2$, $(GaAs)_4/(GaP)_2$, and $(GaAs)_6/(GaP)_2$) have been considered. The $\Delta\omega_c$ and $\Delta\omega_s$ terms represent the frequency shifts due to confinement and strain (i.e., Eq. (46)) calculated in the absence of the other respectively, and the values of $\Delta\omega$ are the total shifts obtained by the model presented previ-

Table I. Frequency shifts of confined LO-phonon modes in GaAs/GaP short-period strained-layer superlattices. The strain from lattice mismatch is accommodated based on the assumption that the superlattices are isolated from the substrates. GaAs stands for the GaAs-like LO modes localized in the GaAs layers, and GaP for the GaP-like LO modes localized in the GaP layers. The $\Delta\omega_c$ and $\Delta\omega_s$ terms represent the shifts due to confinement and strain calculated in the absence of the other, respectively, and the values of $\Delta\omega$ are the total shifts obtained by the model presented in the text.

	GaAs (cm^{-1})		GaP (cm^{-1})	
	$\Delta\omega_c+\Delta\omega_s$	$\Delta\omega$	$\Delta\omega_c+\Delta\omega_s$	$\Delta\omega$
$(GaAs)_2/(GaP)_2$	-4.5	-5.7	-22.6	-21.9
$(GaAs)_4/(GaP)_2$	1.1	0.8	-26.9	-26.0
$(GaAs)_6/(GaP)_2$	1.9	1.8	-29.2	-28.2

Table II. Frequency shifts of confined LO-phonon modes in GaAs/GaP short-period strained-layer superlattices. The strain from lattice mismatch is solely applied to the GaP layers. All of the notations are the same as Table I. Therefore, the values of $\Delta\omega_s$ for the GaAs-like modes are zero in this table.

	GaAs (cm^{-1})		GaP (cm^{-1})	
	$\Delta\omega_c+\Delta\omega_s$	$\Delta\omega$	$\Delta\omega_c+\Delta\omega_s$	$\Delta\omega$
$(GaAs)_2/(GaP)_2$	-12.0	-13.0	-36.5	-35.2
$(GaAs)_4/(GaP)_2$	-4.1	-4.3	-36.5	-35.2
$(GaAs)_6/(GaP)_2$	-2.0	-2.1	-36.5	-35.3

ously.

It can be seen from the tables that the coupling effect (~ $|\Delta\omega - (\Delta\omega_c+\Delta\omega_s)|$) is in general small in GaAs/GaP superlattices. With a 3.7 % lattice mismatch, the largest deviation (or coupling) is only 1.3 cm^{-1} approximately, and decreases as the strength of confinement and strain diminishes in each layer as expected. For the GaAs-like mode (i.e., the LO mode localized in the GaAs layer), six monolayers seem to be thick enough to decouple the shifts due to confinement and strain completely. An interesting result, however, is the sign of deviation. As can be seen in Tables I and II, the model predicts a smaller $\Delta\omega$ for the GaAs-like mode (i.e., more negative) and a larger $\Delta\omega$ for the GaP-like mode (i.e., less negative) compared to $\Delta\omega_c+\Delta\omega_s$ respectively. This tendency can be easily explained by a simple picture suggested by the equivalent wave-vector model [62]. Since the lattice constants are matched in the plane parallel to the interfaces and Poisson's ratio has a negative value, the lattice constants in the normal direction to the interface ($a_\perp^{GaAs}$ and $a_\perp^{GaP}$) are not equal and are always larger for the GaAs layers than for the GaP layers (i.e., $a_\perp^{GaAs} > a_\perp^{GaP}$). Thus, the additive term in the denominator of the equivalent wave-vector should be replaced by a term smaller than 1 for the GaAs-like mode ($a_\perp^{GaP}/a_\perp^{GaAs}$) and a term larger than 1 for the GaP-like mode ($a_\perp^{GaAs}/a_\perp^{GaP}$). As a result, the coupling causes a more negative $\Delta\omega$ for the GaAs-like mode and a less negative $\Delta\omega$ for the GaP-like mode compared to $\Delta\omega_c+\Delta\omega_s$, respectively, as mentioned above. Another interesting point is that the confinement effect for the GaP-like mode is insensitive to the thickness of the GaAs layers as shown in Table II. Hence, given the distribution for strain, the phonon modes in a pseudomorphic thin quantum well structure (not a superlattice) can be effectively studied by this model. Unlike GaAs/GaP superlattices, the effect of coupling may be significant in other material systems. Preliminary results show a considerably large deviation of 4 cm^{-1} in a $(GaAs)_2/(InAs)_2$ superlattice.

The calculated data for frequency shift $\Delta\omega$ have been compared with the Raman measurements of Armelles et al. [56]. The results for the GaP-like mode and the GaAs-like mode are plotted in Fig. 21 and Fig. 22 respectively. In these figures, LO_n represents the nth order confined LO mode. The data for the $(GaAs)_6/(GaP)_2$ superlattice in Tables I and II are denoted as #1 of (a) and #2 of (a) respectively. In

addition, the results for a $(GaAs)_6/(GaP)_4$ superlattice are included with two different configurations for the accommodation of strain: #1 of (b) shows the results when the superlattice is isolated from the substrate (which corresponds to #1 of (a)); and #2 of (b) shows the results with a 0.7 % strain in the GaAs layers and a 3.0 % strain in the GaP layers. The strain distributions used to obtain data #2 of (a) and #2 of (b) are identical to those used in the analysis of Armelles et al.; that is, for #2 of (a) all of the 3.7 % strain is in the GaP layers and for #2 of (b) the strain distribution is as described previously. As can be seen from the figures, the calculated data are in good agreement with the Raman measurements. Indeed, the peaks in the Raman spectra are well placed between the calculated results for the two different strain configurations. This level of agreement suggests that the measured frequency shift can be explained by this linear-chain model with a realistic configuration of strain accommodation. Based on the overall comparison between theoretical predictions and experimental data, it is concluded that the only available Raman frequency shift data [56] on GaAs/GaP short-period strained-layer superlattices are better explained by assuming that the superlattices are isolated from the substrates than by assuming that they are lattice matched to the substrates. While this conclusion has not been reached in previous analyses, it is not unreasonable considering the critical thickness for the formation of misfit dislocation near the substrate-superlattice interface. An alternative explanation is that the Raman measurements by Armelles et al. [56] characterized regions of the GaAs/GaP superlattices that were only partially decoupled from the substrate. However, for a more detailed comparison between experimental and theoretical data, further clarification is essential concerning experimental uncertainties such as the depth of Raman probe, inhomogeneities in the strain distribution along the growth direction, and interface roughness.

An effort has been made to investigate higher modes as well. For the $(GaAs)_6/(GaP)_2$ superlattice, the theoretical calculation for the GaAs-like LO_2 modes predicts ~ 287 cm^{-1} (when isolated from the substrate) and ~ 283 cm^{-1} (when lattice matched to the substrate), respectively. The experimental result is ~ 290 cm^{-1} which shows good agreement with the theoretical calculations. The Raman data for the GaP-like higher modes in the $(GaAs)_6/(GaP)_2$ superlattices were not available for comparison. Due to the simplicity of our model, it is expected that the theoretical prediction for the higher modes deteriorates

rapidly as the corresponding equivalent wave-vector increases.

2.2.6 Simulation of Delta-Doped FETs

This work has focused on electron transport and device performance in delta-doped field effect transistor (FET) structures. The superior conduction property of delta-doped FETs over that of conventional (i.e., uniformly doped) FET structures makes this device one of the most promising candidates for ultra-high speed digital and millimeter-wave applications. High electron mobility, reduced DX center concentration, improved threshold controllability, as well as high breakdown voltage are important advantages of delta-doped FETs. Studies of electron transport and electrical characteristics for such devices are both necessary and important.

Our approach to this research project is two-fold; we employ ensemble Monte Carlo simulations for submicron AlGaAs/GaAs delta-doped HEMTs and two-dimensional drift-diffusion simulations for delta-doped GaAs MESFETs. The objective of Monte Carlo simulations is to provide physical insight into the detailed operation of submicron delta-doped HEMTs. Scattering properties, real space transfer and field dependence of active device dimensions, doping concentration and bias conditions are studied to provide better understanding of device operation. A two-dimensional drift-diffusion model is used to analyze the electrical characteristics of a delta-doped GaAs MESFET, providing a general guide for more practical device design. Currently, we have finished the program-development stage and have started to obtain and analyze preliminary data. Two of papers will be submitted to the journals in the near future. We also plan to submit a paper to the 1990 IEDM which will be held in December. The models used in the simulations and the preliminary data will be discussed briefly as follows:

A. Ensemble Monte Carlo Simulation

The ensemble Monte Carlo program is developed to model transport properties of electrons in heterojunction FET structures. In this program, which incorporates a non-parabolic Γ–L–X analytical band structure, the following scattering mechanisms are included: polar optical phonon, intervalley, ion-

ized impurity, electron-electron, and impact ionization. Electrostatic potential and the electric field distribution within a device are evaluated for each field-adjusted time interval by solving the two-dimensional Poisson equation self-consistently. The effect of carrier degeneracy is considered by employing Fermi statistics with calculated local quasi-Fermi level and energy distribution. Real space transfer of electrons between different materials is also included in the program. A weighted injection scheme is used to improve simulation efficiency. Also, an attempt is made to take the effect of surface-defect-related Fermi-level pinning into account. This program is capable of simulating both delta- and uniformly-doped HEMT structure (hereafter, D-HEMT and U-HEMT, respectively). Theoretical calculations and comparisons are performed for AlGaAs/GaAs D-HEMTs and U-HEMTs. The superior performance of the D-HEMT in terms of device structure, doping and bias condition is demonstrated. Comparison with available experimental results will be made to verify this theoretical study.

Distribution of electron concentration, field, drift velocity, energy, and valley occupancy have been calculated for AlGaAs/GaAs D-HEMTs and U-HEMTs with different device feature sizes, doping, and bias conditions. Comparison of electrical characteristics between the two device structures is made based on these calculations. In order to make the comparison on a one-to-one basis, devices with the same channel length and under the same bias are simulated. Doping of both devices are such that they have equivalent total charge when the impurities are fully ionized. Two specified conditions are chosen for study:

(1) both devices have same distance from gate to channel;

(2) both devices have same threshold voltage.

The parameters used in the simulations are summarized in Table III

>From our preliminary results, we can draw the following conclusions:

- For both conditions (1) and (2), the channel electron density of D-HEMT is higher than that of U-HEMT. For U-HEMT in condition (1), this is due to the fact that comparatively higher field is found in the channel near the drain edge of the gate. High electric field causes local electron heating, and heated

electrons with sufficient energy will experience intervalley scattering and real space transfer. Simulation results show that there are more real space transfer events and intervalley scatterings in this case. For U-HEMT in condition (2), decreased electron density in the channel is caused by the low doping in the AlGaAs layer and the longer distance from gate to channel.

- For both conditions, higher current and higher transconductance are obtained for the D-HEMT. This is partly because of the larger channel electron density in D-HEMTs, as discussed above. In addition, higher drift velocity as a result of relatively smaller electric field in the D-HEMT channel (fewer velocity randomizing collisions) further improves device performance. This trend is in accord with a macroscopic consideration from a simple analytical model. Analytical and measurement results show that the threshold voltage for D-HEMT and U-HEMT can be expressed as:

$$\text{D–HEMT}: \quad V_{th} = -qN_d d(w - 0.5d)/\varepsilon \tag{47}$$

$$\text{U–HEMT}: \quad V_{th} = -qN_d w^2/(2\varepsilon)$$

Thus, for parameters given in condition (1), high V_{th} is expected for the U-HEMT, which in turn results in smaller current and transconductance for a given bias condition. For condition (2), longer distance d from the gate to the channel should be used in order to have the same threshold voltage. However, this deceases the controllability of gate voltage on channel electrons and causes decreased transconductance. Within the Gradual Channel Approximation (GCA), the saturation current and transconductance are inversely proportional to the gate-channel distance. Thus, increasing this distance causes degraded performance.

- Simulation results show that as gate voltage increases above 0 V (both devices are in depletion mode), the transconductance decreases even though the channel field is small. This suggests parallel conduction paths exist in the doped AlGaAs layer, where field is much higher and much more impurity scatterings are expected. This effect is more severe in condition (1) for U-HEMT since the electric field in the AlGaAs layer increases greatly as doping increases and distance decreases.

Our results demonstrate the superior conducting property of D-HEMTs over U-HEMTs. Another feature which further degrades U-HEMTs with doping over 1.0×10^{18} cm^{-3} is due to the presence of a deep-level trap (DX center) in the AlGaAs layer, which is believed to be less prevalent in the D-HEMT structures.

B. Two-Dimensional Drift-Diffusion Simulation

In this program, coupled phenomenological semiconductor equations are solved numerically to simulate electrical characteristics of delta-doped and conventional GaAs MESFETs. These equations are: Poisson equation, current continuity equation, and current density equation. A modified two piece velocity-field relation is employed to take current saturation into account. The Fermi distribution is used in the calculation. A Gaussian doping profile is generated to fit measurement of experimental profiles resulting from ion implantation. Distributions of electron concentration, potential, field, and current density are simulated for various operating conditions. Small signal parameters (capacitance, transconductance) are determined to predict device performance. Comparison is made of delta-doped and conventional uniformly-doped MESFET (hereafter, D-MESFET and U-MESFET, respectively) calculations with experimental results. Using a Crank-Nicolson scheme, the program is able to simulate transient performance. Based on this model, current-voltage and capacitance-voltage characteristics can be easily calculated. Good agreement between simulation and measurement is obtained. Parameters used in calculation and from measuremental results are summarized in Table IV.

Our preliminary results suggest the following conclusions:

- Channel length L and gate-to-channel distance d are the two most important dimensional parameters. The transconductance increases as L and d decrease. However, a decrease in gate-to-channel distance increases the channel field and, thus, deteriorates the breakdown voltage. Spacer distance from gate to drain is crucial in determining the maximum electric field, especially for self-aligned structures. By increasing this distance, the maximum field can be reduced. However, at the same time the parasitic series resistance increases which, in turn, reduces the transconductance. Half maximum doping width is

also an important parameter in terms of transconductance. Trade-off should be made among these parameters in device design in order to get optimized performance.

- Increasing maximum (or peak) doping, N_{max}, in D-MESFET increases electron concentration. This is the main contribution to the high current capability of the structure. However, as N_{max} increases, the maximum field increases as well. This will cause reduced drift velocity and sacrifices the transconductance as N_{max} reaches to a critical point. A slight increase of background doping in the cap layer is useful in reducing the electric field in the channel. For D-MESFETs, where the conducting channel is a heavily-doped layer, a decreased field in this layer improves saturation performance.

- Compared with conventional the U-MESFET, the D-MESFET shows improved performance in current capacity and transconductance. The most important feature of D-MESFET is its very high channel carrier concentration (factor of 10 higher than U-MESFET). Generally, electrons in such a heavily-doped region undergo more impurity scatterings and exhibit low mobility. However, at high temperature and high electric-field, from which the electron can gain energy, impurity scattering becomes less significant on overall mobility. Moreover, when the electric field exceeds a critical value, the saturated velocity determines device performance. Both theory and experimental results show that saturated drift velocity does not depend on the low field mobility, i.e. the same saturation velocity for D-MESFET and U-MESFET is expected. Another feature which makes the D-MESFET performance superior to that of the conventional U-MESFET is that for the same gate-to-channel distance, lower maximum electric field is expected because of the linear conduction band edge dependence on gate-to-channel distance. In a conventional U-MESFET, a quadratic dependence of the conduction band edge on the gate-to-channel distance is expected due to its constant doping concentration under the gate. Reduced field improves saturation and breakdown performance.

2.3 Publications and Presentations

During the last year we have made seven oral presentations at national and international conferences. Also, twelve written manuscripts have been published in the refereed literature. In addition, three

other manuscripts have been accepted for publication and eight manuscripts have been submitted or are currently in preparation. The following paragraphs summarize the presentations and publications made under this program during the last year, and include material not previously reported to ONR in the last renewal proposal as well as material which was accepted for publication in 1989 and has since been published in 1990.

A. Conference Presentations and Seminars

D.L. Woolard, J.L. Pelouard, R.J. Trew, M.A. Littlejohn and C.T. Kelly, "Hydrodynamic Hot-Electron Transport Simulations Based on The Monte Carlo Method", presented at the Sixth International Conference on Hot Carriers in Semiconductors, July 23-28, 1989, Scotttsdale, AZ.

L.F. Register, M.A. Littlejohn and M.A. Stroscio, "Polar Optical Phonon Scattering of Charge Carriers in Alloy Semiconductors: Effects of Phonon Localization", presented at the Sixth International Conference on Hot Carriers in Semiconductors, July 23-28, 1989, Scottsdale, AZ.

J.L. Pelouard, M.A. Littlejohn and H.P. Belgal, "Monte Carlo Study of Ballistic and Quasi-Ballistic Electron Transport in Semiconductors," presented at the Sixth International Conference on the Numerical Analysis of Semiconductor Devices and Integrated Circuits, July 11-14, 1989, Dublin, Ireland.

L.F. Register, M.A. Littlejohn and M.A. Stroscio, "Path-Integral Monte Carlo Methods for Ultra-Small Device Applications," presented at the Sixth International Conference on the Numerical Analysis of Semiconductor Devices and Integrated Circuits, July 11-14, 1989, Dublin, Ireland.

M.A. Littlejohn, J.L. Pelouard, W.C. Koscielniak, and D.L. Woolard, "Device Simulation Augmented by the Monte Carlo Method," presented at the Workshop on Computational Electronics, May 21-25, 1990, Univ. of Illinois, Urbana, IL.

D.L. Woolard, M.A. Stroscio, M.A. Littlejohn, R.J. Trew, and H.L. Grubin, "A New Non-parabolic Hydrodynamic Transport Model with Quantum Corrections," presented at the Workshop on Computational Electronics, May 21-25, 1990, Univ. of Illinois, Urbana, IL.

K.W. Kim, M.A. Stroscio, and J.C. Hall, "Frequencies of Confined Longitudinal-Optical Phonon Modes in Short-Period Strained Semiconductor Superlattices," presented at the SPIE International Symposium on Optical & Optoelectronic Applied Science and Engineering, July 8-13, 1990, San Diego, CA.

B. Refereed Publications, Papers Accepted for Publication, and Papers in Preparation

W.C. Koscielniak, J.L. Pelouard and M.A. Littlejohn, "Dynamic Behavior of Photocurrent in a GaAs Metal-Semiconductor-Metal Photodetector with Sub-Half-Micron Electrode Pattern", Appl. Phys. Lett., 54, 567 (1989).

W.C. Koscielniak, M. A. Littlejohn and J. L. Pelouard, "Analysis of a GaAs Metal-Semiconductor-Metal (MSM) Photodetector with 0.1 μm Finger Spacing", IEEE Electron Dev. Lett., 10, 209 (1989).

L.F. Register, M.A. Stroscio and M.A. Littlejohn, "Efficient Path-Integral Monte Carlo Technique for Ultrasmall Device Applications," Superlattices and Microstructures, 6, 233 (1989).

J.L. Pelouard and M.A. Littlejohn, "Indium-Phosphide-Based Heterojunction Bipolar Transistors," Proceedings of the First International Conference on Indium Phosphide and Related Materials for Advanced Electronics and Optical Devices, Proceedings of SPIE-The International Society for Optical Engineering, vol. 1144, p. 582 (1989).

J.L. Pelouard, M.A. Littlejohn and H.P. Belgal, "Monte Carlo Study of Ballistic and Quasi-Ballistic Electron Transport in Semiconductors," Proceedings of the Sixth International Conference on the Numerical Analysis of Semiconductor Devices and Integrated Circuits, edited by J.J. Miller, Boole Press, Ltd., p. 255, Dublin, Ireland (1989).

L.F. Register, M.A. Littlejohn and M.A. Stroscio, "Path Integral Monte Carlo Methods for Ultra-Small Device Applications," Proceedings of the Sixth International Conference on the Numerical Analysis of Semiconductor Devices and Integrated Circuits, edited by J.J. Miller, Boole Press, Ltd., p. 266, Dublin, Ireland (1989).

D.L. Woolard, J.L. Pelouard, R.J. Trew, M.A. Littlejohn and C.T. Kelly, "Hydrodynamic Hot-Electron Transport Simulations Based on the Monte Carlo Method," Solid State Electronics, 32, 1347 (1989).

L.F. Register, M.A. Littlejohn and M.A. Stroscio, "Polar Optical Phonon Scattering of Charge Carriers in Alloy Semiconductors: Effects of Phonon Localization," Solid State Electronics, 32, 1387 (1989).

W.C. Koscielniak, J.L. Pelouard and M.A. Littlejohn, "Intrinsic and Extrinsic Response of GaAs Metal-Semiconductor-Metal Photodetectors," IEEE Photonics Technol. Lett., 2, 125 (1990).

K.W. Kim, M.A. Stroscio, and J.C. Hall, "Frequencies of Confined Longitudinal-Optical Phonon Modes in GaAs/GaP Short-Period Strained-Layer Superlattices," J. Appl. Phys., 67, 6179 (1990).

W.C. Koscielniak, J.L. Pelouard, and M.A. Littlejohn, "Dark-Current Characteristics of GaAs Metal-Semiconductor-Metal (MSM) Photodetectors," IEEE Trans. Electron Devices, ED-37, 1623 (1990).

K.W. Kim, M.A. Stroscio, and J.C. Hall, "Frequencies of Confined Longitudinal-Optical Phonon Modes in Short-Period Strained Semiconductor Superlattices," accepted for publication in the Proceedings of the SPIE International Symposium on Optical & Optoelectronic Applied Science and Engineering, July 1990.

M.A. Stroscio, K.W. Kim, and J.C. Hall, "Variation in Frequencies of Confined Longitudinal-Optical Phonon Modes due to Changes in the Effective Force Constants Near Heterojunction Interfaces," Superlattices and Microstructures, 7, 115 (1990).

M.A. Littlejohn, J.L. Pelouard, W.C. Koscielniak, and D.L. Woolard, "Device Simulation Augmented by the Monte Carlo Method," accepted for publication in the Proceedings of the Workshop on Computational Electronics, May 21-25, 1990, Univ. of Illinois, Urbana, IL.

D.L. Woolard, M.A. Stroscio, M.A. Littlejohn, R.J. Trew, and H.L. Grubin, "A New Non-parabolic Hydrodynamic Transport Model with Quantum Corrections," presented at the Workshop on Computational Electronics, May 21-25, 1990, Univ. of Illinois, Urbana, IL.

K.W. Kim, H. Tian, and M.A. Littlejohn, "Analysis of Delta-Doped and Uniformly-Doped HEMTs by Ensemble Monte Carlo Simulation," to be submitted to IEEE Electron Device Letters.

L.F. Register, M.A. Littlejohn, and M.A. Stroscio, "Comments on Evaluation of Feynman Path Integrals by Analytic Continuation," in preparation - to be submitted to Physical Review B.

L.F. Register, M.A. Stroscio, and M.A. Littlejohn, "Path Integral Monte Carlo Calculation of Carrier Self-Energies," in preparation - to be submitted to Physical Review B.

J.L. Pelouard and M.A. Littlejohn, "The Role of Nearly-Ballistic Transport in the Emitter-Base Junction of HBTs," in preparation - to be submitted to IEEE Transactions on Electron Devices.

J.L. Pelouard and M.A. Littlejohn, "Transport in the Collector-Base Junction of HBTs," in preparation - to be submitted to the IEEE Transactions on Electron Devices.

D.L. Woolard, M.A. Littlejohn, R.J. Trew, and C.T. Kelly "Hydrodynamic Transport Model with Non-Parabolic Energy Bands," in preparation - to be submitted to Physical Review B.

D.L. Woolard, H.L Grubin, M.A. Littlejohn, M.A. Stroscio, and C.T. Kelly "A Comparison of the Wigner Distribution Function Transport Model with the Quantum-Corrected Hydrodynamic Transport Model," in preparation - to be submitted to Superlattices and Microstructures.

H. Tian, K. W. Kim, and M. A. Littlejohn, "Influence of DX Centers and Surface States on Delta-Doped HEMT Performance," in preparation - to be submitted to J. Appl. Phys.

Appendix B contains the title page of those papers which have been published in 1990. Copies of all published papers have been sent to the ONR contract monitor during the last years grant period.

3.0 LIST OF REFERENCES

1. R. Landauer, "Nanostructure Physics: Fashion or Depth," in Nanostructure Physics and Fabrication, edited by M. A. Reed and W. P. Kirk, Academic Press, New York, pp. 17-30, 1989.

2. G. J. Iafrate, "The Physics of Submicron/Ultrasubmicron Dimensions," in Gallium Arsenide Technology, D. K. Ferry, editor-in-chief, Howard Sams and Co., Indianapolis, Chapter 12, pp. 443-489, 1985.

3. Karl Hess and Gerald J. Iafrate, Proc. IEEE 76, 519 (1988).

4. P.D. Dapkus and S.P. DenBaars, IEDM Tech. Digest, pp. 472-474, 1988.

5. R. P. Feynman and A. R. Hibbs, Quantum Mechanics and Path Integrals, McGraw Hill, New York, 1965.

6. K. K. Thornber, "Use of Feynman Path Integrals in Quantum Transport Theory," presented at the Workshop on Quantum Transport Theory with Application to Nanometer Electronics, San Miniato, Italy, March 2-6, 1987.

7. C. K. Williams, T. H. Glisson, J. R. Hauser, M. A. Littlejohn, and M. F. Abusaid, Solid State Electronics 28, 1105, 1985.

8. W.C. Koscielniak, J.L. Pelouard and M.A. Littlejohn, Appl. Phys. Lett. 54, 567 (1989).

9. N.C. Kluksdahl, A.M. Kriman, D.K. Ferry and C. Ringhofer, Phys. Rev. B 39, 7720 (1989).

10. F. Sols, M. Macucci, U. Ravaioli, and K. Hess, Appl. Phys. Lett. 54, 350 (1989).

11. J.L. Pelouard, M.A. Littlejohn, and H. P. Belgal, "Monte Carlo Study of Ballistic and Quasi-Ballistic Transport in Semiconductors," Proceedings of the Sixth International Conference on the Numerical Analysis of Semiconductor Devices and Integrated Circuits, edited by J. J. Miller, Boole Press, Ltd., p. 255, Dublin, Ireland, 1989.

12. R. P. Feynman, Rev. Mod. Phys. 20, 367 (1948).

13. R. P. Feynman, Phys. Rev. 80, 440 (1950).

14. R. P. Feynman, Phys. Rev. 97, 660 (1954).

15. R. P. Feynman, R. W. Hellwarth, C. K. Iddings, and P. Platzman, Phys. Rev. 127, 1004 (1962).

16. K. K. Thornber and R. P. Feynman, Phys. Rev. B 1, 4099 (1969).

17. B. A. Mason and S. Das Sarma, Phys. Rev. B 33, 1412 (1986).

18. B. Gerlach, H. Löwen, and H. Schliffke, Phys. Rev. B 36, 6320 (1987).

19. C. H. Grein and S. John, Phys. Rev. B 36,

20. D. C. Khandekar, K. V. Bhagwat, and S. V. Lawande, Phys. Rev. B 37, 3085 (1988).

21. R. Bruinsma and Per Bak, Phys. Rev. Lett. 56, 420 (1986).

22. M. Nithisoontorn, R. Lassnig, and E. Gornik, Phys. Rev. B 36, 6225 (1987).

23. M. H. Degani and O. Hipolito, Phys. Rev. Lett. 59, 2820 (1987).

24. See, for example, Monte Carlo Methods in Quantum Problems, edited by M. H. Kalos, D. Reidel Publishing Co., Dordrecht, 1984.

25. L. D. Forsdick, J. Math. Phys. 3, 1261 (1962).

26. L. F. Register, M. A. Stroscio, and M. A. Littlejohn, Superlattices and Microstructures 6, 233 (1989).

27. L. D. Forsdick and H. F. Jordan, Phys. Rev. 143, 58 (1966).

28. B. A. Mason and K. Hess, Superlattices and Microstructures 3, 421 (1987).

29. L. F. Register, M. A. Stroscio, and M. A. Littlejohn, Superlattices and Microstructures 4, 61 (1988).

30. J. D. doll, T. L. Beck, and D. L. Freeman, J. Chem. Phys. 89, 5753 (1988).

31. H. B. Schüttler and D. J. Scalapino, Phys. Rev. B 34, 4744 (1986).

32. D. Thirumalai and B. J. Berne, J. Chem. Phys. 79, 5029 (1983).

33. J. D. Doll, R. D. Coalson, and D. L. Freeman, J. Chem. Phys. 87, 1641 (1987).

34. J. Chang and W. H. Miller, J. Chem . Phys. 87, 1648 (1987).

35. M. H. Degani and O. Hipolito, Superlattices and Microstructures 5, 137 (1989).

36. M. Saitoh, J. Phys. Soc. Jpn. 49, 878 (1980).

37. M. H. Degani and O. Hipolito, Solid State Commun. 65, 1185 (1988).

38. A. F. Levi, J. R. Hayes, and R. Bhat, Appl. Phys. Lett. 48, 1609 (1985).

39. A. F. Levi and Y. Yafet, Appl. Phys. Lett. 51, 42 (1987).

40. M. Heiblum, M. I. Nathan, D. C. Thomas, and C. M. Knoedler, Phys. Rev. Lett. 55, 2200 (1985).

41. M. Heiblum, et al., Phys. Rev. Lett. 58, 816 (1987).

42. K. Hess and G. J. Iafrate, Proc. IEEE 76, 519 (1988).

43. R. J. Trew, R. Sultan, J. R. Hauser, and M. A. Littlejohn, in The Physics of Submicron Structures edited by H. L. Grubin, K. Hess, G. J. Iafrate, and D. K. Ferry, New York, Plenum Press, pp. 177-183, 1984.

44. J.-L. Pelouard and M. A. Littlejohn, "Indium-Phosphide-Based Heterojunction Bipolar Transistors," Proceedings of SPIE-The International Society for Optical Engineering, vol. 1144, p. 582, .989.

45. E. H. Rhoderick, Metal-Semiconductor Contacts, Oxford, Clarendon Press, Chapter 3, pp. 77-96, 1978.

46. H. P. Belgal, Unpublished M.S. Thesis, N. C. State University, June, 1989.

47. D.L. Woolard, et al., Solid State Electronics 31, 371 (1988).

48. D.L. Woolard, et al., Solid State Electronics 32, 1347 (1989).

49. H.L. Grubin and J.P. Kreskovsky, Solid State Electronics 32, 1071 (1989).

50. M. A. Stroscio, Superlattices and Microstructures 2, 83 (1986).

51. M.G. Ancona and G.J. Iafrate, Phys. Rev. B 39, 9536 (1989).

52. W.C. Koscielniak, M.A. Littlejohn and J.L. Pelouard, IEEE Electron Device Lett. 10, 209 (1989).

53. W.C. Koscielniak, J.L. Pelouard, and M.A. Littlejohn, IEEE Photonics Technol. Lett. 2, 125 (1990).

54. W.C. Koscielniak, J.L. Pelouard, and M.A. Littlejohn, IEEE Trans. Electron Devices ED-37, 1623 (1990).

55. B.J. Van Zebhbroeck, W. Patrick, J.M. Halbout, and P. Vettiger, IEEE Electron Device Lett. 9, 527 (1988).

56. G. Armelles, M. Recio, A. Ruiz, and F. Briones, Solid State Commun. 71, 431 (1989).

57. S. Ganesan, A. A. Maradudin, and J. Oitmaa, Ann. Phys. (N.Y.) 56, 556 (1970).

58. F. Cerdeira, C. J. Buchenauer, F. H. Pollak, and M. Cardona, Phys. Rev. B 5, 580 (1972).

59. G. C. Osbourn, J. Appl. Phys. 53, 1586 (1982).

60. Landolt-Börnstein Tables, edited by O. Madelung (Springer, Berlin, 1982), Group III, Vol. 17a.

61. B. A. Weinstein and M. Cardona, Phys. Rev. B 5, 3120 (1972).

62. A. K. Sood, J. Menendez, M. Cardona, and K. Ploog, Phys. Rev. Lett. 54, 2111 (1985).

63. U. Ascher, "Collocation Software for Boundary-Value ODEJ," ACM Transactions on Mathematical Software, vol. 17, no. 4, June 1987.

64. H. B. Keller, "Continuation and Bifurcation in Scientific Computing," lecture notes, 1988.

65. D. L. Smith and C. Mailhiot, J. Appl. Phys. 63, 2717 (1988).

66. E. A. Carridi, T. Y. Chang, K. W. Goossen, and L. F. Eastman, Appl. Phys. Lett. 56, 659 (1990).

67. M. D. Jaffe, Y. Sekiguchi, J. Singh, Y. J. Chen, D. Pavlidis, and M. Quillec, Proc. IEEE/Cornell Conf., pp. 70-79, 1987.

68. See, for example, Jose Menendez, J. Lumin. 44, 285 (1989).

69. G. J. Sullivan, P. M. Ashbeck, M. F. Chang, D. L. Miller, and K. C. Wang, Electron. Lett. 22, 419 (1986).

70. T. P. E. Broekaert, W. Lee, and C. G. Fonstad, Appl. Phys. Lett. 53, 1545 (1988).

71. C. E. C. Wood, G. Metze, J. Berry, and L. F. Eastman, J. Appl. Phys. 51, 383 (1980).

72. E. F. Schubert, A. Fischer, and K. Ploog, IEEE Trans. Electron Devices ED-33, 625 (1986).

4.0 PERSONNEL

Two faculty members in the Electrical and Computer Engineering Department at N.C. State University have been supported by this program during the last reporting period. These faculty members are Dr. M.A. Littlejohn and Dr. K.W. Kim. Dr. Kim joined the NCSU faculty in August, 1988 after completing his Ph.D. degree at the University of Illinois under the direction of Prof. Karl Hess. In addition, Dr. J.R. Hauser and Dr. T.H. Glisson served as consultants on this program without ONR funding. They both have been involved in advising graduate students working on this research. Currently Dr. Glisson serves as the Associate Dean of Academic Affairs in the College of Engineering. Dr. Hauser has recently assumed major technical and administrative responsibilities with the newly - formed NSF Engineering Research Center for Advanced Electronic Materials Processing. Both these former investigators on this ONR project have retained a high degree of technical involvement.

Drs. Littlejohn and Kim serve as co-principal investigators on this research effort. Their resumes are in Appendix C. They are responsible for day-to-day management and direction of the research program aspects. Three graduate students have been supported on this program, and we plan to add a fourth student during the fall semester.

Appendix A

LIST OF REFEREED PUBLICATIONS ON THIS PROGRAM SINCE 1975

1. M. A. Littlejohn, J. R. Hauser, and T. H. Glisson, "Monte Carlo Calculation of Transport Properties of GaN", Appl. Phys. Letters, 26, 625 (1975).

2. J. R. Hauser, M. A. Littlejohn, and T. H. Glisson, "Velocity-Field Relationship for InAs-InP Alloys Including the Effects of Alloy Scattering", Appl. Phys. Letters, 28, 458 (1976).

3. J. W. Harrison and J. R. Hauser, "Theoretical Calculations of Electron Mobility in Ternary III-V Compounds", Jour. Appl. Phys., 47, 292 (1976).

4. J. W. Harrison and J. R. Hauser, "Alloy Scattering in Ternary III-V Compounds", Phys. Rev. B, 13, 5347 (1976).

5. M. A. Littlejohn, J. R. Hauser and T. H. Glisson, "Velocity-Field Characteristics of $Ga_{1-x}In_xP_{1-y}As_y$ Quaternary Alloys", Appl. Phys. Letters, 30, 242 (1977).

6. M. A. Littlejohn, J. R. Hauser, and T. H. Glisson, "Velocity-Field Characteristics of GaAs with Γ_6c–L_6c–X_6c Conduction Band Ordering", Jour. Appl. Phys., 48, 4587 (1977).

7. M. A. Littlejohn, J. R. Hauser, T. H. Glisson, and L. A. Arledge, "High Field Transport and MESFET Performance in Ternary and Quaternary III-V Semiconductors", Proceedings Sixth Biennial Cornell Electrical Engineering Conference: Active Microwave Semiconductor Devices and Circuits, Cornell University, Ithaca, NY, pp. 55-64, August, 1977.

8. T. H. Glisson, J. R. Hauser, M. A. Littlejohn and Williams, "Energy Bandgap and Lattice Constant Contours of III-V Quaternary Alloys", Jour. Electron. Mater. 7, 1 (1978).

9. M. A. Littlejohn, J. R. Hauser, T. H. Glisson, D. K. Ferry, and J. W. Harrison, "Alloy Scattering and High Field Transport in Ternary and Quaternary III-V Semiconductors", Solid-State Electron. 21, 107 (1978).

10. C. K. Williams, T. H. Glisson, J. R. Hauser, and M. A. Littlejohn, "Energy Bandgap and Lattice Constant Contours of III-V Quaternary Alloys of the Form $A_xB_yC_zD$ or $AB_xC_yD_z$", Jour. Electron. Mater. 7, 639 (1978).

11. M. A. Littlejohn, R. Sadler, T. H. Glisson, and J. R. Hauser, "Carrier Compensation and Alloy Scattering in $Ga_{1-x}In_xP_{1-y}As$ Grown by Liquid Phase Epitaxy", Inst. Phys. Conf. Ser. 45, 239 (1979).

12. M. A. Littlejohn, "III-V Compound Semiconductors for Future Electronic Devices", IEEE Conference Record: Proceedings of the Third Biennial University/Government/Industry Microelectronics Symposium, Lubbock, TX, May 21-23, 1979, pp. 6-8.

13. J. R. Hauser, T. H. Glisson, and M. A. Littlejohn, "Peak Velocity and Negative Resistance in the Central (000) Valley of III-V Semiconductors", Solid-State Electron, 22, 487 (1979).

14. H. L. Grubin, D. K. Ferry, J. R. Barker, M. A. Littlejohn, T. H. Glisson, and J. R. Hauser, "Transient Relaxation Effects in Transferred Electron Devices", Proceedings of the Seventh Biennial Cornell Electrical Engineering Conference: Active Microwave Semiconductor Devices and Circuits, Cornell University, Ithaca, NY, pp. 413-422, August, 1979.

15. M. A. Littlejohn, L. A. Arledge, T. H. Glisson, and J. R. Hauser, "The Influence of Central Valley Effective Mass and Alloy Scattering on Transient Velocity in $Ga_{1-x}In_xP_{1-y}As_y$", Electron. Lett., 15, 586 (1979).

16. J. B. Restorff, Bland Houston, R. S. Allsaier, M. A. Littlejohn, and S. Phatak, "The Electron Effective Mass in $In_{1-x}Ga_xAs_yP_{1-y}$ From Shubnikov-de Haas Measurements", Jour. Appl. Phys. 51, 2277 (1980).

17. R. A. Sadler, T. H. Glisson, J. R. Hauser, and M. A. Littlejohn, "Circuit Effects in Time-of-Flight Diffusivity Measurements", Solid-State Electronics, 23, 627 (1980).

18. T. H. Glisson, J. R. Hauser, M. A. Littlejohn, K. Hess, B. G. Streetman, and H. Shichijo, "Monte Carlo Simulation of Real-Space Transfer in GaAs-AlGaAs Heterostructures", Jour. Appl. Phys. 51, 5445 (1980).

19. S. Fujita, S. M. Bedair, M. A. Littlejohn, and J. R. Hauser, "Doping Characteristics and Electrical Properties of Be-doped p-type $Al_xGa_{1-x}As$ by Liquid Phase Epitaxy", Jour. Appl. Phys. 51, 5438 (1980).

20. Y. Takeda, M. A. Littlejohn, and J. R. Hauser, "Electron Hall Mobility Calculations and Alloy Scattering in $Ga_{.47}In_{.53}As$", Electron Lett., 17, 377 (1981).

21. Y. Takeda, M. A. Littlejohn, and J. R. Hauser, "Electron Hall Mobility in $Ga_xIn_{1-x}As_yP_{1-y}$ Calculated with Two-LO-Phonon Model", Appl. Phys. Lett., 39, 620 (1981).

22. Y. Takeda, M. A. Littlejohn, J. A. Hutchby, and R. J. Trew, "Electron Concentration and Alloy Composition Dependence of Hall Factor in $Ga_xIn_{1-x}As_yP_{1-y}$", Electron. Lett., 17, 686 (1981).

23. Y. Takeda and M. A. Littlejohn, "Electron Concentration Dependence of Hall Factor $In_{.53}Ga_{.47}As$", Appl. Phys. Lett., 40, 251 (1982).

24. T. H. Glisson, C. K. Williams, J. R. Hauser, and M. A. Littlejohn, "Transient Response of Electron Transport in GaAs Using the Monte Carlo Method", in VLSI Electronics: Microstructure Science, Vol. IV, pp. 99-145, Academic Press, New York, 1982.

25. Y. Takeda, M. A. Littlejohn, J. A. Hutchby, and R. J. Trew, "Effects of Two-LO-Phonon Modes on Electron Distribution in $Ga_xIn_{1-x}As_yP_{1-y}$", Appl. Phys. Lett., 40, 836 (1982).

26. M. A. Littlejohn, T. H. Glisson, and J. R. Hauser, "Hot Electron Transport in n-Type $Ga_{1-x}In_xAs_yP_{1-y}$ Alloys Lattice-Matched to InP", GaInAsP Alloys Semiconductors, edited by T. P. Pearsall, Chapter 10, pp. 243-274, John Wiley and Sons, London, 1982.

27. M. A. Littlejohn, R. J. Trew, J. R. Hauser, and J. M. Golio, Electron Transport in Planar Doped Barrier Structures Using An Ensemble Monte Carlo Method", Jour. Vac. Sci. Technol. B, 1, 449 (1983).

28. M. A. Littlejohn, W. M. Kwapien, T. H. Glisson, J. R. Hauser, and K. Hess, "Effects of Band Bending on Real Space Transfer in a GaAs/GaAlAs Layered Heterostructure", Jour. Vac. Sci. Technol. B, 1, 445 (1983).

29. C. K. Williams, T. H. Glisson, M. A. Littlejohn, and J. R. Hauser, "Ballistic Transport in GaAs", IEEE Electron Device Letters, EDL-4, 161 (1983).

30. R. J. Trew, R. Sultan, J. R. Hauser, and M. A. Littlejohn, "Ensemble Monte Carlo Studies of High Field Spikes and Planar Doped Barrier Devices", The Physics of Submicron Structures, H. L. Grubin, K. Hess, G. J. Iafrate, and D. K. Ferry, Ed., pp. 177-183, Plenum Press, 1984.

31. C. K. Williams, T. H. Glisson, J. R. Hauser, M. A. Littlejohn, and M. F. Abusaid, "Two-Dimensional Monte Carlo Simulation of A Submicron GaAs MESFET With A Non-Uniformly Doped Channel", Solid-State Electronics, 28, 1105 (1985).

32. J. M. Golio, J. R. Hauser, and P. K. Blakey, "A Large-Signal GaAs MESFET Model Implemented on SPICE," IEEE Trans. on Circuits and Devices, 1, 21 (1985).

33. L. W. Massengill, T. H. Glisson, J. R. Hauser, and M. A. Littlejohn, "Transient Transport in Central-Valley-Dominated Ternary III-V Alloys", Solid State Electronics, September, 29, p. 725 (1986).

34. J. R. Hauser, M. A. Littlejohn, and T. H. Glisson, "Recent Monte Carlo Studies of Transport in Semiconductor Devices", Physics of Semiconductor Devices: Proceedings of the 2nd International Workshop, pp. 526-533, Tata McGraw Hill, Delhi India, 1986 (U.S. edition).

35. J. R. Hauser, C. K. Williams, M. F. Abusaid, T. H. Glisson, and M. A. Littlejohn, "Two-Dimensional Monte Carlo Simulation of GaAs FETs", Large-Scale

Computational Device Modeling, University of Illinois, K. Hess, editor, pp. 65-72, 1986.

36. C. K. Williams, M. A. Littlejohn, T. H. Glisson, and J. R. Hauser, "Monte Carlo, Simulation of the Hall Effect in Degenerate GaAs", Superlattices and Microstructures, 2, 201 (1986).

37. M. F. Abusaid and J. R. Hauser, "Calculations of High Speed Performance For Sub-Micron Ion Implanted GaAs MESFET Device", IEEE Trans. on Elec. Dev., ED-33 913 (1986).

38. M. F. Abusaid and J. R. Hauser, "A Comparative Analysis of GaAs and Si Ion-Implanted MESFET's", IEEE Trans. on Elec. Dev., ED-33, 908 (1986).

39. L. F. Register, M. A. Littlejohn, and M. A. Stroscio, "Feynman Path Integral Study of Confined Carriers Subject to Statistical Potentials", Solid-State Electronics, 31, 563 (1988).

40. D. L. Woolard, R. J. Trew, and M. A. Littlejohn, "Hydrodynamic Hot-Electron Transport Model With Monte Carlo-Generated Transport Parameters", Solid-State Electronics, 31, 571 (1988).

41. L. F. Register, M. A. Stroscio, and M. A. Littlejohn, "Numerical Evaluation of the Feynman Integral-Over-Paths In Real and Imaginary Time", Superlattices and Microstructures, 4, 61 (1988).

42. M. F. Abusaid, C. K. Williams, M. A. Littlejohn, J. R. Hauser, and T. H. Glisson, "Hot Electron Transport in Compound Semiconductor Device Modeling", accepted for publication in Physics of Semiconductor Devices: Proceedings of the 3rd International Workshop.

43 K. F. Brennan, D. H. Park, K. Hess, and M. A. Littlejohn, "Theory of the Velocity-Field Relation in AlGaAs", Journal of Applied Physics, 63, 5004 (1988).

44. W. C. Koscielniak, R. M. Kolbas, and M. A. Littlejohn, "Photocurrent Enhancement in a GaAs Metal-Semiconductor-Metal Photodetector Due To Ultra-Small Au Islands, Appl. Phys. Lett., 52, 987 (1988).

45. W. C. Koscielniak, R. M. Kolbas and M. A. Littlejohn, "Performance of a Near-Infrared GaAs Metal-Semiconductor-Metal Photodetector with Islands", IEEE Electron Dev. Lett., 9, 458 (1988).

46. W. C. Koscielniak, J. L. Pelouard and M.A. Littlejohn, "Dynamic Behavior of Photocurrent in a GaAs Metal-Semiconductor-Metal Photodetector with Sub-Half-Micron Electrode Pattern", Appl. Phys. Lett., 54, 567 (1989).

47. W.C. Koscielniak, M.A. Littlejohn, and J.L. Pelouard, "Analysis of a GaAs Metal-Semiconductor-Metal (MSM) Photodetector with 0.1 μm Finger Spacing", IEEE Electron Dev. Lett., 10, 209 (1989).

48. L.F. Register, M.A. Stroscion, and M.A. Littlejohn, "Efficient Path-Integral Monte Carlo Technique for Ultrasmall Device Applications," Superlattices and Microstructures, 6, 233 (1989).

49. J.L. Pelouard and M.A. Littlejohn, "Indium-Phosphide-Based Heterojunction Bipolar Transistors," Proceedings of the First International Conference on Indium Phosphide and Related Materials for Advanced Electronics and Optical Devices, Proceedings of SPIE-The International Society for Optical Engineering, vol. 1144, p. 582 (1989).

50. J.L. Pelouard, M.A. Littlejohn and H.P. Belgal, "Monte Carlo Study of Ballistic and Quasi-Ballistic Electron Transport in Semiconductors," Proceedings of the Sixth International Conference on the Numerical Analysis of Semiconductor Devices and Integrated Circuits, edited by J.J. Miller, Boole Press, Ltd., p. 255, Dublin, Ireland (1989).

51. L.F. Register, M.A. Littlejohn and M.A. Stroscio, "Path Integral Monte Carlo Methods for Ultra-Small Device Applications," Proceedings of the Sixth International Conference on the Numerical Analysis of Semiconductor Devices and Integrated Circuits, edited by J.J. Miller, Boole Press, Ltd., p. 266, Dublin, Ireland (1989).

52. D.L. Woolard, J.L. Pelouard, R.J. Trew, M.A. Littlejohn and C.T. Kelly, "Hydrodynamic Hot-Electron Transport Simulations Based on the Monte Carlo Method," Solid State Electronics, 32, 1347 (1989).

53. L.F. Register, M.A. Littlejohn and M.A. Stroscio, "Polar Optical Phonon Scattering of Charge Carriers in Alloy Semiconductors: Effects of Phonon Localization," Solid State Electronics, 32, 1387 (1989).

54. W.C. Koscielniak, J.L. Pelouard and M.A. Littlejohn, "Intrinsic and Extrinsic Response of GaAs Metal-Semiconductor-Metal Photodetectors," IEEE Photonics Technol. Lett., 2, 125 (1990).

55. K.W. Kim, M.A. Stroscio, and J.C. Hall, "Frequencies of Confined Longitudinal-Optical Phonon Modes in GaAs/GaP Short-Period Strained-Layer Superlattices," J. Appl. Phys., 67, 6179 (1990).

56. W.C. Koscielniak, J.L. Pelouard, and M.A. Littlejohn, "Dark-Current Characteristics of GaAs Metal-Semiconductor-Metal (MSM) Photodetectors," IEEE Trans. Electron Devices, ED-37, 1623 (1990).

57. K.W. Kim, M.A. Stroscio, and J.C. Hall, "Frequencies of Confined Longitudinal-Optical Phonon Modes in Short-Period Strained Semiconductor Superlattices," accepted for publication in the Proceedings of the SPIE International Symposium on Optical & Optoelectronic Applied Science and Engineering, July, 1990.

58. M.A. Stroscio, K.W. Kim, and J.C. Hall, "Variation in Frequencies of Confined Longitudinal-Optical Phonon Modes due to Changes in the Effective Force Constants Near Heterojunction Interfaces," Superlattices and Microstructures, 7, 115 (1990).

59. M.A. Littlejohn, J.L. Pelouard, W.C. Koscielniak, and D.L. Woolard, "Device Simulation Augmented by the Monte Carlo Method," accepted for publication in the Proceedings of the Workshop on Computational Electronics, May 21-25, 1990, Univ. of Illinois, Urbana, IL.

60. D.L. Woolard, M.A. Stroscio, M.A. Littlejohn, R.J. Trew, and H.L. Grubin, "A New Non-parabolic Hydrodynamic Transport Model with Quantum Corrections," presented at the Workshop on Computational Electronics, May 21-25, 1990, Univ. of Illinois, Urbana, IL.

61. K.W. Kim, H. Tian, and M.A. Littlejohn, "Analysis of Delta-Doped and Uniformly-Doped HEMTs by Ensemble Monte Carlo Simulation," submitted to IEEE Electron Device Letters.

62. L.F. Register, M.A. Littlejohn, and M.A. Stroscio, "Comments on Evaluation of Feynman Path Integrals by Analytic Continuation," in preparation - to be submitted to Physical Review B.

63. L.F. Register. M.A. Stroscio, and M.A. Littlejohn, "Path Integral Monte Carlo Calculation of Carrier Self-Energies," in preparation - to be submitted to Physical Review B.

64. J.L. Pelouard and M.A. Littlejohn, "The Role of Nearly-Ballistic Transport in the Emitter-Base Junction of HBTs," in preparation - to be submitted to IEEE Transactions on Electron Devices.

65. J.L. Pelouard and M.A. Littlejohn, "Transport in the Collector-Base Junction of HBTs," in preparation - to be submitted to the IEEE Transactions on Electron Devices.

66. D.L. Woolard, M.A. Littlejohn, R.J. Trew, and C.T. Kelly "Hydrodynamic Transport Model with Non-Parabolic Energy Bands," in preparation - to be submitted to Physical Review B.

67. D.L. Woolard, H.L Grubin, M.A. Littlejohn, M.A. Stroscio, and C.T. Kelly "A Comparison of the Wigner Distribution Function Transport Model with the Quantum-Corrected Hydrodynamic Transport Model," in preparation - to be submitted to Superlattices and Microstructures.

68. H. Tian, K. W. Kim, and M. A. Littlejohn, Influence of DX Centers and Surface States on Delta-Doped HEMT Performance," in preparation - to be submitted to J. Appl. Phys.

Appendix B

This appendix contains the title page of each paper published in the refereed literature which were supported on the ONR project during the 1989 contract period. Copies of these papers have been sent to the program manager under separate cover. A list of these papers is included below.

1) W. C. Koscielniak, J. L. Pelouard and M.A. Littlejohn, "Dynamic Behavior of Photocurrent in a GaAs Metal-Semiconductor-Metal Photodetector with Sub-Half-Micron Electrode Pattern", Appl. Phys. Lett., 54, 567 (1989).

2) W.C. Koscielniak, M.A. Littlejohn, and J.L. Pelouard, "Analysis of a GaAs Metal-Semiconductor-Metal (MSM) Photodetector with 0.1 μm Finger Spacing", IEEE Electron Dev. Lett., 10, 209 (1989).

3) L.F. Register, M.A. Stroscion, and M.A. Littlejohn, "Efficient Path-Integral Monte Carlo Technique for Ultrasmall Device Applications," Superlattices and Microstructures, 6, 233 (1989).

4) J.L. Pelouard and M.A. Littlejohn, "Indium-Phosphide-Based Heterojunction Bipolar Transistors," Proceedings of the First International Conference on Indium Phosphide and Related Materials for Advanced Electronics and Optical Devices, Proceedings of SPIE-The International Society for Optical Engineering, vol. 1144, p. 582 (1989).

5) J.L. Pelouard, M.A. Littlejohn and H.P. Belgal, "Monte Carlo Study of Ballistic and Quasi-Ballistic Electron Transport in Semiconductors," Proceedings of the Sixth International Conference on the Numerical Analysis of Semiconductor Devices and Integrated Circuits, edited by J.J. Miller, Boole Press, Ltd., p. 255, Dublin, Ireland (1989).

6) L.F. Register, M.A. Littlejohn and M.A. Stroscio, "Path Integral Monte Carlo Methods for Ultra-Small Device Applications," Proceedings of the Sixth International Conference on the Numerical Analysis of Semiconductor Devices and Integrated Circuits, edited by J.J. Miller, Boole Press, Ltd., p. 266, Dublin, Ireland (1989).

7) D.L. Woolard, J.L. Pelouard, R.J. Trew, M.A. Littlejohn and C.T. Kelly, "Hydrodynamic Hot-Electron Transport Simulations Based on the Monte Carlo Method," Solid State Electronics, 32, 1347 (1989).

8) L.F. Register, M.A. Littlejohn and M.A. Stroscio, "Polar Optical Phonon Scattering of Charge Carriers in Alloy Semiconductors: Effects of Phonon Localization," Solid State Electronics, 32, 1387 (1989).

9) W.C. Koscielniak, J.L. Pelouard and M.A. Littlejohn, "Intrinsic and Extrinsic Response of GaAs Metal-Semiconductor-Metal Photodetectors," IEEE Photonics Technol. Lett., 2, 125 (1990).

10) K.W. Kim, M.A. Stroscio, and J.C. Hall, "Frequencies of Confined Longitudinal-Optical Phonon Modes in GaAs/GaP Short-Period Strained-Layer Superlattices," J. Appl. Phys., 67, 6179 (1990).

11) W.C. Koscielniak, J.L. Pelouard, and M.A. Littlejohn, "Dark-Current Characteristics of GaAs Metal-Semiconductor-Metal (MSM) Photodetectors," IEEE Trans. Electron Devices, ED-37, 1623 (1990).

12) M.A. Stroscio, K.W. Kim, and J.C. Hall, "Variation in Frequencies of Confined Longitudinal-Optical Phonon Modes due to Changes in the Effective Force Constants Near Heterojunction Interfaces," Superlattices and Microstructures, 7, 115 (1990).

Dynamic behavior of photocarriers in a GaAs metal-semiconductor-metal photodetector with sub-half-micron electrode pattern

W. C. Koscielniak, J. L. Pelouard,[a] and M. A. Littlejohn
Department of Electrical and Computer Engineering, North Carolina State University, P. O. Box 7911, Raleigh, North Carolina 27695

(Received 26 September 1988; accepted for publication 22 November 1988)

Simulation results of the temporal evolution of photocurrent in an interdigitated GaAs metal-semiconductor-metal photodetector are presented. The dependence of response time on the distance between fingers (0.1 and 0.25 μm) is investigated. The solutions of the time-dependent Schrödinger equation and ensemble Monte Carlo calculations are employed. For a device with 0.1 μm finger spacing, the response time of an intrinsic detector is less than 2 ps, with hole current decay being the major limiting factor. The role of parasitics is shown to significantly increase the simulated response time.

It has recently been shown that GaAs metal-semiconductor-metal (MSM) photodetectors[1-5] can be used as high performance optical detectors in the 0.8–0.87 μm wavelength range. High bandwidth monolithic optoelectronic receivers using MSM photodetectors have already been demonstrated.[6-10] Because of the demand for even faster circuits, there is a need for numerically simulated results, especially for detectors with dimensions even smaller than those considered previously.[5]

In this letter we report theoretical results on the dynamic behavior of photogenerated carriers in GaAs MSM photodetectors with sub-half-micron finger spacings. The time evolution of photocurrent is calculated for detectors with a 0.1 and 0.25 μm distance between metal fingers. The detrimental influence of the extrinsic circuit elements on the device speed is also shown.

The GaAs MSM photodetector is shown schematically in Fig. 1(a). The device is modeled as a one-dimensional structure having an active layer of length L with two ideal Schottky barrier contacts. The background doping level in the active layer was chosen to be 5×10^{14} cm^{-3} (n type). Direct-write electron beam lithography can be used to expose such a sub-half-micron interdigitated finger pattern. Because of the low doping concentration, the optically sensitive regions between the fingers are completely depleted even at very small bias voltages. Thus we may draw the energy-band diagram as shown in Fig. 1(b). Under somewhat simplifying conditions, we assume that carriers are generated halfway between the fingers with a Gaussian spatial distribution.

We have employed two different methods to predict time responses. A quantum mechanical analysis uses numerical solutions of the time-dependent Schrödinger equation in the effective mass approximation. The self-consistent Monte Carlo simulation used in this study is described elsewhere,[11] and employs a set of GaAs parameters published previously.[12] Neither quantum effects (tunneling) nor external parasitic effects (capacitance) have been included in this simulation. The boundary conditions assume the continuity of the quasi-Fermi level through the metal-semiconductor interface for each carrier under reverse bias. Because the barrier heights for electrons and holes (ϕ_e and ϕ_h, respectively) are much larger than kT, the current densities due to injected carriers from the metal into the semiconductor are negligible.

The solutions of the time-dependent Schrödinger wave equation for an electron and a hole are shown in Figs. 2(a)

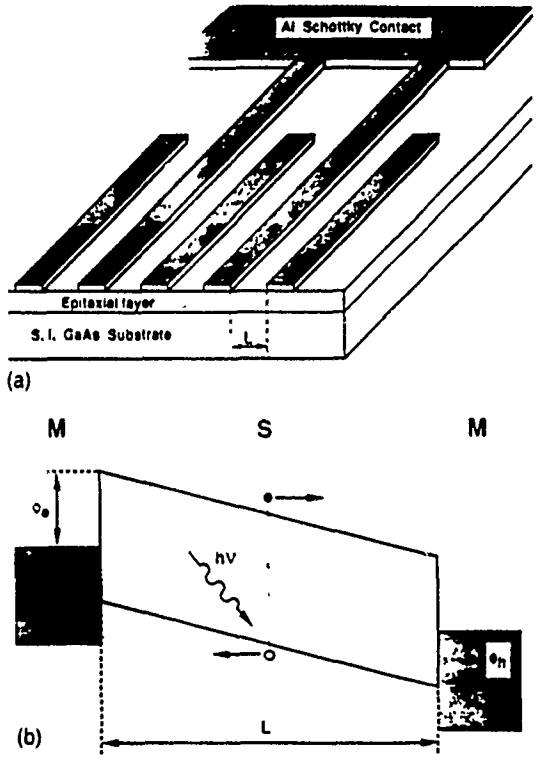

FIG. 1. (a) Schematic view of an interdigitated GaAs MSM photodetector. The distance between fingers is equal to L. (b) Energy band diagram of a detector under bias. The initial ($t=0$) distributions of photocarriers are Gaussian centered in the middle of the device. The initial energies of electrons and holes are 1 and 1 meV, respectively.

[a] Permanent address: Laboratoire de Microstructures et de Microelectonique (CNRS), 196 avenue Henri Ravéra, 92220 Bagneux, France.

 0003-6951/89/060567-03$01.00 © 1989 American Institute of Physics

Analysis of a GaAs Metal–Semiconductor–Metal (MSM) Photodetector with 0.1-μm Finger Spacing

WACLAW C. KOSCIELNIAK, MICHAEL A. LITTLEJOHN, MEMBER, IEEE, AND JEAN-LUC PELOUARD

Abstract—**The temporal response of a GaAs metal-semiconductor-metal (MSM) photodetector with a finger spacing of 0.1 μm has been analyzed. The intrinsic detector has been found to have a minor effect (25-percent increase) on the full width at half-maximum (FWHM) of the temporal response of the device and its parasitic circuit elements. The analysis indicates that a long time constant due to the decay of holes is solely responsible for this increase. The smallest FWHM for this detector is estimated to be less than 2.5 ps.**

I. Introduction

APPLICATIONS of a GaAs metal-semiconductor-metal (MSM) photodetector have been demonstrated by several researchers [1]–[5]. Recently, photodetectors with a very short response time and a high quantum efficiency have been realized [3], [6]. The 0.8–0.87-μm near-infrared wavelength range of GaAs detectors has been extended to 1.3–1.5 μm in InGaAs-based devices [7], [8]. In addition, other ways of increasing the detector's responsivity have been investigated [9]. The availability of high-performance optical detectors compatible with MESFET processing make the MSM device an ideal choice for monolithically integrated optoelectronic circuits [10]–[14].

To our knowledge, there are few reports on simulation results for this device [6], [15]. In this letter, we present a one-dimensional analysis of the temporal response of a GaAs MSM photodetector with sub-half-micrometer finger spacing (0.1 μm). An intrinsic device with low-level optical excitation and different electric field profiles is studied. We also include an extrinsic circuit to determine the importance of parasitic circuit elements on the response speed of this device.

II. Analysis and Results

The photodetector structure is schematically shown in Fig. 1. The unintentionally doped epitaxial layer (n-type) has a background donor concentration of 5×10^{14} cm^{-3}. The use of tungsten silicide (WSi_x) for Schottky contacts would make this device fully compatible with a standard refractory-gate MESFET process [13]. Direct-write electron-beam lithography can be used to expo· 'he multifinger pattern.

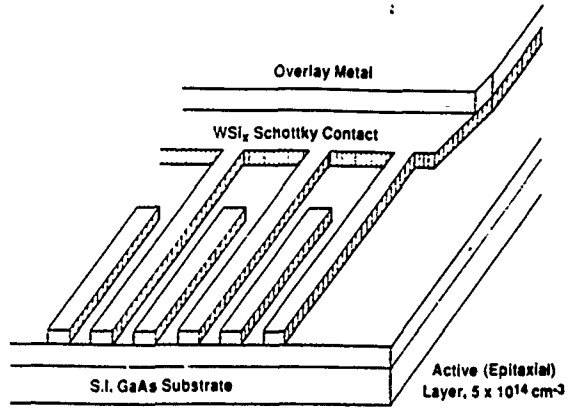

Fig. 1. Structure of an interdigitated GaAs MSM photodetector. The device consists of 30 0.1-μm fingers and the photosensitive area is 5.9 × 8 μm^2.

We use a one ·nensional model to obtain estimates of the minimum time ponse of this device. In order to simulate potential effects ·ithin the intrinsic detector, we introduce spatial variation· f acceptor or donor concentrations to create two built-in electric field profiles, which differ from those of the undoped device. The doping profiles can be created, for example, by focused-ion-beam implantation of the interfinger regions, as illustrated in Fig. 2(a). From Poisson's equation, we find the electrostatic potential variations and the resulting energy-band diagram. For no illumination, the conduction band edges for the three cases considered here are plotted in Fig. 2(b) for an applied voltage of 0.1 V between adjacent fingers. Due to the very low doping concentration of the active layer, our calculations reveal that the regions between fingers are completely depleted of free carriers at 0.1 V for all three doping profiles, and this would remain true if the finger pattern were processed directly on a semi-insulating substrate. The electric field is constant without dopant modification (see the middle curve in Fig. 2(b)). With the acceptor-doping profile (upper curve), an increased electric field occurs at the positively biased electrode (right-hand boundary) forcing the photoexcited electrons to move faster in that region, relative to the undoped case. Conversely, with the donor-doping profile (bottom curve), a higher electric field close to the negatively biased electrode forces the photoexcited holes to move faster in that region, relative to the undoped case. Intuitively, it would appear that the last of these three cases could be the

Manuscript received January 2, 1989; revised January 24, 1989. This work was supported by the Office of Naval Research, Arlington, VA.

W. C. Koscielniak and M. A. Littlejohn are with the Department of Electrical and Computer Engineering, North Carolina State University, Raleigh, NC 27695.

J.-L. Pelouard is with the Department of Electrical and Computer Engineering, North Carolina State University, Raleigh, NC 27695 on leave from the Laboratoire de Microstructures et de Microélectronique (CNRS), 92220 Bagneux, France.

IEEE Log Number 8927908.

0741-3106/89/0500-0209$01.00 © 1989 IEEE

EFFICIENT PATH-INTEGRAL MONTE CARLO TECHNIQUE FOR ULTRASMALL DEVICE APPLICATIONS

L. F. Register[a], M. A. Stroscio[b,a] and M. A. Littlejohn[a,b]

[a]Electrical and Computer
Engineering Department
North Carolina State University
Raleigh, North Carolina 27695-7911

[b]U.S. Army Research Office
Research Triangle Park, North Carolina 27709

(Received 30 September 1988; revised manuscript received 23 January 1989)

The ability to model equilibrium electronic properties of ultrasmall devices using a path-integral Monte Carlo (PIMC) method is demonstrated. First, a direct sampling PIMC method and its advantages over Metropolis importance sampling PIMC methods in this application are described. Then two potential structures typical of ultrasmall devices, a single and a coupled double finite square well potential, are analyzed and the results compared to exact analytic results. The latter example demonstrates the ability to accurately resolve coupling induced energy level splittings at least as small as 2% of the nominal energy. (Lower levels of coupling were not considered.) An additional example given, for which analytic results are not available, is the analysis of a two-dimensional infinite, periodic quantum well array. The PIMC technique described here makes way for the application of the Feynman path-integral formalism, an advantageous formalism for treating scattering processes, to the study of the electronic properties of ultrasmall devices.

1 Introduction

Proper treatment of scattering processes such as charge-carrier-phonon coupling is crucial for accurate modeling of the electronic properties of semiconductor devices. A powerful and conceptually appealing treatment of carrier-phonon coupling is provided by the Feynman Path-Integral (FPI) formalism of quantum mechanics.[1,2] The power of the FPI formalism in treating coupling processes was demonstrated first in quantum electrodynamics (QED),[3] but soon its advantages in the formally similar treatment of carrier-phonon coupling in semiconductors also was realized[4] and, since, several analytic FPI-based studies of the electronic properties of bulk semiconductors have followed (for example, References 5-10 and references therein). In recent years, advances in semiconductor technologies, have led to the realization of devices whose spatial dimensions are on the same scale as the thermal deBroglie wavelength of the charge carriers. These devices exhibit behavior that is either influenced or governed by quantum interference effects, and they must be modeled accordingly. Further, on the ultrasmall spatial and temporal scales at which these devices operate, the semiclassical treatment of carrier-phonon scattering as spatially localized, instantaneous events is of reduced value. However, despite the fully quantum mechanical nature of the FPI formalism, there has not been widespread application of it to the study of the electronic properties of these ultrasmall structures. Despite it's conceptual advantages, application of the FPI formalism poses significant practical problems. For an-

0749-6036/89/070233+12 $02.00/0

© 1989 Academic Press Limited

Invited Paper

Indium Phosphide-based Heterojunction Bipolar Transistors.

Jean-Luc Pelouard* and Michael A. Littlejohn

Department of Electrical and Computer Engineering
North Carolina State University, Raleigh, NC 27695-7911

* Permanent address: Laboratoire de Microstructures et de Microélectronique (CNRS)
196 Ave H. Ravéra - 92220 Bagneux - France

ABSTRACT

The Heterojunction Bipolar Transistor (HBT) is not a new device. In the late 1940's W. Shockley[1] gave the basic ideas and, about ten years later, H. Kroemer[2] published the first paper to show the promising advantages of this new structure. The first device applications have been demonstrated in AlGaAs/GaAs materials, taking advantage of the natural lattice match in this system. Currently, high performance GaAs-based HBTs have been reported and the InP-based transistors are still promising. In this paper we will review the reasons why this device has required more than forty years of development and what its future can be in the InP-based materials systems.

1. INTRODUCTION

In bipolar transistors the main current is carried by electrons injected into the base by the emitter-base junction and collected by the base-collector junction. There is a transistor effect if the collector current is nearly equal to the emitter current. Unfortunately, electron injection (J_n) into the base accompanies hole injection (J_p) into the emitter creating an additional parasitic current. Because the current densities in the homojunction, or Classical Bipolar Transistor (CBT), are given by the Shockley formula for short base diodes, the injection ratio (J_p/J_n) depends on the ratio of base (N_A) to emitter (N_D) doping levels:

$$\left(\frac{J_p}{J_n}\right)_{CBT} \alpha \frac{N_A}{N_D} \qquad (1)$$

In order to obtain an injection ratio small enough for significant current gain, the CBT must have a much higher doping level in the emitter than in the base. Thus, the CBT will have a high resistivity base. This has various well known negative consequences on the behavior of the transistor (Early effect, reduction of f_{max}, etc.).

In contrast, in the first approximation, the energy discontinuity in the HBT emitter-base heterojunction introduces an additional term to the injection ratio equation:

$$\left(\frac{J_p}{J_n}\right)_{CBT} = \left(\frac{J_p}{J_n}\right)_{HBT} \exp\left(\frac{-\Delta E_v}{kT}\right) \qquad (2)$$

PROCEEDINGS OF THE SIXTH INTERNATIONAL NASECODE CONFERENCE
Edited by J. J. H. Miller—Dublin (Ireland) 11th to 14th July 1989 — Boole Press Ltd.

MONTE CARLO STUDY OF BALLISTIC AND QUASI-BALLISTIC TRANSPORT IN SEMICONDUCTORS*

J. L. Pelouard,† H. P. Belgal and M. A. Littlejohn

Electrical and Computer Engineering Department
North Carolina State University
Raleigh, North Carolina 27695-7911

Monte Carlo-generated velocity distribution functions have been utilized to develop criteria to classify electrons contributing to non-stationary transport in semiconductors. These classifications are given in terms of ballistic, quasi-ballistic and velocity-relaxed electron populations. An analytical model has been built which describes these populations. While the results have been obtained for GaAs planar-doped barriers, we believe that the definitions and concepts are valid in a more general sense. To support this proposition, some aspects of InP-based heterojunction bipolar transistors will also be discussed.

1 Introduction

In 1985, two groups reported experimental evidence for hot electron transport in barrier injection devices [1,2]. These and later results established the existence of a peak in the electron energy distribution function at the barrier injection energy [3,4]. This peak, observable a significant distance from the barrier, was attributed to ballistic transport in both homojunction planar-doped barriers and heterojunction barriers.

Recently, Hess and Iafrate explored these results in an effort to elucidate further the processes of ballistic transport and velocity overshoot [5]. They developed definitions for these terms, classified the basic experimental results, and concluded that, while the basic physics of ballistic transport is well understood qualitatively, much quantitative work remains to be done, especially with respect to device applications.

The purpose of this paper is to investigate transport in the base region of GaAs planar-doped barriers used as ballistic launchers. Our results expand the definitions of Hess and Iafrate and further classify electrons in the velocity distribution function as to their role in ballistic and quasi-ballistic transport in semiconductors.

*This paper is in final form and no version of it will be submitted for publication elsewhere.

†Current address: Laboratoire de Microstructures et de Microélectronique (L2M-CNRS), 196 Ave. H. Ravéra, 92220 Bagneux, France.

PROCEEDINGS OF THE SIXTH INTERNATIONAL NASECODE CONFERENCE
Edited by J. J. H. Miller—Dublin (Ireland) 11th to 14th July 1989 — Boole Press Ltd.

PATH-INTEGRAL MONTE CARLO METHODS FOR ULTRASMALL DEVICE APPLICATIONS*

L. F. Register[a], M. A. Littlejohn[a,b] and M. A. Stroscio[b,a]

[a]Electrical and Computer Engineering Department
North Carolina State University
Raleigh, North Carolina 27695-7911

[b]U.S. Army Research Office
Research Triangle Park, North Carolina 27709

The application of Path-Integral Monte Carlo (PIMC) methods to the study of the electronic properties of ultrasmall devices is discussed. First, as an introduction, the advantages of the Feynman path-integral (FPI) formalism for this application are described. Next the FPI formalism itself is reviewed briefly. Then, a practical PIMC method for modeling equilibrium conditions in these devices is described. Last, lacking a nonequilibrium PIMC method proven widely applicable to ultrasmall device modeling, various basic approaches and their limitations are described to exhibit the fundamental problems yet to be overcome.

1 Introduction

Proper treatment of scattering processes such as charge-carrier–phonon coupling is crucial for accurate modeling of the electronic properties of semiconductor devices. A powerful and conceptually appealing treatment of carrier-phonon coupling is provided by the Feynman Path-Integral (FPI) formalism of quantum mechanics [1,2]. The power of the FPI formalism in treating coupling processes was demonstrated first in quantum electrodynamics (QED) [3], but soon its advantages in the formally similar treatment of carrier-phonon coupling in bulk semiconductors also was realized [4]. Further, the reduction in device sizes to dimensions on the order of the thermal de Broglie wavelength of charge carriers offers few conceptual difficulties for the fully quantum mechanical FPI formalism, while greatly reducing the value of the semiclassical treatment of carrier-phonon scattering as spatially localized, instantaneous events. However, the reduction of device dimensions does pose great practical problems to application of the FPI formalism. For

*This paper is in final form and no version of it will be submitted for publication elsewhere.

Solid-State Electronics Vol. 32, No. 12, pp. 1347–1351, 1989
Printed in Great Britain. All rights reserved

0038-1101/89 $3.00 + 0.00
Copyright © 1989 Pergamon Press plc

HYDRODYNAMIC HOT-ELECTRON TRANSPORT SIMULATION BASED ON THE MONTE CARLO METHOD

D. L. Woolard[a], J-L. Pelouard[a,c], R. J. Trew[a], M. A. Littlejohn[a] and C. T. Kelley[b]

[a]Electrical and Computer Engineering Department
North Carolina State University
Raleigh, North Carolina 27695-7911

[b]Department of Mathematics
North Carolina State University
Raleigh, North Carolina 27695-8205

[c]Laboratoire de Microstructures et de Microelectronique (CNRS)
196 Avenue Henri Ravéra, 92220
Bagneux, France

ABSTRACT

A hydrodynamic hot electron model is used to study electron transport through a submicron $N^+ - N - N^+$ GaAs structure. This study is used to investigate improvements which the unique features of this model offer to analysis of devices operating under nonstationary transport conditions. The model is based upon semiclassical "hydrodynamic" conservation equations for the average carrier density, momentum and energy. The general model includes particle relaxation times, momentum relaxation times, energy relaxation times, electron temperature tensors and heat flow vectors as a function of average carrier energy for the Γ, X and L valleys of GaAs. For this study, we utilized a simplified single electron gas version of our model to clearly reveal the impact of the nonstationary terms in the model. Results from both a drift-diffusion model approach and a Monte Carlo analysis are used to show the relative accuracy and facility this new model offers for investigating practical submicron device structures operating under realistic conditions.

KEYWORDS

Hot-electron; hydrodynamic transport model; Monte Carlo method; nonequilibrium transport; nonstationary transport; self-consistent potentials.

INTRODUCTION

Recently, there has been a growing interest in the use of hydrodynamic conservation models to study electron transport (Goldsman and Frey, 1988; Sandborn, Rao and Blakey, 1989). The impetus for choosing this approach is very clear. Hydrodynamic models have the ability to include nonstationary effects (Hess and Iafrate, 1988) and hence are superior in physical detail to simple drift-diffusion models. Also, while Monte Carlo methods can easily incorporate complicated band structure and detailed scattering rates, hydrodynamic models require less computation time to generate solutions and possess macroscopic terms which offer greater physical insight and intuition. However, there has been some question as to the accuracy of these models as opposed to Monte Carlo methods due to the inherit neglect of ensemble effects (Crandle, East and Blakey, 1989). In this paper, we present the results for a transport study of a submicron $N^+ - N - N^+$ GaAs device structure to evaluate the importance of the nonstationary terms in our new hydrodynamic model. Features of this study include : (1) The incorporation of self-consistent potentials by the simultaneous solution of the conservation equations and Poisson's equation. (2) The incorporation of realistic boundary conditions on the device's active region by including an exact doping profile for the entire structure and applying boundary conditions to the contact points of the N^+ regions. The multipoint nonlinear boundary value problem that results from applying the transport model to the device structure is solved using an efficient local nonlinear solver combined with a perturbation-in-doping based continuation method. The electron transport results are compared to results from both a drift-diffusion model and a self-consistent ensemble Monte Carlo analysis of the same GaAs device structure.

POLAR OPTICAL PHONON SCATTERING OF CHARGE CARRIERS IN ALLOY SEMICONDUCTORS: EFFECTS OF PHONON LOCALIZATION

L. F. Register[a], M. A. Littlejohn[a,b] and M. A. Stroscio[b,a]

[a]Electrical and Computer Engineering Department
North Carolina State University
Raleigh, North Carolina 27695-7911

[b]U.S. Army Research Office
Research Triangle Park, North Carolina 27709

ABSTRACT

The effects of spatial localization of phonons or their correlation functions to finite distances in alloy semiconductors on polar optical phonon scattering of hot carriers are modeled analytically. Despite the possibility of increased numbers of carrier-scattering-active phonon modes, it is demonstrated that phonon localization in alloys should have little if any effect on the total polar optical scattering rate for charge carriers coupled to equilibrium phonon populations. Further, it is demonstrated that phonon localization may have a beneficial effect on hot carrier transport by reducing the possibility of exciting nonequilibrium phonon populations. These results are obtained without assuming any specific functional form or degree of phonon localization; rather, calculations rely on the inherent orthogonality and mathematical completeness of the classical vibrational modes over the crystal lattice degrees of freedom.

KEYWORDS

Phonon localization, polar optical phonon scattering, Fröhlich coupi ·. hot electron transport, alloy disorder.

INTRODUCTION

Alloy scattering of charge carriers, the scattering of carriers due to the aperiodic arrangement of atoms in alloy semiconductors, long has been recognized as a significant carrier scattering process in these materials (for example, Littlejohn and colleagues, 1978 and references therein). More recently it has been recognized that alloy disorder similarly may affect phonons: In addition to either one- or two-mode behavior depending on alloy type and possibly composition (for example, Barker and Sievers, 1975), Raman light scattering studies of the phonon spectra of alloy semiconductors $A_xB_{1-x}C$ exhibit broadening and asymmetry in the Raman line shapes that has been ascribed to spatial localization of the phonon modes or at least their correlation functions (Jusserand and Sapriel, 1981; Krabach and colleagues, 1983; Paranthal and Pollak, 1984). In theory, as a consequence of the *Heisenberg uncertainty principle*, the localization of optical phonon states leads to a breakdown in the usual $\vec{q} = 0$ Raman selection rule for the phonon crystal momentum, allowing photon coupling to phonons with a spread of nominal $\vec{q}$ values, and with a corresponding observable spread in energy values. Parayanthal and Pollak (PP) (1984), assuming a Gaussian form for the localization, have calculated correlation lengths based on the degree of observed broadening in the Raman lines of as little as 62 and 80 Å for the $AlAs$-like and $GaAs$-like modes respectively in an $Al_{0.5}Ga_{0.5}As$ alloy sample, values representing significant spreads in the crystal momentum of the Raman active phonon modes. These observable effects of alloy disorder in semiconductors on photon-phonon coupling suggest that alloy disorder also may have a significant effect charge-carrier-phonon coupling — in addition to representing a significant carrier scattering process unto itself. Recently, however, Kash, Jha and Tsang (KJT) (1987) studied alloy hot-electron-optical-phonon coupling both experimentally in two-mode $Al_xGa_{1-x}As$ alloys and one-mode $In_xGa_{1-x}As$ alloys using picosecond time-domain pump-probe Raman techniques, and theoretically for polar (*Fröhlich* (Fröhlich, 1954)) coupling in the former allowing for variations in the phonon frequencies and and polarization strengths of the the two branches of the longitudinal-optical phonon spectrum as a function of alloy composition x. In contrast to the observable effects of alloy disorder on photon-phonon coupling, their experimental measurements of the lifetimes and sizes of small nonequilibrium phonon populations in these alloys exhibit

Intrinsic and Extrinsic Response of GaAs Metal–Semiconductor–Metal Photodetectors

WACLAW C. KOSCIELNIAK, JEAN-LUC PELOUARD, AND MICHAEL A. LITTLEJOHN, SENIOR MEMBER, IEEE

Abstract—**GaAs metal-semiconductor-metal (MSM) photodetectors have been simulated using a self-consistent Monte Carlo (MC) method. Intrinsic device properties are discussed in terms of MC electron and hole transport under low illumination intensity. Parasitic circuit elements are then introduced to more closely model realistic devices using the MC results in a circuit simulator. Intrinsic devices with 0.5 and 1 μm spacing between fingers are dominated by stationary high-field transport. Surprisingly, full-width-half-maximum (FWHM) of 0.5 and 1 μm detectors with parasitics is 4.3 and 3.8 ps, respectively. However, the 1 μm detector exhibits a long hole tail and transient oscillations. Thus, FWHM results (and intrinsic device response) can be inadequate predictors of ultimate frequency response and scaling behavior. However, an estimate of maximum repetition frequency gives f_{max} = 92 GHz for the 0.5 μm device, consistent with experimental data.**

RECENTLY, rapid progress in GaAs metal-semiconductor-metal (MSM) photodetector performance has been achieved [1]–[3]. The fastest reported MSM detector has an intrinsic bandwidth of 105 GHz [3], competitive with other Schottky photodiodes [4], [5]. However, the MSM photodetector is better suited for monolithic integration [6]–[9].

To design MSM photodetectors with a required bandwidth and responsivity, one must identify performance-limiting factors. These factors include intrinsic transport of photoexcited carriers between electrodes and transmission line effects (parasitics) of the contact fingers. Ideally, a coupled field equation/transport equation model is needed to accurately simulate these factors. Such a model is very computer intensive and difficult to interpret.

We have used a self-consistent Monte Carlo (MC) model to simulate intrinsic transport and a lumped-constant circuit model for parasitics. The MC results are used as an input for SPICE simulation of the circuit model. This approach is relatively easy to implement. However, the interpretation of the results depends critically on the parasitic lumped-constant circuit parameters. The purpose of this paper is to present new simulation results from an MC study of MSM photodetectors with 0.5 and 1 μm finger spacings. A modified parasitic circuit gives good agreement with recent experimental data for a device with 0.5 μm interfinger spacing.

The structure of the photodetector with planar multifinger (Al) contacts is shown in Fig. 1(a). Unintentionally doped GaAs ($N_d = 5 \times 10^{14}$ cm^{-3}) simulates devices processed either on epitaxial layers or semi-insulating substrates. The contact barrier heights (0.78 eV and 0.65 eV for electrons and holes, respectively) are much larger than kT. Thus, current injection from the contacts is negligible.

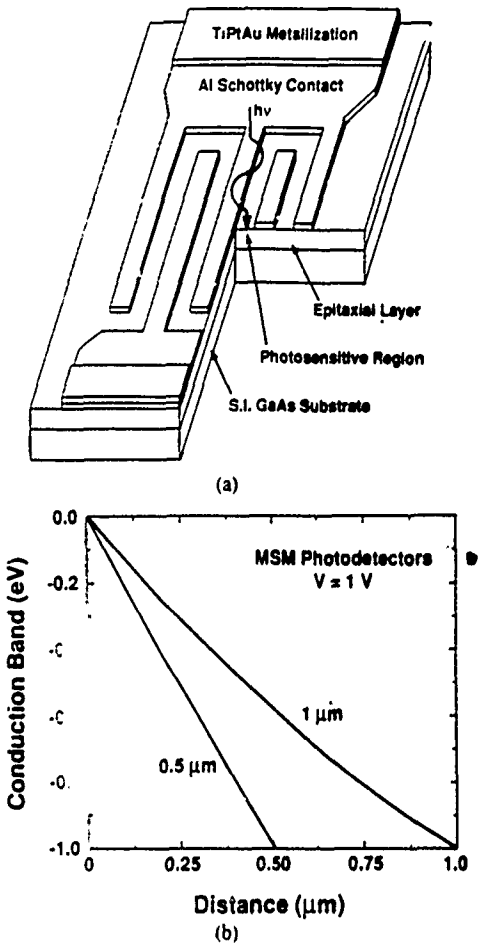

Fig. 1. (a) Schematic structure of a high-speed GaAs MSM photodetector. The finger widths and interfinger spacings are either 0.5 or 1 μm. The photodetectors with a 0.5 and 1 μm interfinger distance have 11 and 6 fingers, respectively. (b) Energy band diagram of photodetectors at a bias of 1 V.

The MC algorithm has been previously described in detail [10]. A 10 fs time step is used in the simulations reported here. Since it is longer than the electromagnetic wave propagation, this value is small enough for accurate numerical analysis yet long enough to retain validity of Poisson's equation. This is indicated in the calculated conduction band profiles shown in Fig. 1(b). The maximum density of photoexcited carriers is 1.3×10^{14} cm^{-3}, which prevents appreciable fluctuations of

Manuscript received April 24, 1989; revised October 17, 1989.

W. C. Koscielniak and M. A. Littlejohn are with the Department of Electrical and Computer Engineering, North Carolina State University, Raleigh, NC 27695.

J.-L. Pelouard is with the Laboratoire de Microstructures et de Microélectronique (CNRS), 92220 Bagneux, France.

IEEE Log Number 8933548.

1041-1135/90/0200-0125$01.00 © 1990 IEEE

Frequencies of confined longitudinal-optical phonon modes in GaAs/GaP short-period strained-layer superlattices

K. W. Kim
Department of Electrical and Computer Engineering, North Carolina State University, Raleigh, North Carolina 27695-7911

M. A. Stroscio
U.S. Army Research Office, Research Triangle Park, North Carolina 27709-2211

J. C. Hall
Department of Electrical and Computer Engineering, North Carolina State University, Raleigh, North Carolina 27695-7911

(Received 7 December 1989; accepted for publication 8 February 1990)

The linear-chain approximation is used to calculate the spectrum of confined longitudinal-optical (LO) phonon frequencies in short-period strained-layer superlattices. The frequencies for confined LO-phonon modes are reported explicitly for the case of GaAs/GaP short-period strained-layer superlattices grown in the ⟨001⟩ direction. These results are compared with the few existing experimental measurements for such superlattices.

I. INTRODUCTION

Recently phonons in semiconductor heterostructures have received much attention. These efforts are due, in part, to the fact that scattering by the longitudinal-optical (LO) phonon modes is an important energy loss mechanism for a wide variety of III-V semiconductor devices.[1] Raman scattering measurements have been used to study the properties of phonon modes in quantum wells and superlattices.[2-8] The binary GaAs/AlAs superlattices have been experimentally investigated most extensively due to the simplicity in analysis (compared to tenary GaAs/AlGaAs superlattices) and the material familiarity.[3-8] In these structures, phonon modes propagating along the direction normal to the heterojunctions are observed to have two different types of characteristics: The phonon modes in the acoustic branch are propagative across the heterojunctions and, as a result, are "folded" into the reduced Brillouin zone,[2] while the modes in the optical branch are "localized" in each layer leading to descriptions of confined modes or slab modes.[4] In addition, the localization of phonon modes near the heterojunctions leads to the well-known interface modes.[5] Furthermore, it is suggested that the Raman frequency shifts for confined LO-phonon modes can be used as a means to determine the bulk phonon dispersion relation (i.e., the equivalent wave-vector model)[4] and as a probe to characterize the quality of interfaces.[8] The frequency shift due to confinement has been analyzed theoretically as well. The results obtained by a simple linear-chain model show a remarkable agreement with experimental data except in the monolayer superlattices.[3] In more detailed analyses, the phonon dispersion relation is calculated in a plane parallel to the heterojunction.[9-11]

The advent of strained-layer (i.e., pseudomorphic) structures adds an interesting effect on the confined phonon modes. The mismatch in lattice constants subjects these structures to the biaxial stress, and results in the strain-induced shifts in optical phonon frequencies. The measurement of Raman shifts for strained-layer quantum wells and superlattices has been accomplished for a relatively small number of III-V systems; most notably the GaSb/AlSb superlattices by Jusserand *et al.*[12] and Santos *et al.*,[13] the GaAs/InAlAs superlattices by Nakayama *et al.*,[14] and the GaAs/GaP superlattices by Armelles *et al.*[15] These experiments clearly exhibit the Raman shifts due to both strain and confinement. In the analysis of experimental data, the contributions by these two effects are in general treated separately considering one effect at a time. This approach is readily justifiable when the mismatch is not large such as in GaSb/AlSb systems (less than 1%). However, as the strain becomes significant (such as in GaAs/InAs systems where the mismatch is approximately 7%), the coupling between two effects may become non-negligible. It is, thus, necessary to study the importance of the coupling effect, and develop a model which can directly predict phonon frequencies in this situation.

In this paper we present a model for determining the frequencies of confined LO phonons in strained-layer III-V superlattices grown in the ⟨001⟩ direction. A discrete (rather than continuum) approach based on a linear-chain model is applied. The frequency shift arising simultaneously from both confinement and strain is accounted for by properly modifying the force constants to incorporate the strain effects into the linear-chain model. For a specific example, the frequency shifts are calculated for GaAs/GaP short-period superlattices, and compared with the existing Raman data of Armelles *et al.*[15] for the lowest order confined LO modes. Our model will be of importance in the strained-layer structures when the strains have to be estimated rather accurately: The diagnosis of heterojunction interface quality[8] is one example, and the study of carrier transport is another. Since the strains in individual layers modify the intrinsic physical properties such as band structures,[16] the strain-induced effects can be applied to tailor the device structures for a possible reduction of carrier-LO-phonon interactions.[17]

II. MODEL

Figure 1 shows a typical schematic drawing for the linear-chain model in a superlattice. As can be seen in the figure, the z axis is chosen as the growth direction of the lattice

 0021-8979/90/106179-05$03.00 © 1990 American Institute of Physics

Dark Current Characteristics of GaAs Metal–Semiconductor–Metal (MSM) Photodetectors

WACŁAW C. KOŚCIELNIAK, JEAN-LUC PELOUARD, ROBERT M. KOLBAS, MEMBER, IEEE, AND MICHAEL A. LITTLEJOHN, SENIOR MEMBER, IEEE

Abstract—**We present calculations of the electron and hole components of dark current in a GaAs metal-semiconductor-metal (MSM) photodetector. A quantum-mechanical model is developed that describes the electron and hole transport behavior in the contact regions which is used to determine dark current as a function of electric field. The model reduces to a conventional thermionic emission model if an ideal barrier transmission coefficient is assumed. In order to assess the accuracy of the model, photodetectors have been fabricated and tested. Theoretical calculations and experimental data are compared and good agreement is obtained. Possible modifications to enhance the usefulness of the model are discussed.**

I. Introduction

GALLIUM ARSENIDE (GaAs) metal-semiconductor-metal (MSM) photodetectors have recently been used to detect ultrashort optical pulses [1]. With a planar, interdigitated pattern delineated by electron-beam lithography, an intrinsic detector bandwidth in excess of 100 GHz has been achieved [2]. Increased research in this area is stimulated by possible development of ultra-high-speed monolithic optoelectronic integrated circuits (IOEC's), in which the MSM photodetector would serve as an input device for optical signals and would be followed by a signal processing circuit. Applications of such circuits for telecommunications and optical data processing are feasible in the near future, especially since monolithic integrated amplifiers operating up to 60 GHz have already been demonstrated [3].

To better understand major factors limiting speed performance of this detector, detailed numerical simulations have been undertaken by the present authors [4]–[6] and others [2]. In order to achieve a large signal-to-noise ratio, detectors with low dark current and low noise are required. However, only basic aspects of dark current of the MSM photodetectors have been addressed [7]–[9]. In the following, we discuss a one-dimensional model for determining the electron and hole components of the dark current. This approach integrates solutions of the time-independent Schrödinger equation with thermionic emission models. The calculations are compared with data from fabricated devices, and good agreement between theory and experiment is obtained. Also, suggestions for further extension of the model are given.

Manuscript received May 23, 1989; revised February 5, 1990. This work was supported by the Office of Naval Research, Arlington, VA, and by the Strategic Defense Initiative Organization/Innovative Science and Technology through the Army Research Office under Contract DAAL-03-87-K0051.

W. C. Kościelniak, R. M. Kolbas, and M. A. Littlejohn are with the Department of Electrical and Computer Engineering, North Carolina State University, Raleigh, NC 27695.

J. L. Pelouard is with the Laboratoire de Microstructures et de Microelectronique (CNRS), 92220 Bagneux, France.

IEEE Log Number 9035768.

II. Device Fabrication

A schematic diagram of the experimental photodetector is shown in Fig. 1. The multifinger pattern was fabricated on a high-purity, undoped substrate. A standard lift-off process (chlorobenzene-soaked positive photoresist) was used to delineate 4000-Å-thick Al fingers. Shortly before Al deposition, the native oxides were removed by immersion of the samples in 1 HCl : 1 H_2O. A recess, approximately 600 Å deep, was etched to remove any photoresist residues between fingers. Etching was performed in a solution of 3 H_3PO_4 : 1 H_2O_2 : 50 H_2O followed by a short immersion in 1 HCl : 1 H_2O. Our experiments indicate that the recess is likely to be responsible for a relatively high breakdown voltage of 80–120 V obtained in the best devices. Experimental results are presented for photodetectors with 3–5-μm distance between fingers and an active area of 83 μm × 83 μm or 100 μm × 100 μm, suitable for coupling to multimode optical fibers.

Simultaneously with the photodetectors, Al Schottky diodes (squares, 7.5×10^{-1} cm^2) were fabricated on Si-doped (2×10^{17} cm^{-3}) substrates. Earlier, AuGeNi/Au ohmic contacts were alloyed to the back sides of the n-type samples. The barrier height (ϕ_n = 0.75–0.77 eV) and the ideality factor (n = 1.04–1.05) were determined from I–V characteristics of these diodes. The near-unity ideality factor indicates a high-quality Al-GaAs interface and absence of native interfacial oxides. This information is important since we neglect the native oxides in the model development. In addition, the change in I–V characteristics upon various annealing temperature cycles up to 470°C was measured in order to obtain additional information about the nature of the metal–semiconductor interface. There is an initial increase in barrier height for temperatures up to 250°C, followed by a slow

0018-9383/90/0700-1623$01.00 © 1990 IEEE

VARIATION IN FREQUENCIES OF CONFINED LONGITUDINAL-OPTICAL PHONON MODES DUE TO CHANGES IN THE EFFECTIVE FORCE CONSTANTS NEAR HETEROJUNCTION INTERFACES

M. A. Stroscio,[a] K. W. Kim,[b] and J. C. Hall[b]

[a]U. S. Army Research Office
Research Triangle Park, NC 27709-2211

[b]Department of Electrical and Computer Engineering
North Carolina State University
Raleigh, NC 27695-7911

(Received 2 January 1990)

A linear-chain model with variable force constants for the couplings at heterojunctions is used to calculate the spectrum of confined longitudinal-optical (LO) phonon frequencies in a short-period strained-layer superlattice. Even for the case of a superlattice with only two atomic monolayers in each superlattice layer, it is demonstrated that the frequencies of confined LO-phonon modes are only weakly dependent on variations in interfacial force constants.

1. Introduction

Phonons in semiconductor heterostructures have received much attention. These efforts are due, in part, to the fact that scattering by the longitudinal-optical (LO) phonon modes is an important energy loss mechanism for electrons in a wide variety of III-V semiconductor devices.[1] In addition, Raman scattering measurements have been applied to study the properties of phonon modes in quantum wells and superlattices.[2–8] Recently, Raman spectra have been used to characterize monolayer variations in the thicknesses of quantum wells.[8] In the analysis and interpretation of Raman data for confined LO-phonon modes, it is convenient to model the confined LO modes as modes in a uniform isolated dielectric slab.[8–11] Such an approximate model is based on the assumption that atomic force constants at heterojunction interfaces are identical with those of the bulk or of uniform pseudomorphic layers. In this paper, the effect of varying force constants at the heterojunction interfaces of a strained-layer, short-period superlattice is analyzed by using a linear-chain model to determine the corresponding changes in the frequencies of the confined LO-phonon modes. In the studies reported herein, a superlattice with only two atomic monolayers in each superlattice layer is modeled in order to determine the importance of perturbations in heterojunction interface force constants for a system where such effects should be large. In particular, frequencies of confined LO-phonon modes are determined for a GaAs/GaP short-period superlattice with two monolayers per superlattice layer. It is found that varying interfacial force constants by values as extreme as 10% results in only about a 2% change in the frequencies of the confined LO-phonon modes. As a practical matter, changes in the frequencies of confined LO-phonon modes will generally be considerably less than 2% since in most superlattices and quantum wells the ratio of the number of bonds at interfaces to the number of bonds removed from interfaces is less than for the two-monolayer per layer case examined herein.

2. Linear-Chain Model with Variable Interfacial Force Constants

In order to introduce the basic properties of the linear-chain model used in this analysis, we will consider initially the case where interface effects are absent. Figure 1 depicts a schematic for the linear-chain system used to study the role of force-constant variations at heterojunction interfaces. The z axis is chosen as the growth direction of the lattice. Hence, for the longitudinal modes of interest, the atomic displacements are in the z direction. In the absence of strain, the force constant in each layer is estimated based on the frequencies of the

0749-6036/90/020115–04 $02.00/0
© 1990 Academic Press Limited

Appendix C

Resumes for Principal Investigators, Dr. M. A. Littlejohn and Dr. K. W. Kim.

BIOGRAPHICAL SUMMARY FOR MICHAEL A. LITTLEJOHN

Business Address

Department of Electrical and Computer Engineering
North Carolina State University
Box 7911
Raleigh, North Carolina 27695-7911
(919) 737-2336

Education

North Carolina State University	1962	B.S.	Electrical Engineering
North Carolina State University	1964	M.S.	Electrical Engineering
North Carolina State University	1967	Ph.D.	Electrical Engineering

Industrial and Academic Experience

1967-present	Assistant Professor/Associate Professor/Professor, Department of Electrical and Computer Engineering, North Carolina State University, Raleigh, North Carolina.
1977-1981, 1985-present	Technical Staff Member, U.S. Army Research Office, Research Triangle Park, North Carolina.
1981-1983	Director, Microelectronics Programs, School of Engineering, North Carolina State University, Raleigh, North Carolina.
1984-1985	Associate Dean of Engineering for Research Programs, North Carolina State University, Raleigh, North Carolina.
1988-1989	Associate Director, NSF Engineering Research Center On Advanced Electronic Materials Processing.

Professional Activities

Member at Large, Executive Committee of the Electronics Division of the Electrochemical Society, 1983-1988.
Member, National Academy of Sciences National Research Council Committee on Recommendations for U.S. Army Basic Scientific Research, 1985-1986.
Member, Technical Advisory Board, IEEE Engineering Research and Development Committee, 1986-1989.
Associate Editor, Electronics Division, Journal of the Electrochemical Society, 1987-1990.
Member, NSF Committee on Research Trends and Opportunities for the Metallurgy, Polymers, and Ceramics Section, Division of Materials Research, 1983-1985.
Organizer and Program Chairman, NSF Workshop on The Future of Microstructure Technology, 1985.
Co-organizer, NSF Workshop on Cooperation and Sharing Among U.S. Microelectronics Centers, 1983.

Society Memberships and Honors

Institute of Electrical and Electronics Engineers
American Society for Engineering Education
American Physical Society
Electrochemical Society
Certification of Achievement For Patriotic Civilian Service, U.S. Army, 1989
R.J. Reynolds Industries, Inc., Award for Excellence in Teaching and Research, 1983-1987
Alcoa Foundation Distinguished Research Award, 1983
N.C. State University Alumni Award — University Distinguished Alumni Professor, 1980
Western Electric — ASEE Fund Award for Excellence in Teaching and Research (1978)
Sigma Xi Outstanding Young Scientist Award, 1976
Eta Kappa Nu Outstanding Teacher Award, 1974 & 1975

Field of Research Interest

Semiconductor device simulation and modeling, III-V compound semiconductor materials and devices, hot electron transport in semiconductors, ion implantation and radiation damage in semiconductors, thin films and oxides on semiconductors, defects in semiconductors.

Ten Most Recent Refereed Publications (From a total of 93)

1. W.C. Koscielniak, J.L. Pelouard and M.A. Littlejohn, "Intrinsic and Extrinsic Response of GaAs Metal-Semiconductor-Metal Photodetectors," Photonics Tech. Lett., 2, 125, 1990.
2. L.F. Register, M.A. Littlejohn and M.A. Stroscio, "Polar Optical Phonon Scattering of Charge Carriers in Alloy Semiconductors: Effects of Phonon Localization," Solid-State Electron., 32, 1387, 1989.
3. D.L. Woolard, J.L. Pelouard, R.J. Trew, M.A. Littlejohn and C.T. Kelley, "Hydrodynamic Hot-Electron Transport Simulation Based on the Monte Carlo Method," Solid-State Electron., 32, 1347, 1989.
4. W.C. Koscielniak, M.A. Littlejohn and J.L. Pelouard, "Analysis of a High-Speed GaAs Metal-Semiconductor-Metal (MSM) Photodetector with 0.1 μm Finger Spacing," IEEE Electron Dev. Lett., 10, 221 (1989).
5. W.C. Koscielniak, J.L. Pelouard and M.A. Littlejohn, "Dynamic Behavior of Photocurrent in a GaAs Metal-Semiconductor-Metal Photodetector with Sub-Half Micron Electrode Pattern," Appl. Phys. Lett., 54, 567 (1989).
6. K.F. Brennan, D.H. Park, K. Hess and M.A. Littlejohn, "Theory of the Velocity Field Relation in AlGaAs," Jour. Appl. Phys., 63, 5004 (1988).
7. D.L. Woolard, R.J. Trew and M.A. Littlejohn, "Hydrodynamic Hot Electron Transport Model With Monte Carlo-Generated Transport Parameters," Solid State Electronics, 31, 571 (1988).
8. L.F. Register, M.A. Littlejohn and M.A. Stroscio, "Feynman Path Integral Study of Confined Carriers Subject to a Statistical Potential," Solid State Electronics, 31, 563 (1988).
9. L.F. Register, M.A. Stroscio and M.A. Littlejohn, "Numerical Evaluation of the Feynman Integral-Over-Paths in Real and Imaginary Time," Superlattices and Microstructures, 4, 61 (1988).
10. C.K. Williams, M.A. Littlejohn, T.H. Glisson and J.R. Hauser, "Monte Carlo Simulation of the Hall Effect in Degenerate GaAs," Superlattices and Microstructures, 29, p. 725, 1986.

Associations With Graduate Students/Post-Doctoral Scholars For Last Five Years

(From a total of 57 graduate students and 7 post-doctorals sponsored)

1. H.P. Belgal, M.S.E.E., 1988.
2. L.F. register, Ph.D., 1989.
3. D.L. Woolard, Ph.D, 1990.
4. W.C. Koscielniak, Ph.D, 1990.
5. K.J. Kim, Ph.D.
6. J.E. Monaghan, Ph.D.
7. J.L. Pelouard, Visiting Assistant Professor, 1988-1989.
8. H.H. Tian, Visiting Assistant Professor, 1989-1990.

Scientific Collaborators During Last Four Years

1. Dr. M.A. Stroscio, U.S. Army Research Office, RTP, NC
2. Dr. K.F. Brennan, Georgia Institute of Technology, Atlanta, GA.
3. Dr. K. Hess, University of Illinois, Urbana, IL.

Ki Wook Kim

Dept. of Electrical and Computer Engineering
Box 7911
North Carolina State University
Raleigh, NC 27695-7911

Phone: (919) 737-5229
Birthdate: September 14, 1960

EDUCATION

08/88 Ph.D. in Electrical Engineering
University of Illinois, Urbana, Illinois
Thesis Title: Monte Carlo Studies of Nonlinear Electron Transport in III-V Semiconductors

05/85 M.S. in Electrical Engineering
University of Illinois, Urbana, Illinois

02/83 B.S. in Electronics Engineering
Seoul National University, Seoul, Korea

WORK EXPERIENCE

08/88 - present: Assistant Professor (Visiting), Department of Electrical and Computer Engineering, North Carolina State University, Raleigh, North Carolina

06/85 - 08/88: Graduate Research Assistant, Coordinated Science Laboratory, University of Illinois, Urbana, Illinois

06/83 - 05/85: Graduate Research Assistant, Department of Electrical Engineering, University of Illinois, Urbana, Illinois

ACADEMIC HONORS

IBM Predoctoral Fellowship (1986-1988)

RESEARCH INTERESTS

Semiconductor physics and modeling of electronic and optoelectronic devices, carrier transport in bulk and heterostructures, quantum effects, Monte Carlo simulation.

PUBLICATIONS

Refereed Articles in Journals

1. K. Kim, K. Kahen, J.P. Leburton, and K. Hess, "Band-structure dependence of impact ionization rate in GaAs," *J. Appl. Phys.* 59, 2595 (1986).

2. K. Kim and K. Hess, "Simulations of electron impact ionization rate in GaAs in nonuniform electric fields," *J. Appl. Phys.* 60, 2626 (1986).

3. D. Arnold, K. Kim, and K. Hess, "Effects of field fluctuation on impact ionization rates in semiconductor devices due to the discreteness and distribution of dopants," *J. Appl. Phys.* 61, 1456 (1987).

4. K. Kim, K. Hess, and F. Capasso, "New effects of structure in momentum and real space on nonlinear transport across heterojunction band discontinuities," *Appl. Phys. Lett.* 51, 508 (1987).

5. K. Kim, B. Mason, and K. Hess, "Inclusion of collision broadening in semiconductor electron transport simulations," *Phys. Rev.* B36, 6547 (1987).

6. K. Kim and K. Hess, "Ensemble Monte Carlo simulations of semiclassical nonlinear electron transport across heterojunction band discontinuities," *Solid-State Electron.* 31, 877 (1988).

7. K. Kim, K. Hess, and F. Capasso, "A Monte Carlo study of electron heating and enhanced thermionic emission by hot phonons in heterolayers," *Appl. Phys. Lett.* 52, 1167 (1988).

8. M. Kuzuhara, K. Kim, D. Arnold, and K. Hess, "Ballistic electron transport across collector barriers in AlGaAs/GaAs hot-electron transistors," *Appl. Phys. Lett.* 52, 1252 (1988).

9. K. Kim and K. Hess, "Electron transport in AlGaAs/GaAs tunneling hot electron transfer amplifiers," *J. Appl. Phys.* 64, 3057 (1988).

10. J. M. Higman, K. Kim, K. Hess, T. van Zutphen, and H. M. J. Boots, "Monte Carlo simulation of Si and GaAs avalanche electron emitting diodes," *J. Appl. Phys.* 65, 1384 (1989).

11. M. Kuzuhara, K. Kim, and K. Hess, "Transient simulation of AlGaAs/GaAs/AlGaAs and AlGaAs/InGaAs/AlGaAs hot-electron transistors," *IEEE Trans. Electron Devices* ED-36, 118 (1989).

12. K. W. Kim, M. A. Stroscio, and J. C. Hall, "Frequencies of confined longitudinal-optical phonon modes in GaAs/GaP short-period strained-layer superlattices," *J. Appl. Phys.* 67, 6179 (1990).

13. M. A. Stroscio, K. W. Kim, and J. C. Hall, "Variation in frequencies of confined longitudinal-optical phonon modes due to changes in the effective force constants near heterojunction interfaces," *Superlatt. Microstruct.* 7, 115 (1990).

14. M. A. Stroscio, K. W. Kim, M. A. Littlejohn, and H. Chuang, "Polarization Eigenvectors of Surface-Optical-Phonon Modes in a Rectangular Quantum Wire," *Phys. Rev. B.* 42, 1488 (1990).

15. K. W. Kim and M. A. Stroscio, "Electron-Optical-Phonon Interaction in Binary/Ternary Heterostructures," submitted to *Appl. Phys. Lett.*

16. M. A. Stroscio, K. W. Kim, and S. Rudin, "Scattering Rate for the Electron-LO-Phonon Interaction in Polar Semiconductor Quantum Wires," accepted for publication in *Phys. Rev. B.*

17. K. W. Kim, H. Tian, and M. A. Littlejohn, "Analysis of Delta-Doped and Uniformly-Doped HEMTs by Ensemble Monte Carlo Simulation," submitted to *IEEE Electron Device Lett.*

18. K. W. Kim, M. A. Stroscio, and A. Bhatt, "Electron-Optical-Phonon Scattering Rates in a Rectangular Semiconductor Quantum Wire," to be submitted to *Phys. Rev. B.*

19. H. Tian, K. W. Kim, and M. A. Littlejohn, "Influence of DX Centers and Surface States on Delta-Doped HEMT Performance," to be submitted to *J. Appl. Phys.*

Refereed Articles in Proceedings of Conferences

1. K. Kim, K. Hess, and F. Capasso, "Simulations of nonlinear transport in AlGaAs/GaAs single well heterostructures," presented at the 5th Int. Conf. on Hot Carriers in Semiconductors (July, 1987, Boston, Mass.), published in *Solid-State Electron.* 31, 349 (1988).

2. K. W. Kim, M. A. Stroscio, and J. C. Hall, "Frequencies of Confined Longitudinal-Optical Phonon Modes in Short-Period Strained Semiconductor Superlattices," presented at the SPIE Int. Symp. on Optical & Optoelectronic Applied Science and Engineering (July, 1990, San Diego, Calif.), Proceedings to be published.

3. M. A. Stroscio, K. W. Kim, and M. A. Littlejohn, "Theory of Optical-Phonon Interactions in Quantum Wells and Quantum Wires (Invited)," to be presented at the SPIE Int. Conf. on Physical Concepts of Materials for Novel Optoelectronic Device Applications (October, 1990, Aachen, Germany), Proceedings to be published.